DER MATERIALS QUARTERLY PROGRESS REPORT

For the Period
January 1, 2002 to March 31, 2002

Prepared by:

David P. Stinton, Manager, and
Roxanne A. Raschke
DER Materials Research
Oak Ridge National Laboratory

For:

Department of Energy
Office of Power Technologies
Energy Efficiency and Renewable Energy

DER MATERIALS QUARTERLY PROGRESS REPORT

January—March 2002

TABLE OF CONTENTS

Advanced Materials for Exhaust Components of Recripracating Engines

P. J. Maziasz
Oak Ridge National Laboratory, Oak Ridge, Tennessee

RECUPERATORS

Advanced Alloys for High Temperature Recuperators

P. J. Maziasz, B. A. Pint, R. W. Swindeman, K. L. Moore, and M. L. Santella
Metals and Ceramics Division
Oak Ridge National Laboratory
P.O. Box 2008, Oak Ridge, TN 37831-6115
Phone: (865) 574-5082, E-mail: maziaszpj@ornl.gov

Objective

The main objective of this program is to work with commercial materials suppliers (foil and thin sheet) and recuperator manufacturers to develop the improved or advanced materials they need for their near-term and longer-term microturbine applications. The near term portion of this program will identify or develop low-cost stainless steels and alloys (no more than 1.5 times the cost of commercial 347 stainless steel) with more creep- and corrosion-resistance for better performance and durability at about 704°C (1300°F). The longer-term portion of this program will identify or develop stainless alloys or materials that can perform reliably at 760°C (1400°F) and higher. Near-term success should have an immediate impact on current microturbines, particularly those using alternate or more corrosive fuels. Longer-term solutions will benefit advanced microturbines which are being designed today to operate at higher temperatures.

Currently, the specific compact recuperator technologies being addressed in this program included primary surface recuperators (PSR) and the brazed plate and fin recuperators (PFR). Other types of advanced recuperator technology can be included in the future. ORNL will collaborate with materials suppliers to test the properties (tensile, creep, corrosion) of candidate foils related to component manufacturability and in-service performance, while the OEM's obtain sufficient and appropriate material to test actual recuperator manufacturing processes, and make recuperator components for evaluation and testing. There is synergy and coordination between this particular materials program and other ORNL programs that are: a) evaluating the corrosion resistance of recuperator foils at 650-800°C in 10% water vapor, and b) developing an engine-based advanced recuperator materials and component test facility.

Highlights

<u>Materials for use to about 704°C (1300°F)</u>

The most promising materials for this goal range from standard 347 stainless steel with modified processing for more creep-resistance, to compositionally modified 347 stainless steels with modified processing with significantly better creep-resistance and aging resistance. This group could also include stainless steels with more Cr and Ni than standard 347 steel. This quarter, direct evaluation of fresh and engine-tested recuperator components began. Such data will enable ORNL to define the optimum performance upgrade solution for each microturbine manufacturer. This quarter, another ORNL modified 347 steel (#4) was tested and lasted about

575 h during creep at 750°C and 100 MPa, with about the same creep rate found in alloy 625. New oxidation/corrosion data on these ORNL modified 347 steels at 800°C and 10% water vapor showed significantly better behavior than standard 347 stainless steel up to 1000 h. New data on weldability showed the new ORNL modified 347 steels to be as weldable as standard, commercial 347 steel.

Materials for use at 760°C (1400°F) or higher

The most promising materials with significantly better creep-resistance and corrosion-resistance in this temperature range at 3-4 times the cost of 347 stainless steel are HR120 (Haynes) or modified alloy 803 (Special Metals). These Fe-based austenitic stainless alloys have about 25%Cr and 35%Ni. Alloys with even higher performance would include HR230, alloy 740, or alloy 625, or HR214 at 5-10 times the cost of 347 steel, and these are mainly Ni-based alloys with significant amounts of Cr, Co, Mo, W or Al added. This quarter, creep-rupture screening at 750°C and 100 MPa was completed, with variations in processing to vary grain size all showing relatively similar good creep behavior. Fine-grained HR120 lasted almost 900 h and had about 30% rupture ductility, but also a higher creep rate. Discussions about producing commercial foils of these alloys began this quarter. Weld screening of HR120 and the modified 803 alloy relative to standard, commercial 347 steel also began this quarter. Oxidation screening of both HR120 and the modified 803 alloy showed excellent oxidation resistance after 1000 h at 800°C.

Technical Progress

Current natural gas microturbines in service today have recuperators made of 347 stainless steel and generally do not exceed 650-675°C. While higher efficiency, larger turbines sizes and alternate fuels all require more performance as well as higher reliability from the recuperator, economic factors limit more costly solutions for recuperators, which are already about 30% of the total system first cost. This recuperator materials program is driven by the need to provide microturbine OEMs with the most affordable materials that upgrade the performance of their specific recuperator technologies. This ORNL program has two essential parts: (a) analysis and evaluation of engine-tested recuperator components to exactly define the performance and manufacturing details related to improved recuperators for each OEM, and (b) commercial-scale trials of processing and alloy compositional modifications of type 347 stainless steel and of alloy 120, and possibly of modified alloy 803, with benchmarking to establish the performance relative to standard, commercial 347 stainless steel foils and sheets for comparison. There is close coordination with another ORNL program that has converted a Capstone 60 kW microturbine into an advanced recuperator test facility.

Recuperator Component Analysis

Several different microturbine OEMs have provided pieces of fresh and engine-tested PFR and PSR recuperators made from standard 347 stainless steel for analysis and testing last quarter, and sectioning and characterization began this quarter. These components are manufactured

from coils of standard, commercial 347 steel that range from 3-4 mil foil up to 10 mil sheet, and include the additional manufacturing steps of welding and/or brazing. ORNL is characterizing the engine-tested components and measuring the changes relative to fresh (as-manufactured) components. In addition, samples of some fresh recuperator components began lab testing in air + 10% water vapor at several different temperatures to help understand and interpret the engine-tested component behavior. This engine-exposed 347 stainless component data will define the performance and/or life increases that can be achieved by substituting the advanced materials. Detailed component analysis is also important feedback to the OEM's, and will be used to help define the best way to use advanced materials to make recuperators capable of better performance at higher temperatures for each different microturbine OEM.

Selection and Commercial Scale-Up of Advanced Recuperator Materials:
a) Materials for use to about 704°C (1300°F)

A summary of the room-temperature tensile properties of 4 mil foils of the advanced alloys down-selected from the previous ORNL advanced alloy screening program are given in Table 1, including several more modified 347 steels tested this quarter (ORNL modified 347 #3 and #4), together with cost relative to standard, commercial 347 stainless steel. Foils of the standard stainless steels and alloys were produced by lab-scale processing methods at ORNL from commercial plate or tubing stock. The ORNL developmental modified 347 stainless steels were melted as 10-15 lb ingots, and then hot-rolled into plate and processed into foil at ORNL. Creep-rupture properties for these foils testing in air at 750°C and 100 MPa (high-stress creep for accelerated testing) are given in Fig. 1. Last quarter, a new 20Cr-15Ni austenitic stainless steel (ORNL mod 3) was produced and tested, and this quarter another modified 347 (19Cr-12.5Ni, ORNL mod 4) was also produced and tested. The new ORNL 347 mod 4 showed exceptional creep-strength (as good as or better than alloy 625 in terms of primary creep and secondary creep rate), and lasted about 575 h and ruptured with almost 3% elongation. This quarter, several more very similar modified heats of 347 were made with small adjustments in Nb and C content and other minor impurities to boost the rupture ductility without reducing the creep strength, and they will be creep-tested next quarter.

Table 1. Tensile Properties of Advanced Heat-Resistant Austenitic Stainless Steel and Alloy Foils Tested at Room Temperature

Alloy	Yield Strength (MPa)	Total Elongation (%)	Approximate Normalized Cost
Materials for use to about 704°C (1300°F)			
347 HFG steel	283	50	1.0
347 standard steel	173	47	1.0
ORNL mod. 347 #1	281	33	1.0
ORNL mod. 347 #2	232	23	1.0
ORNL mod. 347 #3	259	36	1.0
ORNL mod. 347 #4	285	29	1.0

Materials for use at 760°C (1400°F) or higher

alloy 803 (standard)	242	39	3
modified alloy 803 (1A)	294	30	3
alloy 120 (standard)	415	34	3.5

(0.004 inch thick foils processed at ORNL at different conditions tailored to each particular steel or alloy)

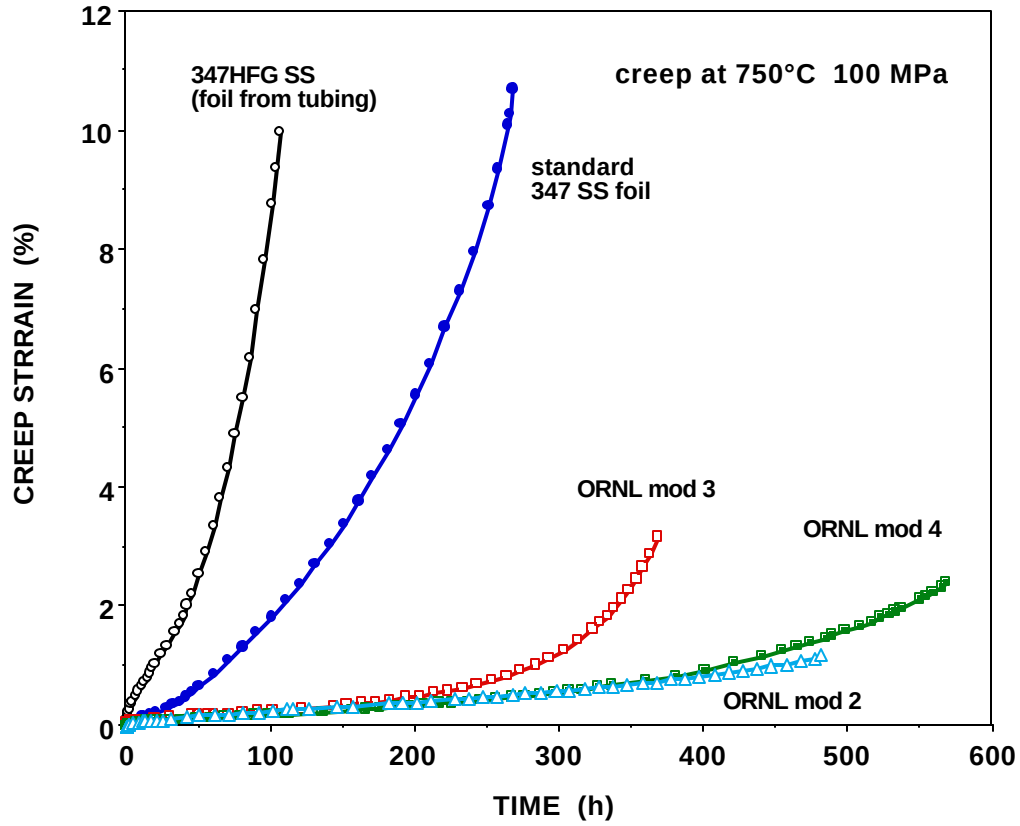

Figure 1. Plot of creep-strain versus time for three new ORNL modified laboratory heats of type 347 stainless steel (17-18Cr, 10-13Ni, ORNL mod 2 and 4, and 20Cr-15Ni, ORNL mod 3) tested in air at 750°C. For comparison, foil from standard commercial 347 stainless steel, and from foil produced by splitting, flattening and rolling commercial 347H tubing (Sumitomo, H – high carbon, FG – fine grained), both with similar ORNL lab-scale foil processing, are also included.

This quarter, ORNL began oxidation studies of these new modified 347 steels together with other advanced alloy, including the 120 and 803 austenitic alloys. Tests to 1000 h were completed at 750°C and 800°C with 10% water vapor this quarter, and new testing began at 650 and 700°C. Specimens were also made from portions of fresh 347 stainless steel recuperator components and put into the oxidation test at 700°C. Results of the testing at 800°C are shown in Fig. 2. These are greatly accelerated tests for the purpose of screening the alloys and ranking them relative to each other, not tests to qualifying alloys for use at these conditions. Clearly, the standard commercial 347 stainless steels suffer rapid and catastrophic

corrosion attack, but the new ORNL modified 347 steels all show much better corrosion resistance, and fall closer to the behavior of NF709 (Fe-20Cr-25Ni-Nb) and alloy 625 for this limited testing time. Longer time testing at 700 and 750°C will be more relevant to extended microturbine service at about 700°C, but clearly, the ORNL modified 347 steels that show improved creep resistance also show improved corrosion resistance relative to standard commercial 347 stainless steel. Such behavior is consistent with at least higher levels of Cr and Ni in the modified 347 steels, as well as other new elements added to stabilize the austenite phase at high temperatures.

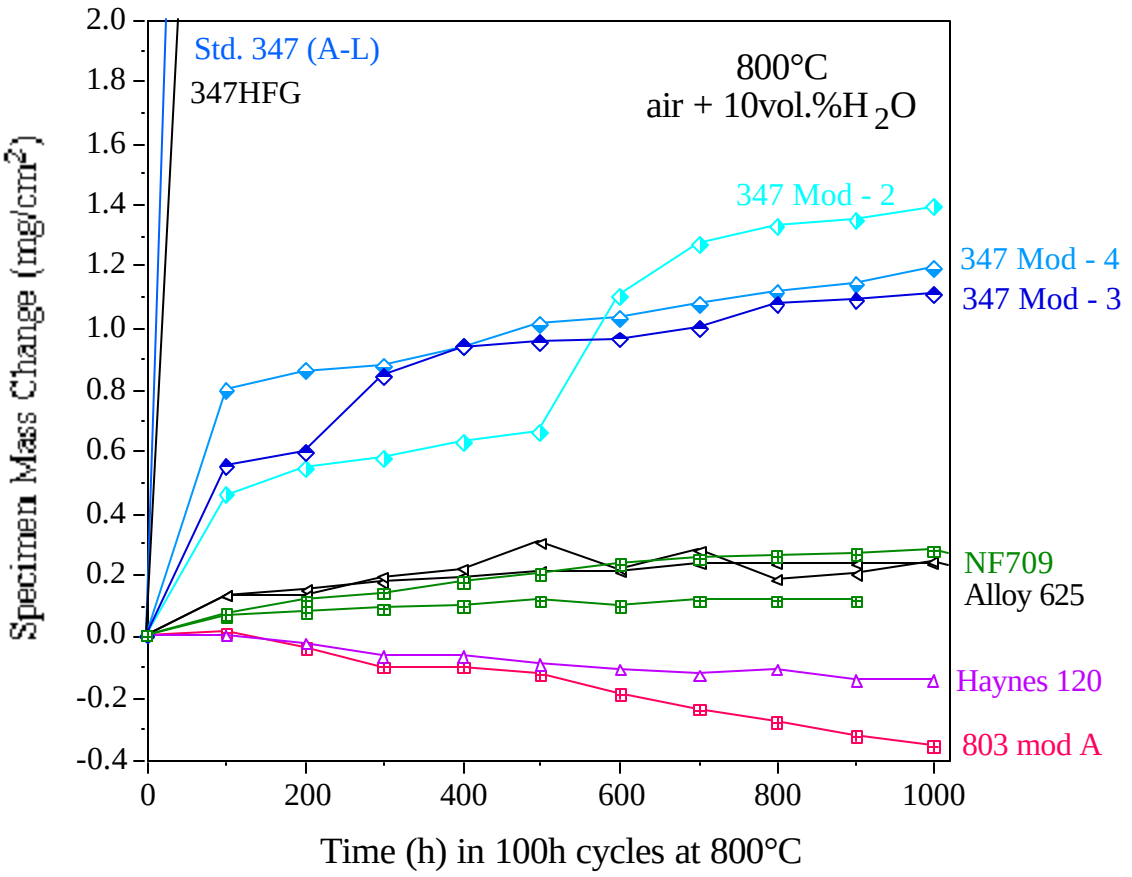

Figure 2. Oxidation testing of foil coupons in air + 10% water vapor at 800°C, with cycling to room temperature every 100h for weight measurements. Foils of both commercial stainless steels, alloys and superalloys and ORNL developmental steels were lab-scale processed at ORNL and were also used to make tensile/creep specimens. All foils were made from plate stock, except for 347 HFG and NF709, which were made from split and flattened boiler tubing. All foils are in the solution-annealed condition.

This quarter, new testing began on both the weldability and the thermal aging resistance of all the candidate advanced recuperator stainless steels and alloys. Weldability was investigated because welding is a critical manufacturing step in making any recuperator component, and

there is the general perception that more stable austenitic stainless steels and alloys (Cr and Ni equivalents of alloying elements, with Cr and elements that behave like it promoting ferrite stability, and Ni and elements that behave like it promoting austenite stability) are more difficult to weld. Weldability was tested by using gas-tungsten-arc (argon shielded) welding to produce autogeneous, partial penetration welds on all of the thicker plate stock (0.1 to 0.03 inches thick) of the commercial, or ORNL developmental steels and alloys used to produce foils. This is a much more severe test than welding foils. The data so far indicates that all of the ORNL modified 347 steels are as weldable as standard, commercial 347 steel (Allegheny-Ludlum), with no hot or cold-cracking. Cross-sections of these welds will be examined metallographically next quarter, as well as some testing of other welding methods (i.e. laser welding).

This quarter, thermal aging began of foil tensile specimens at 700 and 750°C for 2500 h to measure the room-temperature ductility remaining after aging. 300 series stainless steels are prone to significant ductility loss after aging at 650°C and above, and cold cracking is a concern for recuperator components that must endure cycling or thermal shocks due to rapid heating or cooling. This testing will be another measure of the improvements of the modified 347 stainless steels or the advanced austenitic alloys in terms of retaining ductility by resisting the effects of aging.

Discussions with microturbine OEMs and 347 stainless steel foil producers continued this quarter to define their interest in selecting one or two of the ORNL modified 347 steels for commercial scale-up and foil production, as well as modifying the processing of standard 347 stainless steels to improve its performance.

b) Materials for use at 760°C (1400°F) or higher

The advanced austenitic alloys with more Cr and Ni than 347 stainless steel represent a substantial upgrade in high temperature strength and creep-resistance relative to standard 347 stainless steels, particularly with appropriately modified foil processing. Standard alloy 803 (Special Metals, Fe-25Cr-35Ni-Ti-Nb) has very good creep-rupture ductility but much less creep-resistance than standard 347 stainless steel, as shown in Fig. 3. The modified 803 alloys were developed in a joint project between ORNL and Special Metals to improve its creep resistance, and several different processing conditions (1A and 1A.1, varying primarily grain size) still produce consistent improvements in creep-strength and rupture ductility relative to standard 347 stainless steel. Better fracture ductility and better creep strength will make this alloy have better performance and reliability for recuperator applications. Standard HR120 (Haynes International, Fe-25Cr-35Ni-Nb-N) alloy processed into foil at ORNL (A) has similarly good creep behavior. A second sample of HR120 alloy was processed differently (B, much shorter annealing times to refine the grain size, similar to the modified 803 alloy), and it lasted about 900 h and ruptured with about 30% ductility after creep testing at 750°C and 100 MPa. While all of these alloys show good rupture lives and ductility, their creep rates are considerably higher than the ORNL modified 347 stainless steels (alloy 120 and modified 803

reach 2-3% creep strain in about 200 h), which exhibit creep resistance similar to the Ni-based superalloy 625. Total creep-strain is also a consideration and constraint in most recuperator designs.

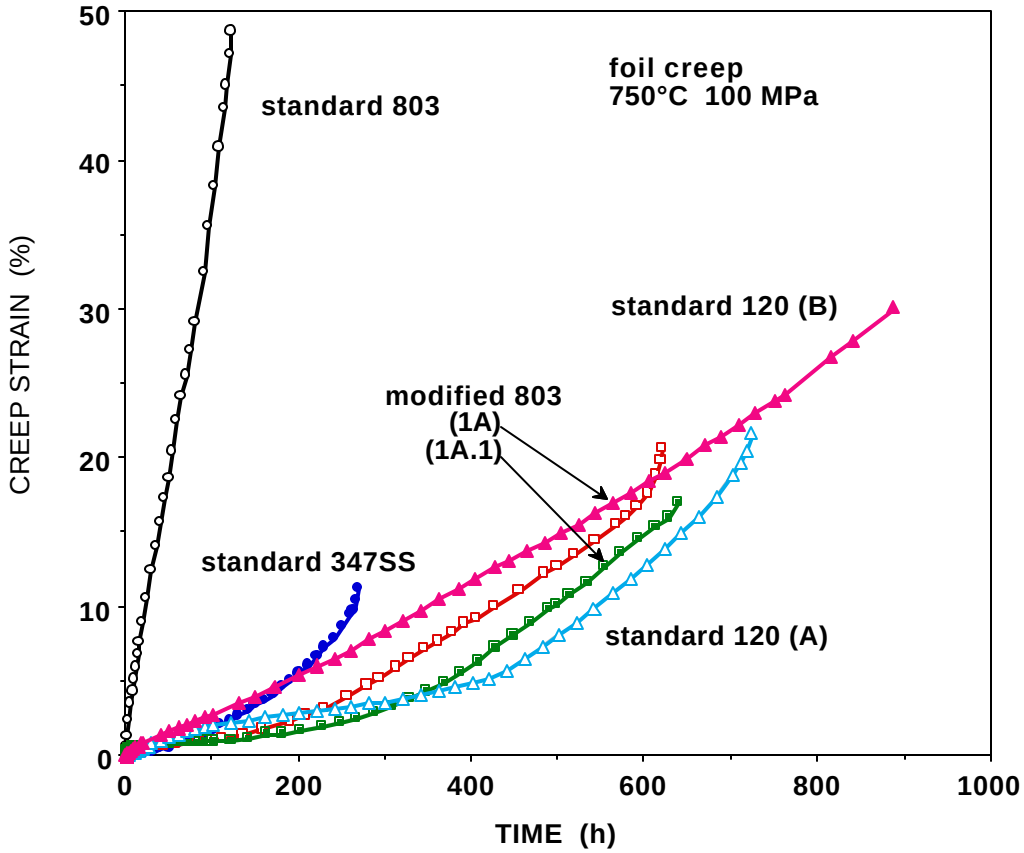

Figure 3. Plot of creep strain (%) versus time for creep-rupture tests at 750°C and 100 MPa run in air for the commercial advanced stainless alloys processed into 0.004 inch thick foils using laboratory-scale processing methods at ORNL, and down-selected for commercial scale-up. All alloys are in the solution-annealed (SA) condition.

The advanced alloys were also evaluated for oxidation/corrosion resistance at 750 and 800°C, and data at 800°C is also shown in Fig. 2. Both HR120 and modified 803 show good resistance to oxidation mass gain, consistent with higher Cr contents. Their high-temperature oxidation/corrosion resistance, even for more corrosive alternate fuels, should be far superior to 347 stainless steel. They also should have similar manufacturing characteristics relative to 347 steel, particularly the modified 803 (Table 1). Their corrosion resistance and creep strength indicate capability of being used at 760°C or above relative to standard 347 stainless steel without having to increase section thickness to compensate for increased temperature.

This quarter, tensile specimens of the advanced HR120 and modified 803 were also included in the thermal aging experiments at 700 and 750°C for 2500 h to determine their resistance to ductility loss at room temperature. Plate stock of both alloys was also included in the welding tests, and results will be evaluated next quarter.

In summary, ORNL began a new advanced recuperator materials technology program in FY 2002 to complete lab-scale studies and then to scale them up to commercially produced foil and sheet products that microturbine OEMs can then use to make upgraded recuperator components with more performance and reliability at higher temperatures. The goal is manufacturing on a trial basis and engine-testing. This project expands and applies its unique and systematic data base on mechanical behavior and oxidation/corrosion effects of stainless steel and alloy foils, focused on addressing and meeting the needs of the U.S. microturbines industry for improved recuperators.

Status of Milestones

New Program

FY2002 – Develop stainless steel near type 347 stainless steel composition and cost with maximum performance in foil form at 700-750°C (complete by June 2002) – on schedule.

Industry Interactions

Discussions continued with the microturbine OEMs Ingersoll-Rand Energy Systems and Capstone Turbines during this quarter. Ingersoll-Rand shipped engine-tested and fresh recuperator components to ORNL for analysis and evaluation, and Capstone agreed to provide some standard, commercial 347 stainless steel foils for baseline properties testing. Discussion about advanced alloy commercial foil production continued with Elgiloy, Haynes International and Special Metals. Elgiloy does produce standard HR120 foil, and provided some to ORNL this quarter. Since the modified 803 alloy is developmental and has only been produced in small quantities, discussions continued this quarter to obtain a larger heat of the new modified alloy 803 from Special Metals for Elgiloy to process into foil. Discussions with General Motors Global Alternative Propulsion Center, who have needs for heat-exchanger/reformer technology for fuel-cell applications that are similar to advanced microturbine recuperators, continued this quarter as well. More detailed interactions and discussions began this quarter with United Technology Research Center to define and describe their microturbine recuperator interests and needs.

Problems Encountered

None.

Publications/Presentations

A presentation on Advanced Alloys for High Temperature Recuperators was made by P. J. Maziasz, B. A. Pint, R. W. Swindeman, K. L. More and E Lara-Curzio at the DOE/DER Microturbines and Industrial Gas Turbines Peer Review, held March 12-14, 2002 in Fairfax, VA.

Recuperator Alloys – Composition Optimization for Corrosion Resistance

R. Peraldi and B. A. Pint
Metals and Ceramics Division
Oak Ridge National Laboratory
P.O. Box 2008, Oak Ridge, TN 37831-6156
Phone:(865) 576-2897, E-mail: pintba@ornl.gov

Objective

In order to provide a clear, fundamental understanding of alloy composition effects on corrosion resistance of stainless steel components used in recuperators, the oxidation behavior of model alloys is being studied. The first goal of this study was to determine the critical Cr content and the effect of Ni concentration required to minimize the accelerated corrosion attack caused by water vapor. Other factors to be investigated include the effects of temperature, alloy grain size, phase composition and minor alloy additions. The composition and microstructure effects also will provide data for life-prediction models and may suggest a mechanistic explanation for the effect of water vapor on the oxidation of steels. This information will be used to select cost-effective alloys for higher temperature recuperators.

Highlights

Comparing the performance of austenitic and ferritic alloys, the fine-grained austenitic alloys generally performed better at lower temperatures, 650-700°C, while the coarser-grained ferritic alloys performed better at 800°C. Using Cr diffusivity data in ferritic and austenitic alloys from the literature, the superior performance of ferritic alloys at 800°C can be explained because of the faster Cr diffusivity in ferritic alloys, compared to austenitic alloys. However, the Cr diffusivities are similar at the lower temperatures. This suggests that the addition of Ni plays an important role in improving the corrosion resistance at 650-700°C.

Technical Progress

Experimental Procedure

As outlined in previous reports, several model austenitic and ferritic cast alloys were vacuum annealed for 4h at 1100°C prior to testing. Rolled alloys were prepared from these cast materials. Pieces of cast material were hot forged and hot rolled at 1100°C to 2.5mm thickness, followed by cold rolling to 1.25mm. Annealing was done for rolled materials under Ar + 4%H_2 for 2 minutes at 900 and 1000°C for ferritic and austenitic alloys, respectively. Oxidation specimens were cut from the rolled plate materials with dimensions (1x12x18mm) to produce a similar surface/volume ratio (about 2.3) as the cast coupons. All specimens were polished to 600-grit SiC paper and cleaned in acetone and methanol. From light microscopy of etched specimens (Figure 1), characterization of the average grain size was calculated as ≈150μm for cast alloys, and ≈100μm and ≈10μm for rolled ferritic and austenitic specimens, respectively. All of the cast and rolled alloys were oxidized in air + 10vol.% water vapor with 1h cycles between 650 and 800°C.

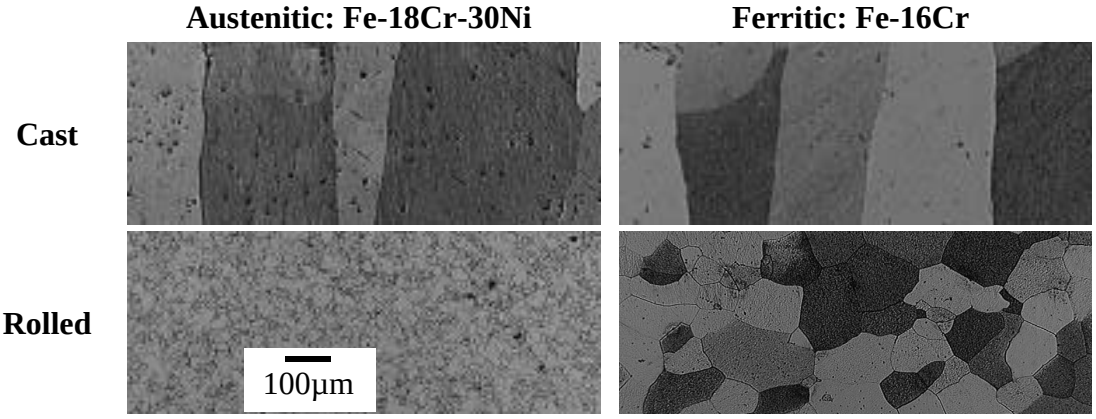

Figure 1: Light microscopy of etched austenitic Fe-18Cr-30Ni (left column) and ferritic Fe-16Cr (right column) for cast and rolled samples after annealing.

Volume and grain boundary Cr diffusivity.

Comparison of Cr diffusivity in austenitic and ferritic alloys was made from diffusion data measured by Tokei et al. [1]. In Figure 2, effective diffusion coefficients (dashed lines), taking into account both volume diffusion and grain-boundary diffusion with an average grain size of 150µm corresponding to the cast alloys, are shown and compared to the volume diffusion coefficient (solid lines). In the temperature range of 597-805°C, the average grain size of the cast alloys was too large to strongly enhance the Cr diffusivity in both ferritic and austenitic alloys, Figure 2.

Austenitic vs. ferritic.

Figure 2 also includes the different oxidation performances observed in air + 10% water vapor: either a thin protective oxide scale (POS) was observed or accelerated attack (AA) occurred which sometimes included spallation. Increasing the temperature delayed the breakaway observed on ferritic alloys whereas it reduced the protective oxide growth stage for austenitic alloys. In Figure 2, white points represent the good oxidation performance as they can maintain a protective oxide scale after 100x1h cycles and black points represent accelerated attack. At 800°C, the Cr diffusivity was calculated to be more than one order of magnitude higher in the ferritic than in austenitic alloys (Figure 2) providing a plausible explanation for the better corrosion resistance of ferritic alloys at higher temperatures. Between 600 and 650°C, the calculated Cr diffusion was similar for ferritic and austenitic alloys. Without an advantage in Cr diffusivity, the superior performance of the austenitic alloys at lower temperatures, suggests some beneficial role of Ni in improving resistance to water vapor.

Cast vs. rolled.

If ferritic alloys were more oxidation resistant than austenitic alloys because of their higher Cr diffusivity, then, in the same way, a fine alloy grain size would increase the Cr diffusivity and therefore the corrosion resistance of the alloy. Figure 3 is based on a similar calculation as was used for Figure 2, but for rolled materials, taking into account a grain size of 100µm for austenitic and 10µm for ferritic alloys. Previous experimental results have shown that rolled austenitic alloys delayed the AA or AAS compared to cast specimens. The higher Cr diffusivity in fine-grained austenitic alloys explains these results, Figure 3. For ferritic alloys, rolled and cast specimens had a similar behavior as both alloys have a similar grain size and thus a similar Cr diffusivity.

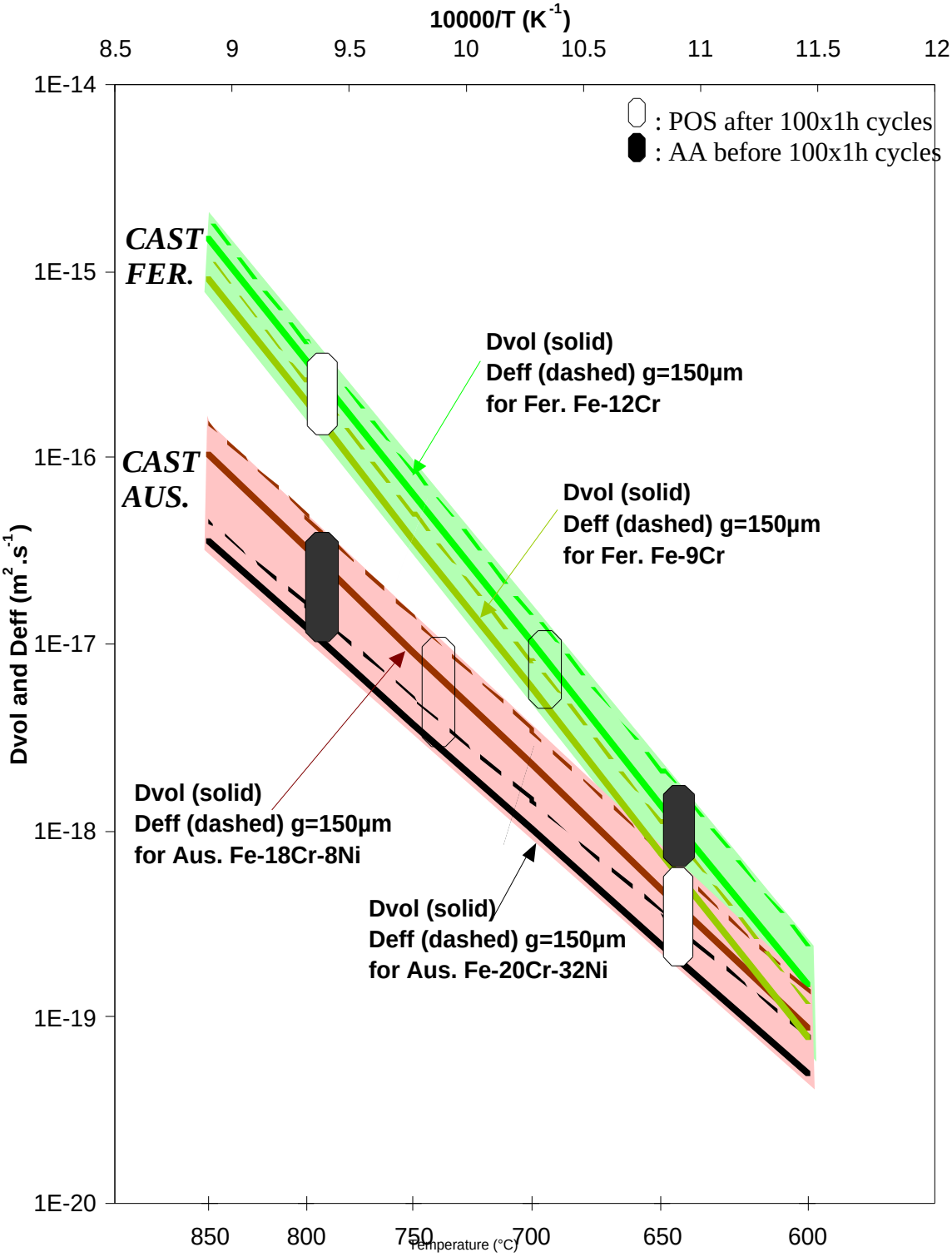

Figure 2: Arrhenius plot of Cr coefficient diffusion in cast austenitic and ferritic alloys calculated from Tökei et al. data [1] for bulk diffusion (solid lines) and bulk + grain boundary diffusion with an average grain size of g = 150 µm (dashed lines). Upper and lower areas correspond to the Cr diffusivity in cast ferritic and austenitic alloys, respectively.

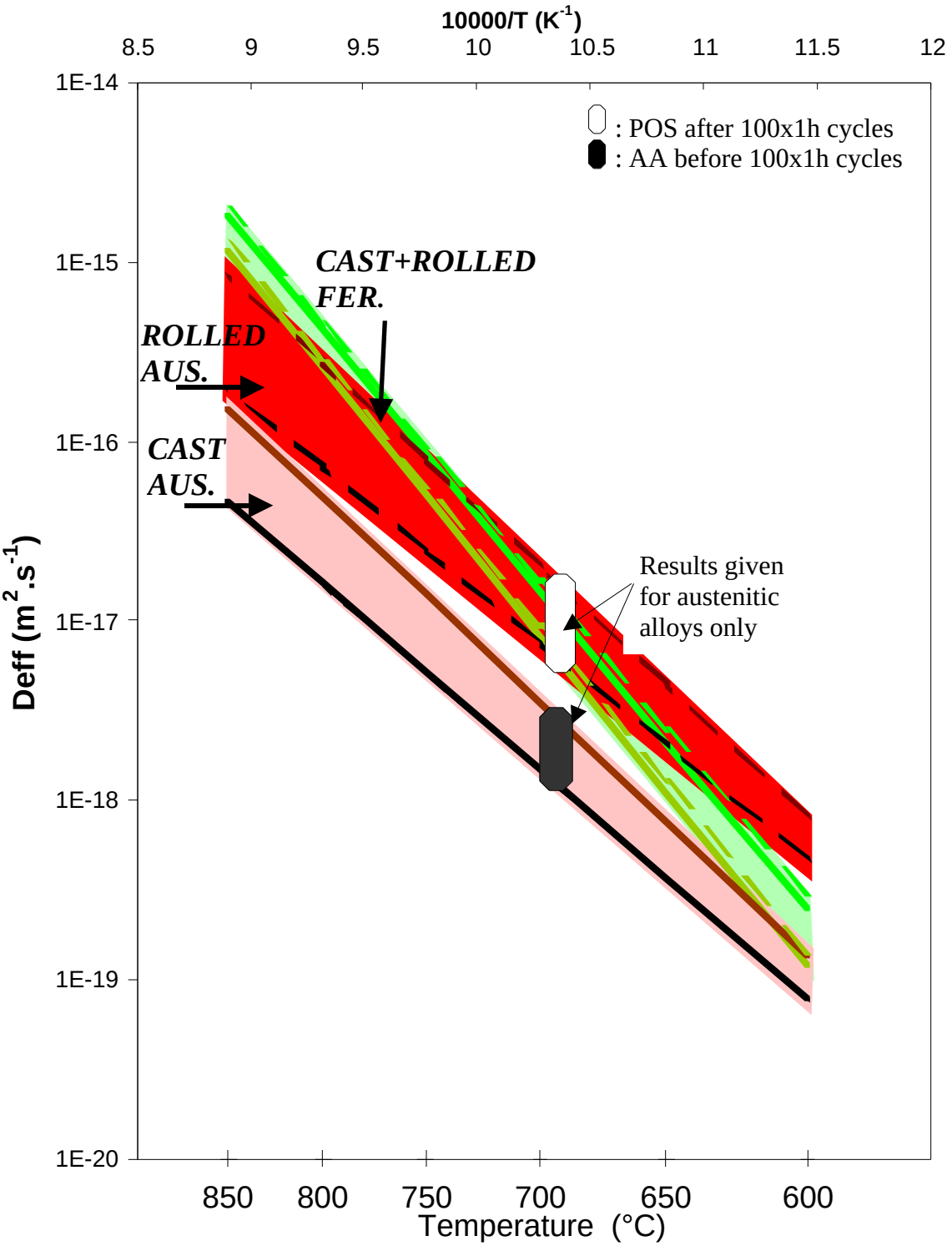

Figure 3: Arrhenius plot of Cr coefficient diffusion calculated from Tökei et al. data [1] for bulk + grain boundary diffusion with an average grain size of g = 150 µm for cast ferritic and austenitic (solid lines), g = 100µm for rolled ferritic (dashed lines) and g = 10µm for rolled austenitic (dashed lines). For ferritic alloys, Cr diffusivity are superimposed for cast and rolled materials.

Status of Milestones

Open literature publication of experimental results. (August, 2002)

Industry Interactions

Discussed materials needs with Bowman Power Systems and André Mom from the Dutch Gas Turbine Association

Problems Encountered

None.

Publications/Presentations

Oral presentation at the TMS Annual Meeting, Seattle, USA, (February, 17-21st 2002).
"Effect of chromium and nickel contents on high temperature oxidation of stainless steels in mixed air and water vapor.", R. Peraldi and B. A. Pint.

Publication submitted to Materials at High Temperatures:
"Effect of chromium and nickel contents on the oxidation behavior of ferritic and austenitic model alloys in air with water vapor.", R. Peraldi and B. A. Pint.

Reference

[1]: Tökei Zs., K. Hennesen, H. Viefhaus and H. J. Grabke, Materials Science Technology, Vol 16 (2000), pp 1129-1138.

Recuperator Materials Testing and Evaluation

E. Lara-Curzio
Metals and Ceramics Division
Oak Ridge National Laboratory
P.O. Box 2008, Oak Ridge, TN 37831-6069
Phone: (865) 574-1749, E-mail: laracurzioe@ornl.gov

Objective

The objective of this sub-task is to screen and evaluate candidate materials for the next generation of advanced microturbine recuperators. To attain this objective, a commercially-available microturbine was acquired and in coordination and collaboration with its manufacturer, it was modified to operate at recuperator inlet temperatures as high as 843°C. The durability of candidate recuperator materials will be determined by placing test specimens at a location upstream of the recuperator, followed by determination of the evolution of the material's physical and mechanical properties as a function of time of exposure. During exposure tests inside the microturbine, it will be possible to subject test specimens to various levels of mechanical stress by using a specially-designed sample holder and pressurized air. The selection of materials to be evaluated in the modified microturbine will be made in coordination and collaboration with other tasks of this program and with manufacturers of microturbines and recuperators.

Highlights

A procedure was developed, in collaboration with personnel from the Materials Joining & NDT Group at ORNL, to laser-weld thin (plain or corrugated) metallic foils to a sample holder for evaluation inside a microturbine. The sample holder will enable the application of mechanical stresses to the metallic foil test specimens through internal pressurization. The critical parameters for laser-welding thin metallic foils were found by trial and error and the final procedure is capable of producing leak-tight structures.

Technical progress

During this reporting period significant progress was made towards the operational readiness of the microturbine test facility. Although original plans included the indoor installation of this test facility, these plans had to be modified as a result of restrictions placed by various organizations within Oak Ridge National Laboratory. After several environmental and safety reviews, the test facility is finally in progress of becoming operational. Figure 1 is a photograph of the modified 60kW Capstone microturbine and its gas compressor in their current outdoor location behind the High Temperature Materials Laboratory at ORNL. Gas and air lines have been installed, and electrical connections are being finalized. Solid-state power electronics in the microturbine will

allow it to operate in grid-connect mode and hence, it will supply electrical power to ORNL.

Progress has also been made in the preparation of test specimens and the validation of the sample holder design. In collaboration with Dr. Michael Santella of the Materials Joining & NDT Group at ORNL, a study was initiated to determine the optimum parameters for laser-welding foil test specimens to sample holders. To date, flat and stamped foils of 347 stainless steel and different Haynes alloys (120, 214, 230) have been laser-welded to sample holders fabricated with the same alloy (to avoid stresses that would result from a possible mismatch in thermal expansion behavior). Figure 2, which is a photograph of a sample holder, shows flat and corrugated foils at locations 1 and 3 of the sample holder, respectively. Visible at locations 2 and 4 are holes that allow the placement of thermocouples next to test specimens to monitor their temperature during the test. Another role of the holes is to allow the passage of air to pressurize the cavity that is formed when a foil test specimen is welded to the sample holder. Dimensions for the sample holder are shown in Figure 3.

Figure 1. Microturbine test facility. On the left is a100 psi gas compressor. On the right is the modified 60kW Capstone microturbine. Next to the microturbine is an exhaust noise suppressor.

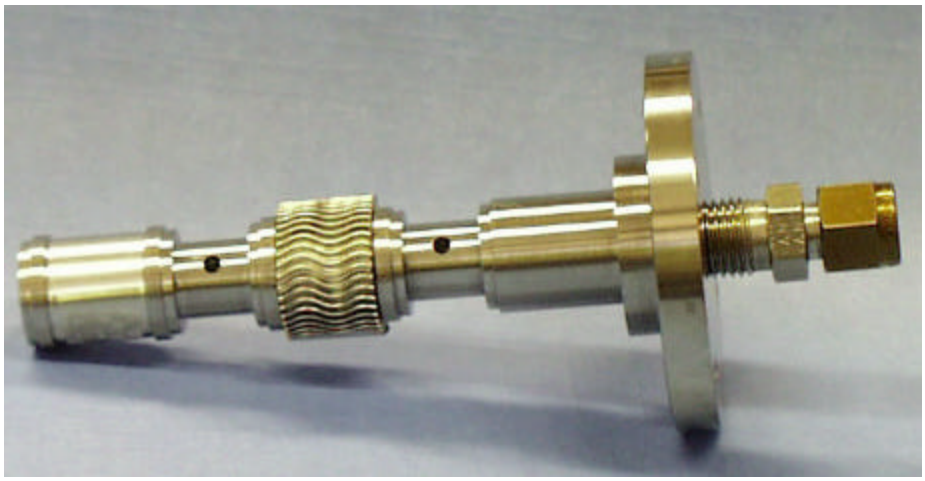

Figure 2. Photograph of sample holder for evaluation of foil test specimens. Note plain and corrugated foil test specimens at locations 1 and 3 of the sample holder.

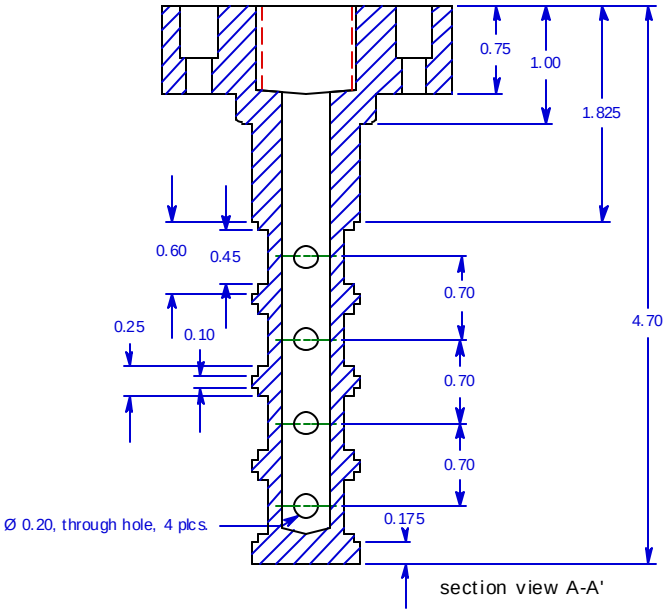

Figure 3. Dimensions of sample holder.

When the sample holder is pressurized, the foil test specimens will be subjected to a multiaxial state of stress that will be dominated by tangential (hoop) stresses. Figure 4 shows the tangential stress distribution obtained by the finite-element method in a section of the sample holder with a foil test specimen. The results presented in Figure 4 correspond to an axisymmetric elastic analysis with symmetric boundary conditions at the bottom of the model and unitary pressure in the cavity formed by the sample holder and the foil. Work is currently under way to extend this analysis by including plasticity and creep deformation. With respect to the results in Figure 4 note that the maximum tangential stress occurs in the unsupported section of the foil and at the location where

the foil test specimen is welded to the sample holder. The magnitude of the maximum tangential stress in the unsupported section of the foil agrees well with the value predicted by a simple strength of materials analysis for a pressurized thin-walled vessel. In this case, the magnitude of the maximum tangential stress is given by the following relation:

$$s_q = P\frac{r}{t} \tag{1}$$

where P is the magnitude of the pressure inside the vessel, r the radius of the cylinder and t the thickness of the wall. For the analysis in Figure 4, the ratio (r/t) is approximately equal to 10.

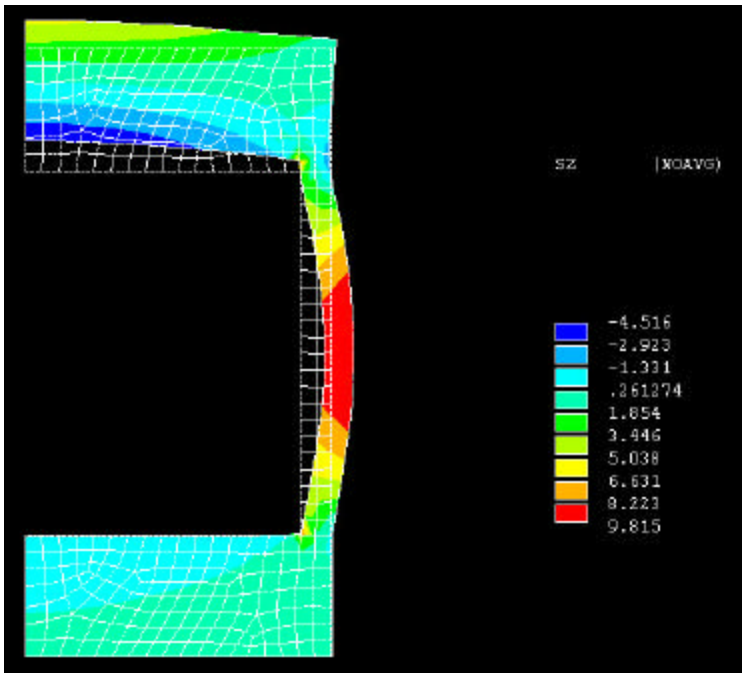

Figure 4. Stress distribution in foil specimen when subjected to internal pressurization.

Status of Milestones

FY 2001 - To acquire a commercially available microturbine, and initiate a testing campaign using a modified recuperator. Met.

Problems Encountered

None.

Publications/Presentations

None.

CERAMIC RELIABILITY FOR MICROTURBINE HOT-SECTION COMPONENTS

Reliability Evaluation of Microturbine Components

H-T Lin, M. K. Ferber, and P. F. Becher
Metals and Ceramics Division
Oak Ridge National Laboratory
P.O. Box 2008, Oak Ridge, TN 37831-6068
Phone: (865) 576-8857, E-mail: linh@ornl.gov

Objective

Evaluate and document the long-term mechanical properties of very small specimens machined from ceramic components (e.g., blades, nozzles, vanes, and rotors) in as processed and after engine testing at ambient and elevated temperatures under various controlled environments. This work will allow microturbine companies to verify mechanical properties of components and apply the generated database in advanced design and lifetime prediction methodologies. The work also provides a critical insight into how the microturbine environments influence the microstructure and chemistry, thus mechanical performance, of materials.

Highlights

A meeting was held between HT Lin (ORNL) and Vimal Pujari (Saint-Gobain) during Cocoa Beach Meeting to discuss the mechanical testing plan for Norton NT154 silicon nitride ceramic. A preliminary testing matrix and the number of billets needed were outlined. Mechanical testing for bend bars with the as-processed and as-machined surface will be carried out. In addition, mechanical testing for other potential silicon nitride materials developed by Saint-Gobain was also discussed. The test matrix proposed for NT154 will be refined based on the operating conditions provided by microturbine companies when the materials are ready for testing.

Technical Progress

Characterization and mechanical testing for Rolls-Royce Allison uncoated SN282 and coated AS800 silicon nitride vanes was completed during this reporting period. Analysis of x-ray diffraction and SEM indicated that the microstructure and intergranular phase composition were stable with time. However, both uncoated SN282 and plasma-sprayed-oxide (PSO) coated AS800 vanes did experience significant material recession. The recession rate appeared to be controlled by temperature and to a minor extent upon the sintering additives. Results also indicated that the experimental Honeywell PSO EBC employed in the present engine tests did not provide an adequate protection (diffusion barrier) from gas turbine environments. Thus, the PSO coated AS800 vanes exhibited similar recession rate and materials degradation to those uncoated AS800 vanes evaluated in the Phase I engine test. Finally the strength measured for biaxial disks machined from the uncoated SN282 airfoil surfaces did not change significantly with time. On the other hand, the strength of samples machined from PSO coated AS800 airfoil surfaces

decreased with an increase in exposure time due to the formation of a very rough surface and/or subsurface damage zone. These observations indicate that the lifetime of the silicon nitride vanes is mostly controlled by dimensional and not mechanical considerations. Therefore, alternative EBC systems need to be explored and developed to inhibit material recession and ensure a long-term stability and performance in gas turbine environments.

Dynamic fatigue tests on commercially available siliconized silicon carbide (Si-SiC) materials were continued during this reporting period. The objective of dynamic fatigue tests is to generate mechanical database for microturbine companies for their component lifetime modeling tasks. Two commercial Si-SiC materials, i.e., CoorsTek SCRB210 and Schunk, were evaluated under this subtask. Dynamic fatigue tests were conducted in four-point bending using 20mm/40mm, α-SiC, semi-articulating fixtures at 1150°C in air. Stressing rates of 30 and 0.003 MPa/s were employed to evaluate the fatigue effect. Load was continuously measured as a function of time, and flexure strength was calculated using ASTM C1161. Mechanical results showed that both CoorsTeck and Schunk Si-SiC materials exhibited little or no strength degradation when tested at 1150°C, as shown in Table 1 and Figs. 1-4). Results also showed that the Weibull modulus obtained was not sensitive to the test temperature. On the other hand, the strength obtained at 0.003 MPa/s for CoorsTek Si-SiC was about 20% higher than that obtained at 30 MPa/s, while the strength of Schunk Si-SiC was not influenced by the stressing rate at 1150°C. The increased strength observed for CoorsTek Si-SiC could be attributed to the softening of Si. The dynamic fatigue results showed that the Schunk Si-SiC exhibited a higher dynamic fatigue exponent (N = 702) than that obtained for the CoorsTek Si-SiC (51) at 1150°C, suggestive of a better slow crack growth (fatigue) resistance, as shown in Figs. 5 and 6. The difference in characteristic strength and Weibull modulus between CoorsTek and Schunk Si-SiC material could arise from the difference in matrix SiC grain size and Si content.

Table 1. Summary of uncensored Weibull strength distributions for CoorsTek and Schunk Si-SiC materials (longitudinally machined) per ASTM C1161.

Material	# of Spmns. Tested	Stressing Rate (MPa/s)	Temp. (°C)	Uncens. Weibull Modulus	± 95% Uncens. Weibull Modulus	Uncens. Chrctstic Strength (MPa)	± 95% Uncens. Chrctstic Strength (MPa)
CoorsTek	20	30	20	13.03	9.13, 17.54	356	343, 369
CoorsTek	20	0.003	20	10.38	7.07, 14.46	329	313, 344
Schunk	20	30	20	8.4	5.76, 11.60	295	278, 312
Schunk	20	0.003	20	7.68	5.21, 10.69	274	257, 291
CoorsTek	20	30	1150	16.64	11.58, 21.83	336	326, 346
CoorsTek	20	0.003	1150	15.05	10.47, 20.48	403	389, 415
Schunk	20	30	1150	10.52	7.35, 14.24	290	277, 304
Schunk	20	0.003	1150	11.37	7.86, 15.56	294	281, 306

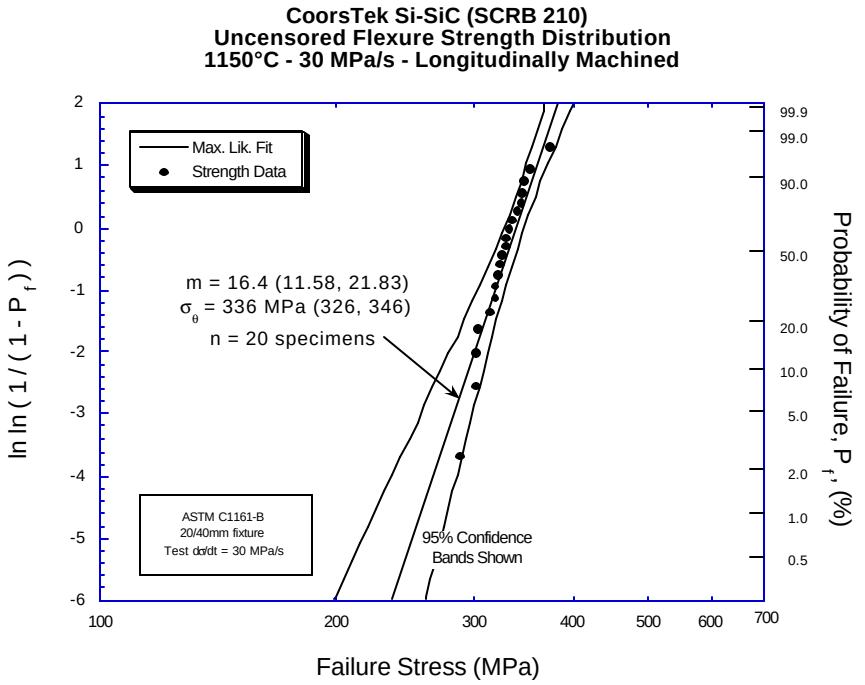

Figure 1. Strength distribution of CoorsTek Si-SiC tested at 1150°C and at 30 MPa/s.

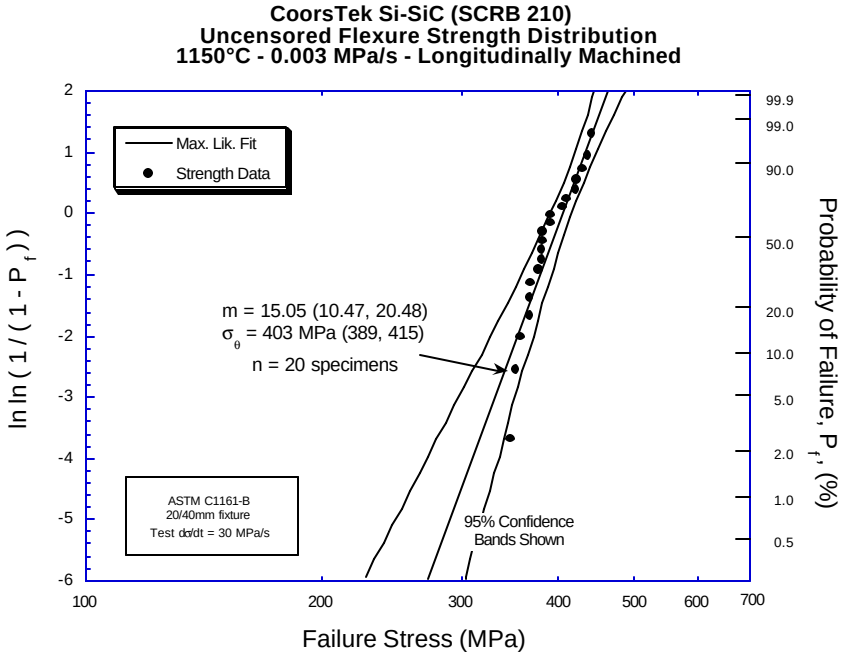

Figure 2. Strength distribution of CoorsTek Si-SiC tested at 1150°C and at 0.003 MPa/s.

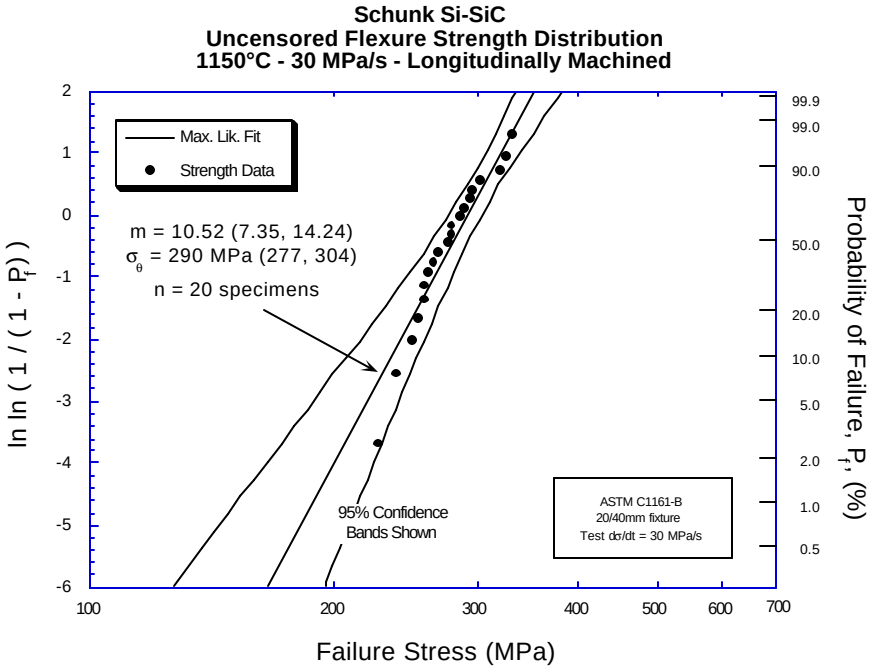

Figure 3. Strength distribution of Schunk Si-SiC tested at 1150°C and at 30 MPa/s.

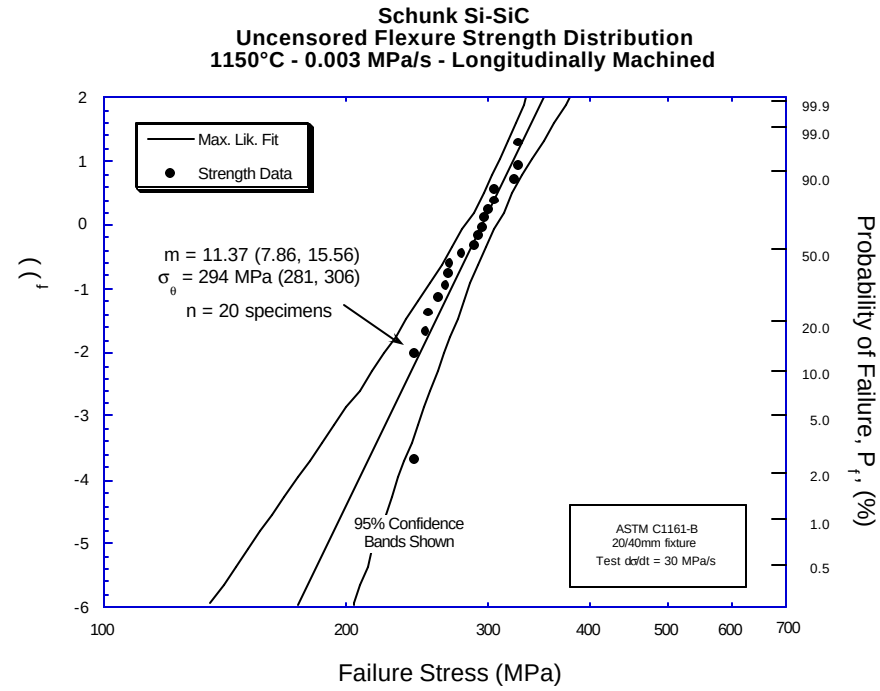

Figure 4. Strength distribution of Schunk Si-SiC tested at 1150°C and at 0.003 MPa/s.

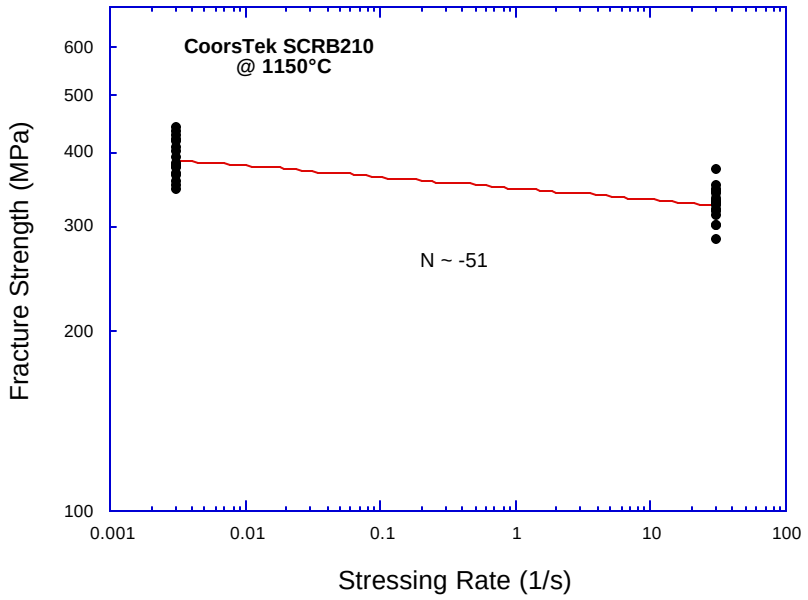

Figure 5. Dynamic fatigue exponent of CoorsTek Si-SiC tested at 1150°C.

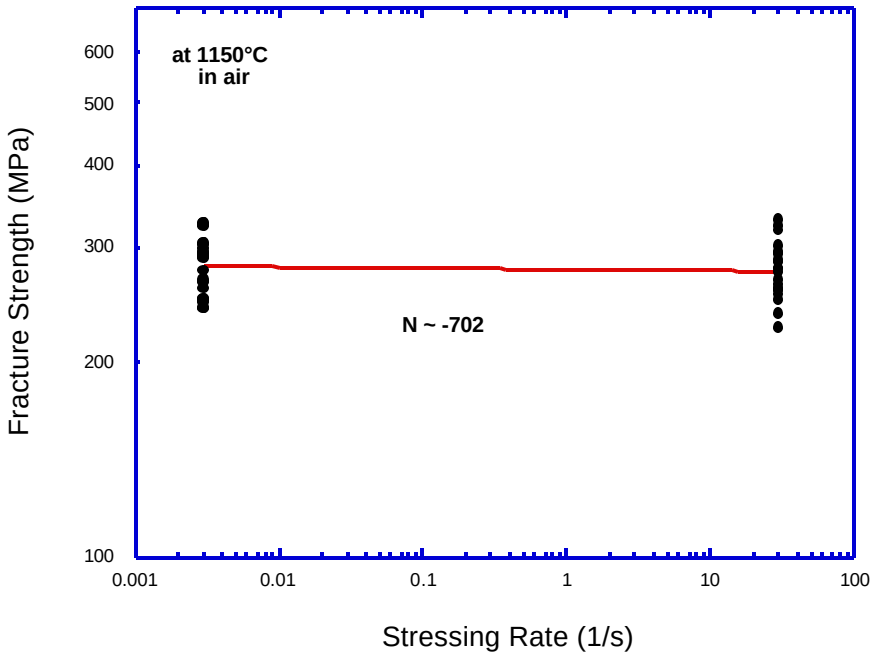

Figure 6. Dynamic fatigue exponent of Schunk Si-SiC tested at 1150°C.

The SASiC MOR bars with and without EBC, which was developed by UTRC, were received from Greg Ojard at UTRC for mechanical property evaluation. The purpose of

this study is to provide an understanding on the effect of EBC system on the mechanical response of the substrates. Preliminary test results at room temperature will be reported in the next quarterly report.

Status of Milestones

Complete characterization of microstructure and mechanical properties for UTRC silicon nitride microturbine components by September 2002. On schedule.

Complete the database generation of commercial Si-SiC materials for microturbine companies' lifetime modeling task by June 2002. On schedule.

Industry Interactions

Communication with John Holowczak at UTRC to discuss the delivery status of the Kyocera SN281 and SN282 microturbine rotors and machining status of the co-processed billets.

Communication with Greg Ojard at UTRC to discuss the mechanical testing status of SASiC bend bars with and without UTRC EBC, and also the test matrix of Kyocera SN282 silicon nitride.

Communication with Josh Kimmel and Mark van Roode at Solar Turbines on the mechanical testing results of SN88 silicon nitride bend bars with EBC.

Communication with David Bath at Kyocera on the test matrix for SN282 silicon nitride manufactured with various green machining parameters.

Communication with Vimal Pujari at Saint-Gobain to discuss the mechanical testing of Norton NT154 silicon nitride materials.

Communication with Russ Yeckley at Kennametal to discuss the mechanical testing of α/β SiAlON materials.

Problems Encountered

None.

Publications

H. T. Lin and M. K. Ferber, "Mechanical Reliability Evaluation of Silicon Nitride Ceramic Components After Exposure in Industrial Gas Turbines," to be published in a special issue of *Journal of European Ceramic Society* for the United Engineering Foundation International Conference on "Structural Ceramics and Ceramic Composites for High-Temperature Application," October 7-12, 2001, Seville, Spain.

Long-Term Testing in Water Vapor Environments

M. K. Ferber, and H-T Lin
Metals and Ceramics Division
Oak Ridge National Laboratory
P.O. Box 2008, Oak Ridge, TN 37831-6068
Phone: (865) 576-0818, E-mail: ferbermk@ornl.gov

Objective

The objective of this project is to develop test facilities for evaluating the influence of high-pressure and high-temperature water vapor upon the long-term mechanical behavior of monolithic ceramics having environmental barrier coatings.

Highlights

The prototype environmental containment system, which was modified to provide for more uniform introduction of steam into the gage section of the button-head tensile specimen, was evaluated. Preliminary tests of an NT154 silicon nitride (manufactured by Saint-Gobain Ceramics & Plastics, Inc., Northboro, MA) indicated that this approach resulted in both localized recession and enhanced oxidation

Technical Progress

The effort this period focused on the design and fabrication of hardware for injecting steam into the hot-zone of existing creep/stress rupture test machines. Based upon previous work, the most effective method involves using either SiC or alumina tubes to inject steam onto the gage section of the tensile specimen (see Figure 1). Based upon preliminary testing, this approach has been extremely effective in simulating recession and enhanced oxidation. For example, Figure 2 illustrates the NT154 specimen after 500h of exposure in a water vapor saturated environment at 1 atm total pressure and 1200°C. The loss of material in the vicinity of the injection tube is indicated by the white line. Scanning electron microscopy (SEM) of the surface in the SiC injection tube contact region (Figure 3) revealed localized attack of the silicon nitride grains. No silica was detected in this region.

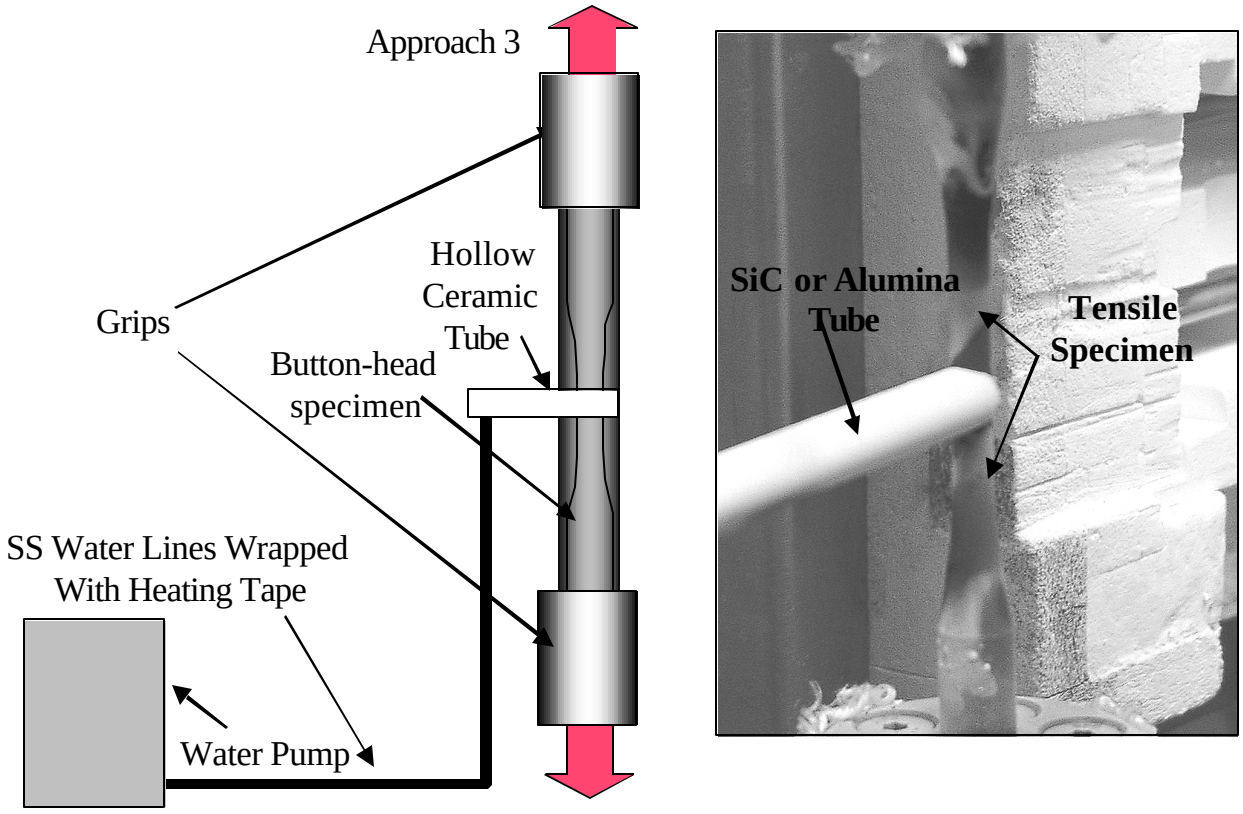

Figure 1: Direct Steam Injection System.

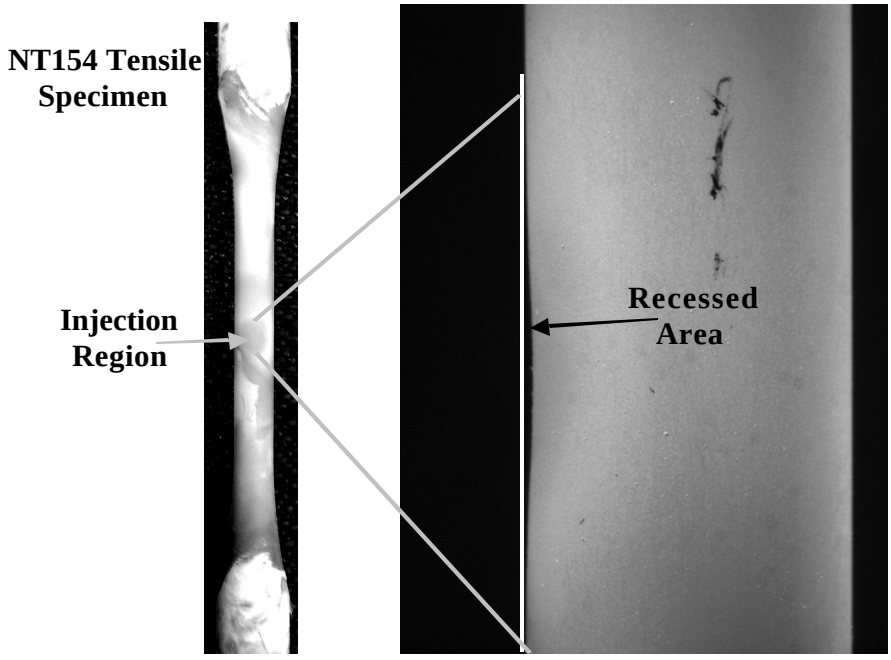

Figure 2: NT154 Tensile Specimen after 500 h Exposure to Saturated Water Vapor Environment at 1200°C.

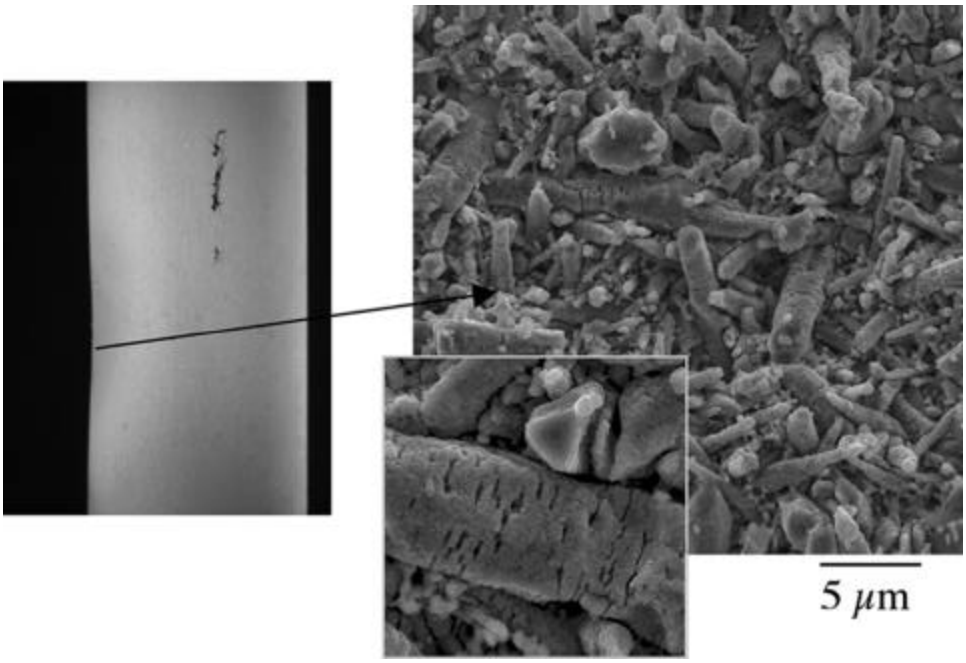

Figure 3: Surface of NT154 Specimen Surface in SiC Tube Contact Region.

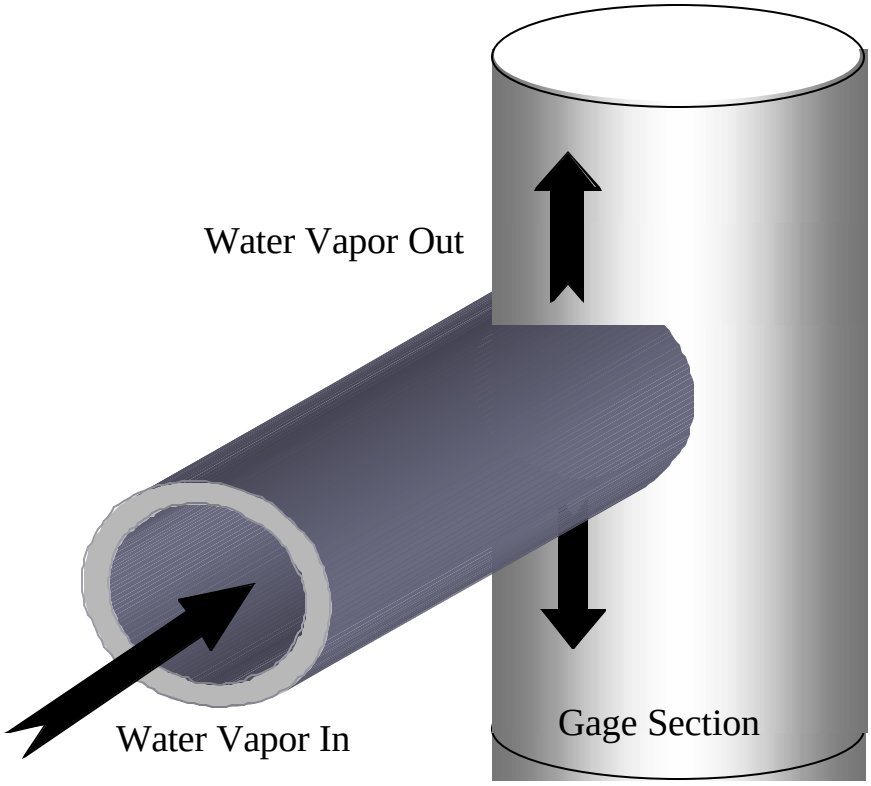

Figure 4: Schematic Illustration of the Water Vapor Flow for the Direct Injection System.

The reason for the relatively high recession may be a result of the higher than expected velocity of the water vapor resulting from the confinement of gas in the small volume of the injection tube and forced

flow through the narrow gap that separates the injection tube from the tensile specimen (Figure 4). For example, in the NT154 test, water at 25°C was introduced into the heated injection system at a rate of 0.1 cc/s. Based upon the density difference between steam at temperature and the water, this rate increases to 673 cc/s. The linear velocity in the injection tube is estimated to be 34 m/s. An even higher velocity is expected as the water vapor is forced to flow through the narrow gap between the gage surface and injection tube.

One can use this information in conjunction with the NASA-Glenn volatility model [1] to calculate the loss of material expected for the NT154 tensile test. For a water vapor pressure was 1 atm, a temperature of 1200°C, and a gas velocity of 34 m/s, the recession is estimated to be 49 µm which is about a factor of 3 lower that the measured value of 126 µm.

Status of Milestones

Milestone 1: Design, fabricate, and evaluate steam containment system for existing creep-stress rupture rigs and issue letter report (April 1, 2001/Delayed 12 months/Completed April 10, 2002).

Milestone 2: Conduct preliminary environmental stability tests on uncoated SN282 and issue letter report (July, 2002/On schedule/ Delayed 4 months).

Milestone 3: Modify 4 test frames to accommodate direct steam injection system (March 2002).

Industry Interactions

Held several discussions with Jim Kesseli of Ingersoll-Rand Energy Systems concerning material availability and database access.

Held discussions with Curt Johnson and Reza Sarrafi-Nour of GE concerning database and future materials testing.

Held extensive discussions with Greg Ojard of UTRC concerning implementation of an ongoing study for EBC development for silicon nitride ceramics.

Problems Encountered

None.

Publications/Presentations

A presentation on ceramics was made by Matt K. Ferber at the Peer Review of the Microturbine and Industrial Gas Turbine Programs, held on March 12-14, 2002 in Fairfax, VA.

Reference

J. L. Smialek, R. C. Robinson, E. J. Opila, D. S. Fox, and N. Jacobson, "SiC and Si_3N_4 Recession due to SiO_2 Scale Volatility Under Combustor Conditions, " *Advanced Composite Materials*, Vol. 8, No. 1, pp. 33-45, (1999).

Reliability Analysis of Microturbine Components

S. F. Duffy, E. H. Baker, and J. L. Palko
Connecticut Reserve Technologies, LLC
2997 Sussex Ct., Stow, OH 44224
Phone: (216) 687-3874, E-mail: sduffy@crtechnologies.com

Objective

The work under this contract is separated into four tasks as outlined below:

Task 1 - Connecticut Reserve Technologies, LLC (CRT) will interface WeibPar, an in-house Weibull parameter estimation software package, with the reliability modules of NASA GRC's CARES/*Life*.

Task 2 - CRT will provide development and design expertise in support of the companies involved in the DoE Microturbine project. CRT will aid design engineers in order to assess the life of micro-turbine ceramic components. This will help to establish life cycle costs. These predictions will be based on the finite element results as well as the material specific information generated from the laboratory tests. The CARES/Life programs will provide the estimates for the component life.

Task 3 – Transient Reliability Analysis will be added to NASA's existing CARES/Life ceramic reliability algorithm software. Work will entail coding the algorithm within the Fortran module and integrating the Fortran modules with a Windows GUI.

Task 4 –Develop a ceramics material reliability database graphical user interface (GUI) for Windows PC computers. Cooperate with ORNL, GRC and UDRI personnel to specify formats and capabilities of a ceramic specimen database for fast-fracture, fatigue, creep, and recession properties of materials. The database should have the ability to integrate with CARES/Life and CARES/Creep life prediction codes.

Highlights

Working with Matt Ferber and Ingersoll Rand to produce a graphical tool to analyze strength at temperature databases relative to a specific structural component.

Technical Progress

Task 1 – The revised scope for this task has been stated above. CRT has a verbal agreement with ORNL to substitute WeibPar as the Weibull parameter estimation software portion of this task. The necessary modifications to the software have been outlined. It has been determined that WeibPar will act as the controlling application. WeibPar will therefore execute CARES/*Life* as a background function. All user input and output to CARES/*Life* will controlled by WeibPar.

Task 2 –CRT provided Ingersoll Rand with the ability to assess baseline failure data at temperature using the pooling techniques provided by the WeibPar algorithm. A spreadsheet was developed that utilizes estimates of the Weibull material scale parameter (as a function of temperature) and the Weibull modulus as well as the size scaling relationship inherent to Weibull analysis. The result is a characteristic strength versus temperature graph where the user can input the characteristic volume or characteristic area of a component. The resulting curve adjusts up or down based on the geometry and load applied to the structural component being analyzed. An example was provided using AS800 material data provided by Matt Ferber at ORNL. This approach provides industry with a graphical screening tool where the design engineer can quickly assess a particular material relative to a specific component. Knowing the maximum stress and use temperature for a given component, the design engineer can see graphically whether the material is worth considering for the design application. This feature will be incorporated in the WeibPar algorithm under the next phase of this contract.

Task 3 – Batdorf reliability routines have been added to the transient reliability module of CARES/*Life*. Example problems are being created to test and demonstrate the transient capabilities. An updated input file structure is being reviewed. Once the input file structure is fixed the Windows GUI will be updated accordingly.

Task 4 – Discussions with Matt Ferber at ORNL has led to structuring material data based on use. The three use categories will be: (1) Structural Ceramics, (2) Thermal Ceramics, and (3) Electrical Ceramics. Each use classification has material properties specific to a design application. This will simplify the data storage format.

Status of Milestones

Milestones are on schedule.

Industry Interactions

See Task 2 progress note above.

Problems Encountered

None.

Publications/Presentations

None.

NDE Technology Development for Microturbines

W. A. Ellingson, E. R. Koehl, A. Parikh, and J. Stainbrook
Argonne National Laboratory
9700 South Cass Avenue
Argonne, IL 60439
Phone: (630) 252-5068, E-mail: ellingson@ornl.gov

Objective

The objective of this project is development of nondestructive evaluation/characterization (NDE/C) technologies for: (1) evaluating low-cost monolithic ceramics for hot section components of microturbines or industrial gas turbines, (2) evaluating environmental barrier coatings (EBCs) for monolithic ceramics or ceramic matrix composites, and (3) evaluating other materials which are part of the technology to advance DER technologies such as ceramic-metal joints. The project is directly coupled to other OPT-DER projects focused on materials developments directed towards low-cost, high volume monolithic ceramics, environmental barrier coating systems and related technologies such as ceramic-metal joining.

Highlights

There are two highlights this period. First, we have set up the new 6-axis articulated robot arm so that NDE methods can be applied to complex shaped vanes and blades. Second, we received the new 80 μm pixel, CMOS-electronic based X-ray detector which will allow very high spatial resolution for small flaw detection.

Technical progress

Technical work this period focused on 3 areas: (1) getting the robot arm set up and software developed so it will accept CAD files of turbine vanes and blades, (2) further developments towards high speed X-ray imaging for low-cost monolithic ceramic materials, and (3) continued work on NDE for EBCs on SiC/SiC composites.

1. Robot Arm

The articulated robot arm is being set up to allow NDE of complicated geometries such as vanes and blades. The major tasks include: path programming the robot, coordinating data acquisition and robot path, computer connection between the robot and a personal computer. Further tasks will include studying resulting data as a function of the part geometry mapping the damage/data onto the 3D part surface.

Robot System:

The system includes ABB's 6 axis articulated robot arm model IRB 140 (M2000), controlled by ABB S4C+ controller with a teach pendant. The path programs for the robot are developed using the offline programming and simulation package RobotSTUDIO from ABB. The Robot Arm is mechanically mounted on an optical worktable. The software allows virtual robot simulation without actually running the commands/programs on the real robot.

Software and Interfacing:

The software used to control the robot includes RobotSTUDIO, an offline programming and simulation software from ABB. The Data Acquisition (DAQ) software being developed is written in LabVIEW so that there is a "user friendly" interface. The procedure we follow is to do simulation of the actual system in RobotSTUDIO, then export the program to the Robot controller's language (RAPID) and port that into the robot's programmable logic controller (PLC). Depending on the task to be accomplished, minor modifications

(add/delete routines, change velocity, etc.) can be added to the robot program in the PC. In our case we interface the robot program to the DAQ program for NDE data acquisition. We must insert a line of code to send signal/data to the serial port of the controller at certain desired positions (start and end of scan lines). This is accomplished because the controller is connected directly to the DAQ computer via a RS-232 serial link cable. The structure of the DAQ program is listed below in Table 1.

Table 1. Procedure for Robot

```
SET the port address for SERIAL PORT
SET the port address for POWER METER
CHECK CONTINUOUSLY for signal from SERIAL PORT
CONTINUOUSLY receive data from the POWER METER
WAIT for START OF LINE signal from robot controller
        START WRITING DATA TO FILE
          IF (SIGNAL FROM CONTROLLER = 0)
                STOP WRITING DATA TO FILE
          ELSE
          CONTINUE WRITING DATA TO FILE
END PROGRAM AFTER SCANNING IS DONE
```

Obtaining Laser Scatter NDE Data:

In order for the robot to be coupled to the NDE laser scatter device to study delams and thickness of EBCs on vane and blades, several software modifications were needed for the DAQ software.

For example, at the end we get a laser-scatter data file containing the detected laser power and then we need to re-set the scan line. For the first test, to test our software, we produced a simple 50 mm square plate (see Fig. 1), and we decided to take 100 data points per line. As part of this we must set the speed of the robot arm to match our requirement of 100 data points. The speed and data points are governed by the response of the power meter. Considering that the spot size of laser beam ~ 1-2 mm, the distance to be scanned ~ 50 mm; number of data points we want in 50 mm is 100, the max readout speed of the power meter is 100 Hz, meaning that in 1 second it can receive 100 data points (maximum). Thus, to receive 100 data points (in 50 mm) takes 1 second. This implies we could set the speed of robot to be 50 mm/s (maximum speed). We also need to take into account the data transfer rates of signal to and from PC/Robot controller.

There are several steps involved when using the robot. These include:

1) Mount the sample on the robot
2) Import the CAD file into RobotSTUDIO (RS).
3) Position and manipulate the robot to match actual orientations.
4) Define tool path and work object in RobotSTUDIO.
5) Make target points on test object by intersecting the surface of interest with a imaginary plane
6) Orient test object surface to keep normal to laser beam
7) Make a path from these targets by chaining them together
8) Repeat steps 5-7 by changing the position of intersecting plane to get a number of paths (scan lines).
9) Export the program from RobotSTUDIO.
10) Edit the program file to insert commands to interrupt data writing to file when it's the end of a line and restart it at the start of a new line.
11) Transfer the robot program to the programmable logic controller (PLC) via FTP from the computer.
12) Start the DAQ program then start the robot control program

As noted earlier, in order to study the robot motion and attempt to acquire our first NDE laser scatter data set, we had a simple 50 mm square flat plate made with 1.6 mm holes drilled at various locations. Figure 1 shows a diagram of the plate.

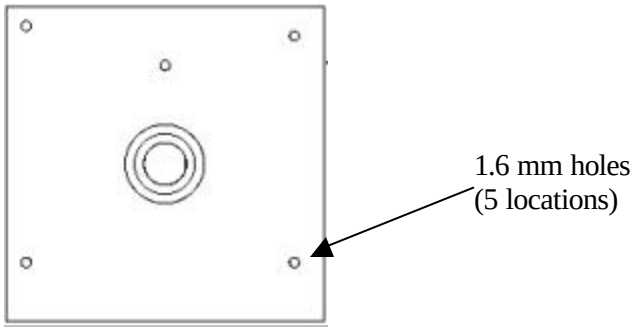

Fig. 1. Robot arm – NDE data acquisition test plate, 50 mm x 50 mm x 12.5 mm

Part of the laser back-scatter NDE effort for EBCs on vanes and blades, concerns the way the laser light is incident upon the sample. Two configurations have been studied: (a) normal incidence, and (b) oblique incidence. For the robot arm to be used, it must be controlled in such a way that the local surface normal is always known. Figure 2 shows schematically this concept. This shows angle-of-incidence scattering but normal incidence with normal reflectance can also be achieved.

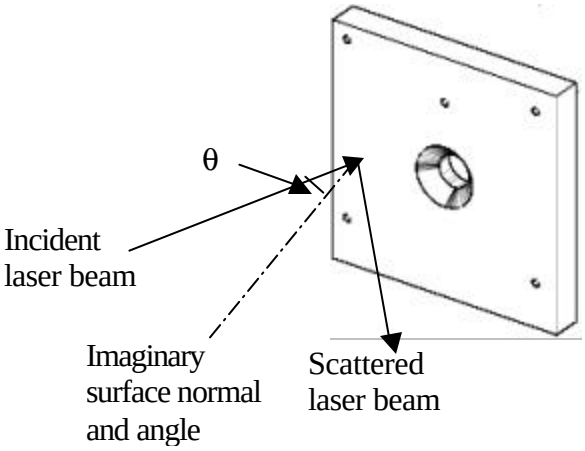

Fig. 2. Schematic diagram of the laser-scatter concept and local surface normal.
The example shown is for angle-of-incidence scattering.

It was noted earlier that for the robot scan data to be acquired, the data are only acquired in one direction. That currently is left to right but can be reversed. Figure 3 shows schematically this idea.

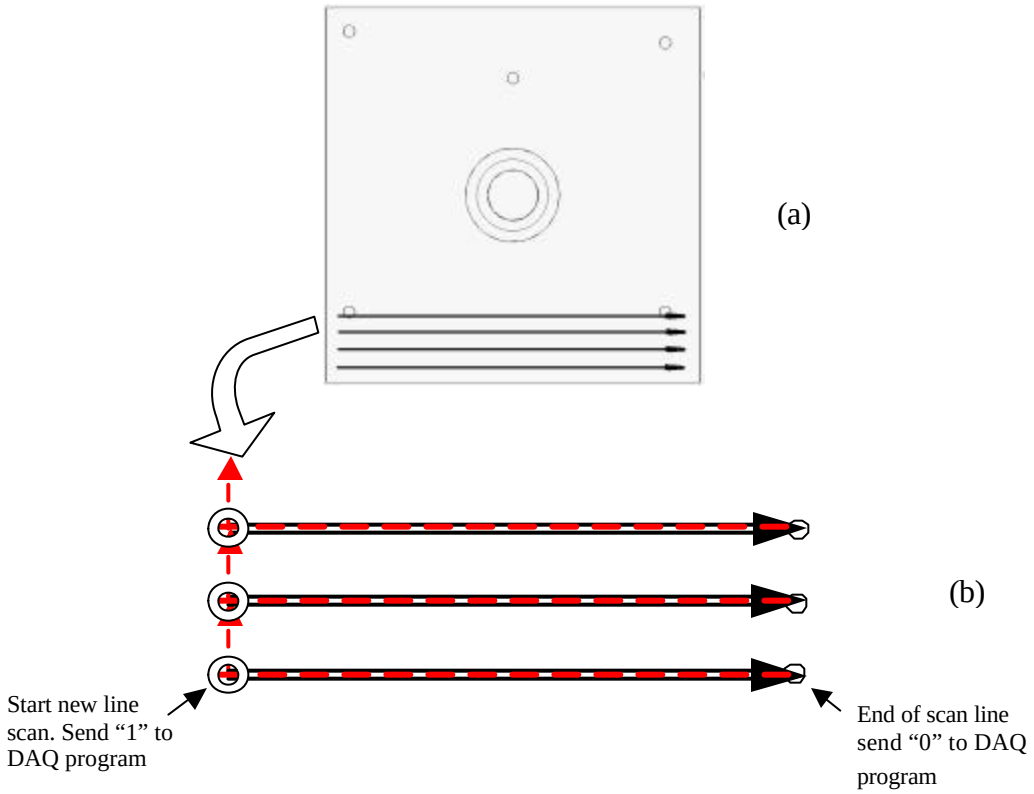

Fig. 3. Schematic diagram showing the left-justified data acquisition scan path from the robot. (a) Schematic of path on object; (b) detail of start-stop of line scan.

2. NDE development for on-line low-cost monolithics

Work this period focused on two areas: (1) initial installation and check out of the new 80 µm CMOS-based electronic X-ray detector, and (2) continued evaluation of the spatial resolution capabilities of the large 40 cm by 40 cm amorphous silicon flat panel detector being used for full scale 3D imaging.

80 µm linear detector

This period we received the new 80-µm square pixel detector from Envision. We interfaced the detector to new software to allow initial images to be acquired. Figure 4 shows a schematic of the set up using lead letters, ANL, for the first image. Shown in Fig. 5 is the resulting first projection image.

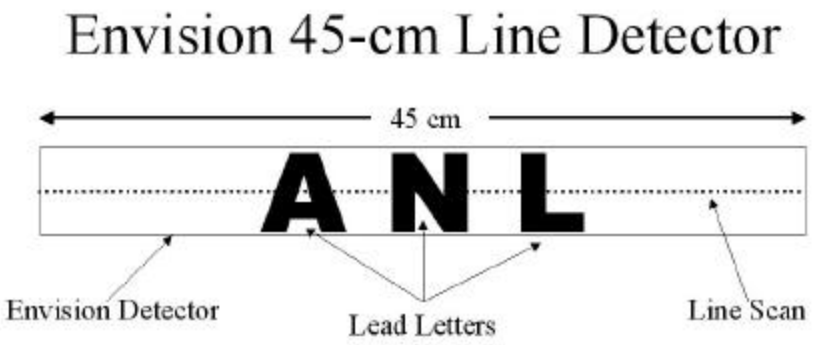

Fig. 4. Schematic diagram showing location of lead letters used for first CMOs X-ray image acquisition.

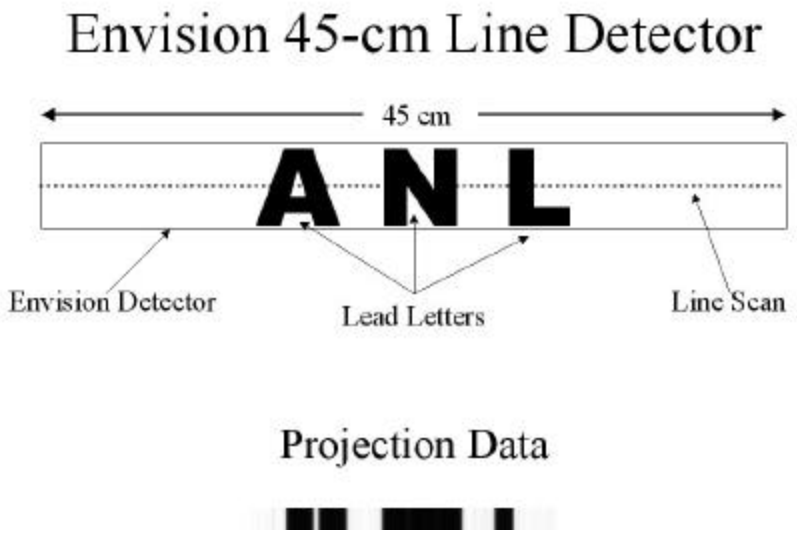

Fig. 5. Schematic diagram and resulting X-ray image taken of section of the letter.

Large Flat Panel for Direct Digital Imaging

We continued this period to evaluate our large flat panel detector in order to evaluate the spatial resolution capability. We began the effort to experimentally determine the detail-detection diagram for the 3D CT scanner. Figure 6 below shows the resulting defect-detection diagram. Note this is for existing 400 µm square pixel detector and the new 200 µm square pixel detector is expected to arrive in July. A new defect-detection diagram will then be generated.

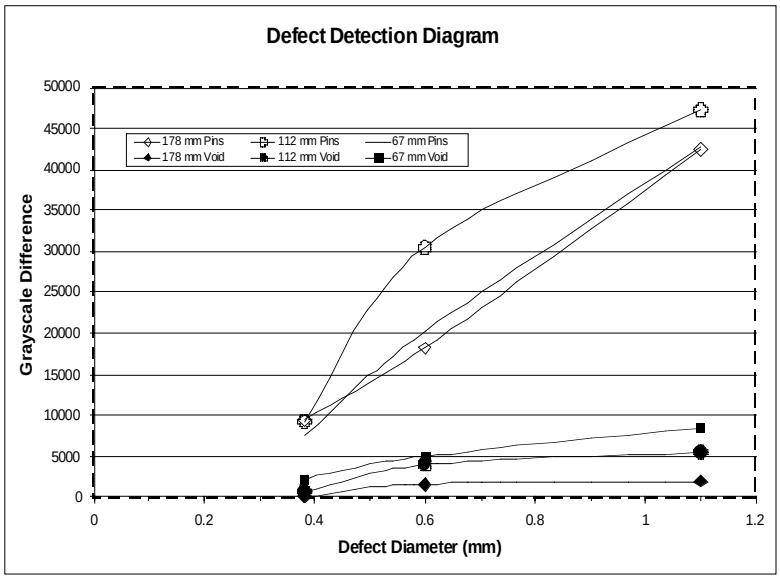

Fig. 6. Defect-detection Diagram for large area (40 cm by 40 cm) flat panel detector with 400 μm pixels and a 200 μm square X-ray source size.

In order to establish the defect-detection diagram, we used three cylindrical discs of different diameters: 67 mm, 112 mm and 178 mm. These were made of gelcast AS800 and were cut from sections of an unbladed rotor. These sections were each about one cm thick. In each disc we drilled three holes using an ultrasonic drilling machine. The three holes were 390 μm, 600 μm and 1.1 mm in diameter. X-ray acquisition tests were conducted with nothing in the drilled holes as well as with stainless steel inserts in the holes. We used two reconstruction algorithms for the reconstructed images from which the measurements were made. One algorithm is called a "parallel" beam code and the other is called a "cone" beam code. These each provide different attributes. Shown below in Fig. 7 is one of the discs used for the defect-detection diagram. It is the middle disc that is 112 mm in diameter. Also shown in Fig. 7 are two of the X-ray computed tomography images for each of the reconstruction algorithms. By using the X-ray CT images as the data sets, a line profile across the features of interest was drawn and the full width-half max (FWHM) values were used to obtain the feature sizes. This kind of analysis was also used to establish the gray scale value. The difference of the gray scale value at this peak was subtracted from the "air" or background value and this difference was then plotted against known feature size as shown in Fig. 7.

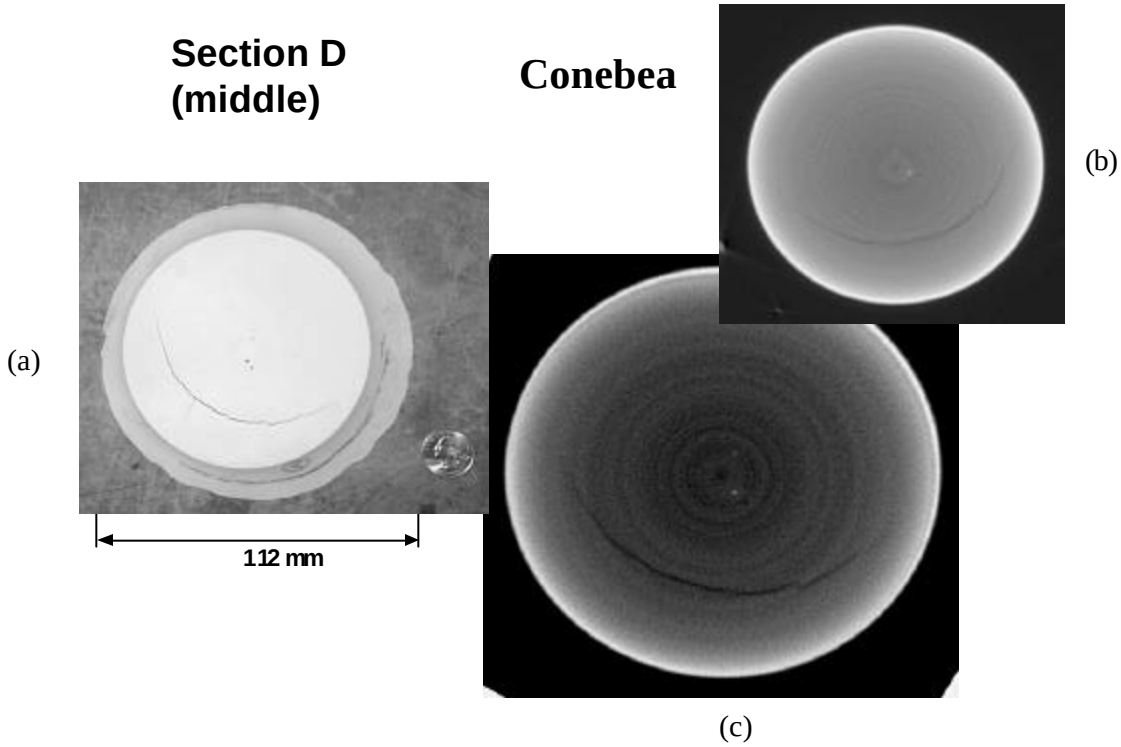

Fig. 7. One of the AS800 discs used for x-ray computed tomography studies for defect-detection diagram. (a) Optical photomicrograph of the disc showing the ultrasonically drilled holes as well as the existence of a natural crack, (b) X-ray computed cross section using the cone beam algorithm, (c) X-ray computed tomography cross section using the parallel beam algorithm

2. NDE development for EBC coated monolithics and Composites
We received additional samples this period of EBC monolithics and the results will be reported next period. We also conducted tests on EBC-CMC. These will be reported next period.

Status of milestones

Milestones are on schedule

Industry/National Lab Interactions

Discussions took place this period with a variety of institutions involved with the efforts of this project.

Discussions were held with Matt Ferber of ORNL relative to the EBC coated vanes from Rolls Royce/Allison

Problems encountered

None.

Publications/Presentations

Two papers were written and submitted to the 46th ASME Gas Turbine and Aeroengine Technical Congress to be held June 3-6 in Amsterdam, The Netherlands.

Trips/Meetings

W. A. Ellingson attended the 26th annual International Conference on Advanced ceramics and Composites sponsored by the American Ceramic Society January 13-18, 2002, in Cocoa Beach, FL.

W. A. Ellingson attended the 26th annual Conference on Composites, materials and Structures sponsored by the United States Advanced Ceramics Association, USACA, The National Institute of Ceramic Engineers, NICE, as well as the US Department of Defense and NASA held January 28-31, 2002, in Cocoa Beach, FL.

W. A. Ellingson participated in the International Conference on Advances in Life Assessment and Optimization of Fossil Power Plants sponsored by the EPRI held March 11-13, 2002, in Orlando, FL.

CHARACTERIZATION OF ADVANCED CERAMICS FOR INDUSTRIAL GAS TURBINE/ MICROTURBINE APPLICATIONS

Oxidation/Corrosion Characterization of Monolithic Si_3N_4 and EBCs

K. L. More and P. F. Tortorelli
Metals and Ceramics Division
Oak Ridge National Laboratory
P. O. Box, Oak Ridge, Tennessee 37831-6064
Phone: (865) 574-7788, E-mail: morekl1@ornl.gov

Objectives

Characterization and corrosion analyses of Si_3N_4 materials provided to ORNL as part of the Hot-Section Materials/Component Development Program

Exposures of candidate Si_3N_4 materials to high water-vapor pressures (in Keiser Rig) to simulate high-temperature, high-pressure environmental effects associated with microturbines

Evaluate the reliability of environmental barrier coatings (EBCs) on silicon nitrides for selected microturbine applications

Highlights

Residual strength measurements were made on three different Honeywell Si_3N_4 materials (uncoated) after exposure in the Keiser Rig for 500, 1000, 1500, and 2000h at 1315°C and 3% or 20% H_2O. After exposure for 2000h at 3% H_2O, there was a loss of ~20% in strength for AS800 Si_3N_4 and no measurable strength loss for AS950 Si_3N_4. As expected, the loss of strength for AS800 Si_3N_4 exposed for 2000h at 20% H_2O was greater than that observed after 2000h at 3% H_2O. After 2000h at 20% H_2O, the AS800 material lost ~33% of its strength. The AS950 appears to be performing somewhat better than the AS800. However, 2000h data at 20% H_2O for AS950 is not yet available for direct comparison with the AS800 data.

Technical Progress

A furnace system that provides a high-temperature, high-pressure, low-flow-velocity (< 0.1 fps) mixed-gas environment (ORNL's Keiser Rig) serves as a means to conduct first-stage evaluations of Si_3N_4 and Si_3N_4+EBC coupons provided by Honeywell Ceramic Components (HCC) in support of hot section materials/component development for microturbines. A summary of the specimen runs conducted in the Keiser Rig for this project was given in a previous quarterly report (DER Quarterly Progress Report for July 1, 2001 – September 30, 2001). Since this report was published, four more runs have been conducted in the Keiser Rig at 1315°C completing 2000h exposure at 3% and 20% H_2O for all three types of Si_3N_4 being evaluated in this study (slipcast AS800, gelcast AS800, and slipcast AS950). Several HCC experimental environmental barrier coatings (EBCs) have also been exposed in the Keiser Rig (DER Quarterly Report for October 1, 2001 – December 31, 2001).

During this quarter, extensive mechanical property evaluations were conducted on uncoated Si_3N_4 after exposure to 3% and 20% H_2O at 1315°C for 500, 1000, 1500, and 2000h in the Keiser Rig. The starting Si_3N_4 specimens were 2.54 cm X 5.08 cm plates with one as-processed surface and one machined surface. The plates are hung from an alumina rod in the Keiser Rig. Enough plates of each of the three Si_3N_4 materials were exposed in the Keiser Rig at 1315°C to finish with three plates of each type of Si_3N_4 exposed at either 3% or 20% H_2O for each of four times of 500, 1000, 1500, 2000h. Four-point bend specimens were machined from each plate after exposure. Three four-point bend specimens were machined from each Si_3N_4 plate for a total of nine four-point bend test specimens at each operating condition and time. The as-processed surface was always on the tensile face during mechanical testing since as-processed surfaces have been shown to have lower oxidation rates than machined surfaces.

A summary of the strength results for all three Si_3N_4 materials exposed at 1315°C and 3% H_2O are shown in Figure 1. Strength loss for each of the AS800 materials exposed was approximately the same after 2000h, 16-17%, whereas no measurable loss was observed after 2000h exposure at 1315°C for the AS950 Si_3N_4 in the Keiser Rig. When the three Si_3N_4 materials were exposed in the Keiser Rig at 1315°C and 20% H_2O, significant strength losses was observed for all the Si_3N_4 materials after exposure. As shown in Figure 2, which summarizes the strength data for Si_3N_4 exposed at 1315°C and 20% H_2O, the gelcast AS800 lost ~33% of its strength after 2000h. The strengths of slipcast AS800 and slipcast AS950 exposed for 2000h at 20% H_2O have not been measured yet, however, after exposure for only 1500h, the strength of the slipcast AS800 decreased by ~35% and the strength of the AS950 decreased by ~20%. At both water-vapor pressures, AS950 had the least amount of strength reduction of the three different Si_3N_4 materials and of the two AS800 compositions, the gelcast material appears to be superior to the slipcast material.

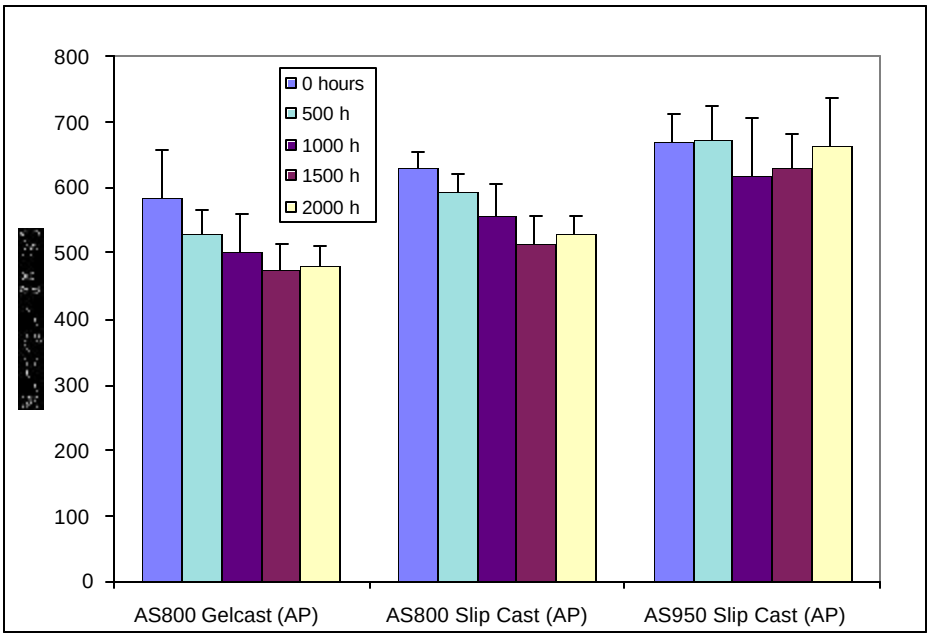

Figure 1. Summary of Si_3N_4 materials exposed for 0-2000h at 1315°C and 3% H_2O in Keiser Rig.

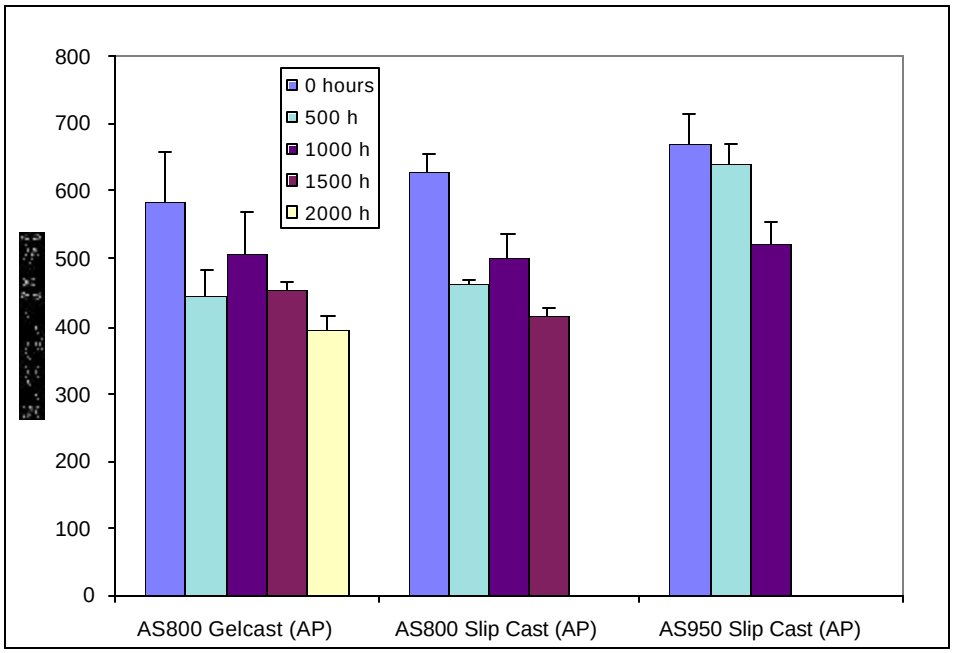

Figure 2. Summary of Si_3N_4 materials exposed for 0-2000h at 1315°C and 20% H_2O in Keiser Rig.

Status of Milestones

08/2001 Complete 2000 h exposures on three different Honeywell Si_3N_4 materials in ORNL's Keiser Rig, characterize microstructural changes, and determine material recession rates. Report results.
Milestone is complete. Results were reported/presented at Honeywell Engines & Systems on March 20, 2002.

Industry Interactions

Attended Workshop on Microturbine Application, January 17-18, 2002, College Park, MD. Discussed ongoing collaborative work with several microturbine industries.

Visited Honeywell Engines & Systems, Phoenix, AZ on March 20, 2002 to discuss current status of silicon nitride microturbine materials work (described herein). Presented results on Keiser Rig exposures of coated and uncoated silicon nitride.

Honeywell Ceramic Components is supplying the silicon nitrides (with and without coatings) for exposures in the Keiser Rig and characterization at ORNL. Collaborations (meetings, conference calls, e-mails) with Honeywell Ceramic Components, Honeywell Corporate Technology, and Honeywell Engines & Systems are ongoing.

Problems Encountered

None.

Publications/Presentations

K. L. More and P. F. Tortorelli, "Current Status of Si_3N_4 Exposures at ORNL," presented during visit to Honeywell Engines & Systems, Phoenix, AZ, March 20, 2002.

Mechanical Characterization of Monolithic Silicon Si_3N_4

R. R. Wills, S. Hilton, and S. Goodrich
University of Dayton Research Institute,
300 College Park, KL-165, Dayton, OH 45469-0162
Phone: (937) 229-4341, E-mail: roger.wills@udri.udayton.edu

Objective

The objective of this project is to work closely with microturbine materials suppliers to characterize monolithic ceramics and provide the data obtained to microturbine manufacturers via the Web site database as well as user-friendly software which will allow perspective users to readily compare different silicon nitrides. This project consists of the following four tasks:

- Task 1: Evaluate Strength and Slow Crack Growth of New Materials
- Task 2: Modify Six Existing Creep Frames to Allow Introduction of Water Vapor
- Task 3: Evaluate the Effects of Water Vapor Upon Honeywell's Silicon Nitride Ceramics
- Task 4: Develop "User Friendly" Software for Searching Existing Mechanical Properties Database

Task 1 is motivated by material needs of both Ingersoll- Rand (IR) Energy Systems and UTRC. The ceramic materials being considered by IR Energy Systems include Kyocera's SN235 and SN237 for which the required mechanical property data are somewhat limited. In the case of the UTRC microturbine, Si-SiC is a prime candidate for the combustor. The goal of Task 2 is to modify existing facilities to evaluate the effects of water vapor upon the strength and creep rupture behavior of both uncoated and coated Si_3N_4 ceramics. In Task 3, the facilities developed in Task 2 will be used to evaluate the mechanical behavior of specimens with and without an environmental barrier coating (EBC).

Highlights

Strength, creep and slow crack growth data were generated for a siliconized silicon carbide (Coorstek SC-2) this reporting period. This material is of interest to UTRC for their microturbine project.

Technical Progress

Rectangular billets and rods of a commercial siliconized silicon carbide were procured. In siliconized (or reaction sintered) SiC, SiC and C mixtures are first formed into shaped compact. This compact is then exposed at high temperatures to molten Si, which infiltrates into the pore structure and reacts with C to form SiC. The resulting material consists of the original SiC grains, newly formed SiC, and residual Si.

Four-point flexure bars having approximate dimensions of 3 by 4 by 50 mm were machined from the

billets. Fast fracture at room temperature is complete. Dynamic stressing rate data collected so far at 1100°C, 1200°C and 1300°C is presented below together with Weibull plots.

Dynamic Fatigue Strength as a Function of Stressing Rate

CoorsTek SC-2

April 2, 2002

Test Temperature (°C)	Stressing Rate (MPa/s)	Specimens Tested	Flexural Strength (MPa)	Standard Deviation (MPa)	Weibull Modulus
20	30	15	415	22	25
1100	30	15	386	8	59
1200	30	15	432	21	25
1300	30	15	402	31	16
20	0.003	0	-	-	-
1100	0.003	12	300	15	-
1200	0.003	15	285	22	17
1300	0.003	6	254	11	-

Four Point Flexure Test Results at 20°C

CoorsTek; SC-2

April 2, 2002

Specimen Number	Stressing Rate (MPa/s)	Load (lbs)	Flexural Strength (MPa)
16	30	117	431
17	30	111	407
18	30	120	440
19	30	112	410
20	30	122	446
21	30	102	376
22	30	115	423
23	30	117	427
24	30	112	409
25	30	116	425
26	30	105	386
27	30	113	415
28	30	117	428
29	30	116	426

30	30	103	376

Four Point Flexure Test Results AT 1100°C

CoorsTek; SC-2

April 2, 2002

Specimen Number	Stressing Rate (MPa/s)	Load (lbs)	Flexural Strength (MPa)
41	30	105	384
42	30	105	387
43	30	100	366
45	30	108	393
46	30	106	387
47	30	104	379
48	30	108	397
50	30	107	391
51	30	104	379
52	30	106	389
53	30	108	397
79	30	106	389
80	30	104	381
82	30	103	377
83	30	107	392
100	0.003	79	289
101	0.003	84	303
102	0.003	84	308
103	0.003	73	265
104	0.003	87	316
105	0.003	86	313
106	0.003	83	303
107	0.003	85	309
108	0.003	84	309
109	0.003	86	312
110	0.003	78	287
111	0.003	80	292

Four Point Flexure Test Results AT 1200°C

CoorsTek; SC-2

April 2, 2002

Specimen Number	Stressing Rate (MPa/s)	Load (lbs)	Flexural Strength (MPa)
34	30	118	432
35	30	106	389
36	30	122	444
54	30	118	432
55	30	119	435
56	30	126	461
57	30	111	405
58	30	126	462
59	30	114	416
60	30	112	409
61	30	125	458
62	30	121	442
63	30	117	426
64	30	121	439
65	30	120	436
89	0.003	84	305
90	0.003	75	272
91	0.003	73	265
92	0.003	80	290
93	0.003	80	288
95	0.003	81	294
96	0.003	74	270
97	0.003	78	284
98	0.003	77	282
99	0.003	76	280
115	0.003	85	310
116	0.003	83	302
118	0.003	62	226
119	0.003	87	317
120	0.003	80	294

Four Point Flexure Test Results AT 1300°C

CoorsTek; SC-2

April 2, 2002

Specimen Number	Stressing Rate (MPa/s)	Load (lbs)	Flexural Strength (MPa)
37	30	115	421
39	30	97	354
66	30	119	436
67	30	117	427
68	30	102	371
69	30	120	438
70	30	116	424
71	30	101	372
72	30	105	385
73	30	121	444
74	30	115	419
75	30	105	382
76	30	112	409
77	30	107	393
78	30	97	355
84	0.003	70	253
85	0.003	75	272
86	0.003	65	238
87	0.003	69	252
88	0.003	68	248
121	0.003	71	259

Weibull Modulus	25.2	RWMT	0.0396	WCS	424
Average Strength	415	Std. Dev.	22	BO	-153
Median Strength	418				

15 Specimens

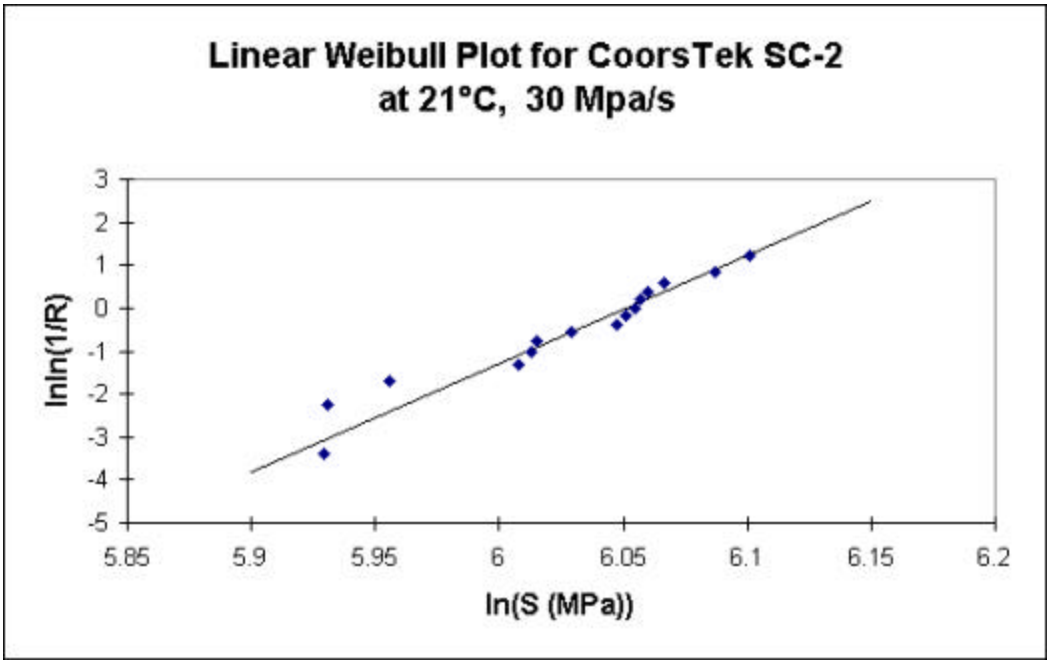

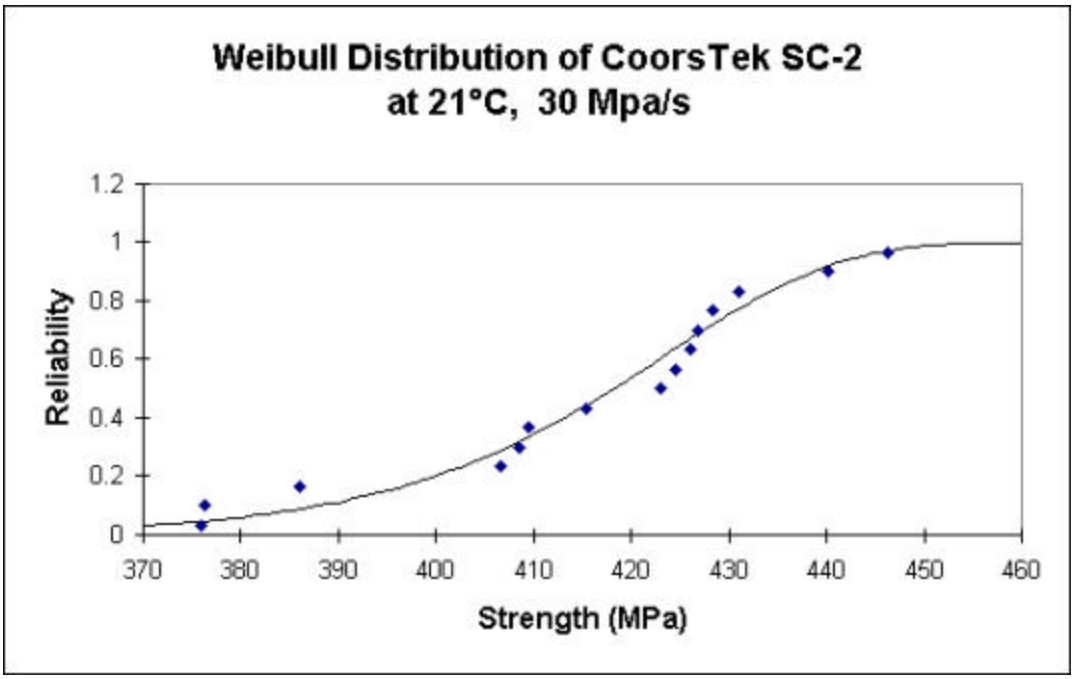

Weibull Modulus	59.0	RWMT	0.0170	WCS	389
Average Strength	386	Std. Dev.	8	BO	-352
Median Strength	387				

15 Specimens

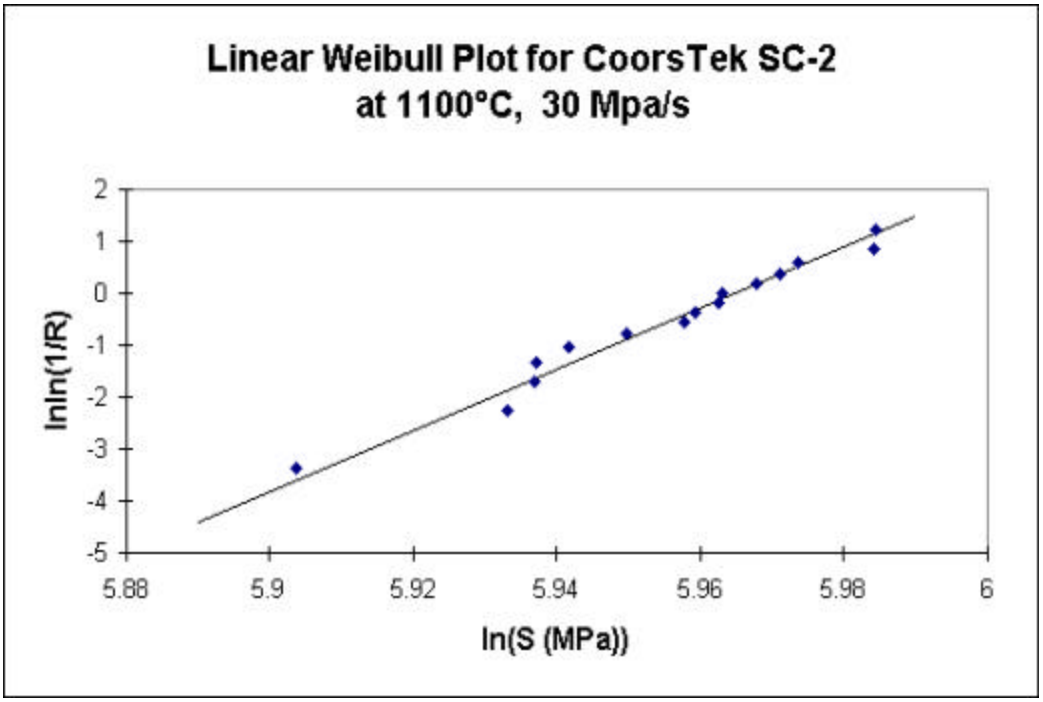

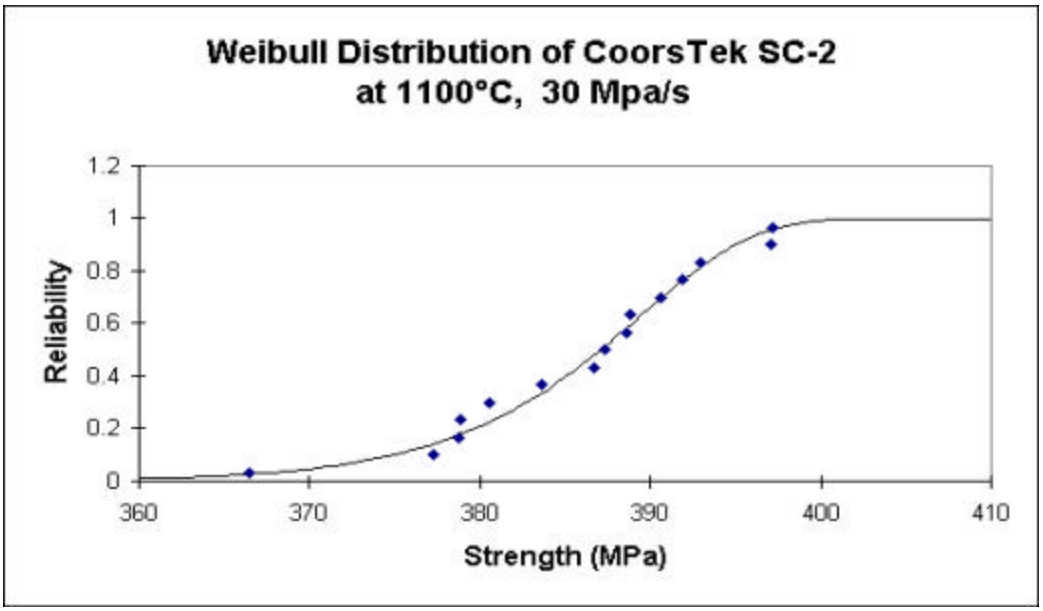

Weibull Modulus	25.1	RWMT	0.0398	WCS	442
Average Strength	432	Std. Dev.	21	BO	-153
Median Strength	435				

15 Specimens

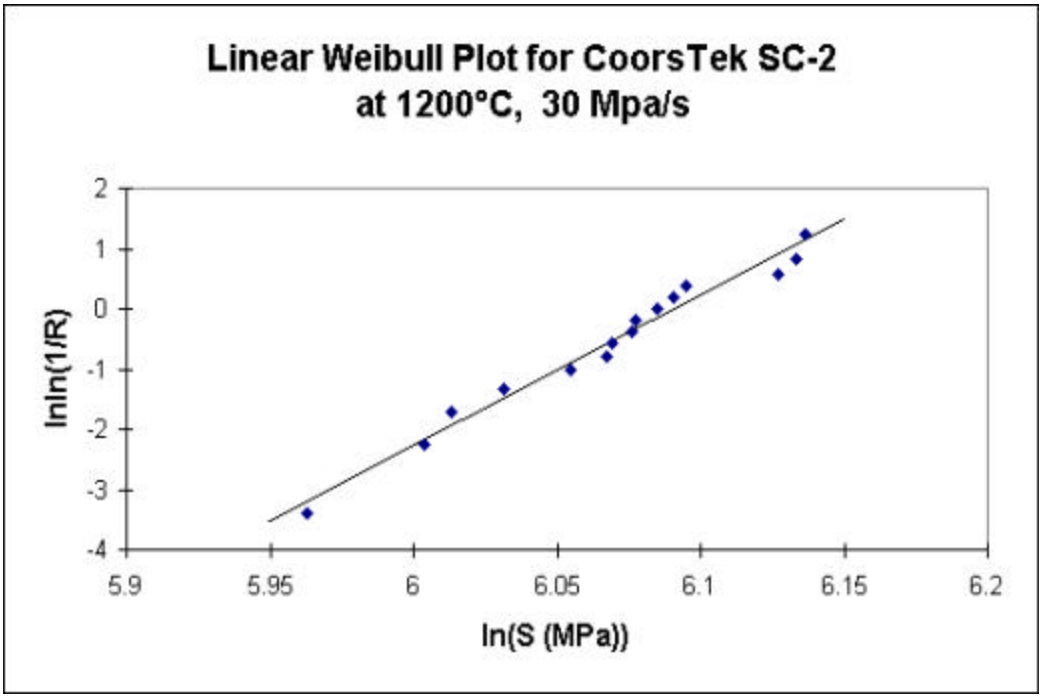

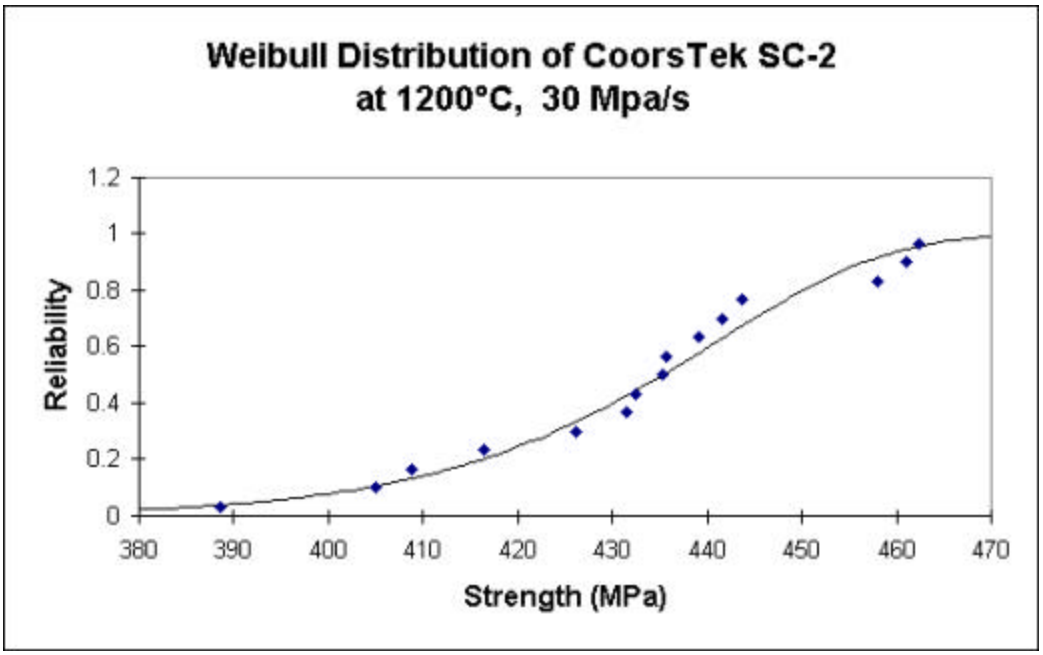

Weibull Modulus	17.4	RWMT	0.0575	WCS	294
Average Strength	285	Std. Dev.	22	BO	-99
Median Strength	288				

15 Specimens

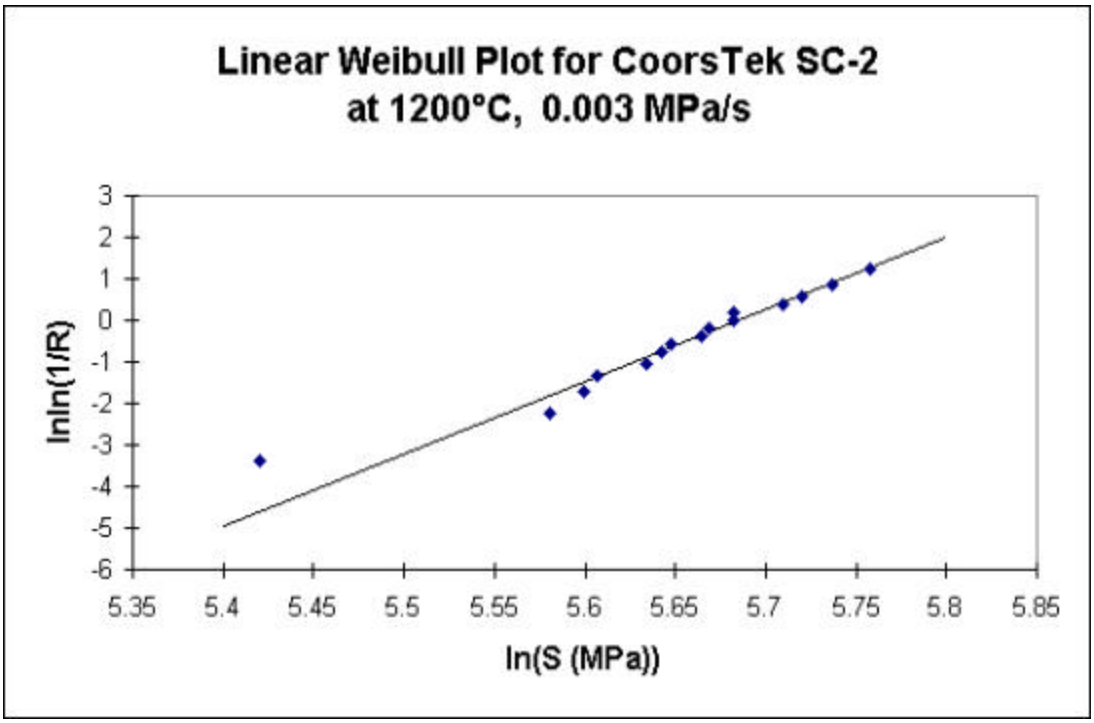

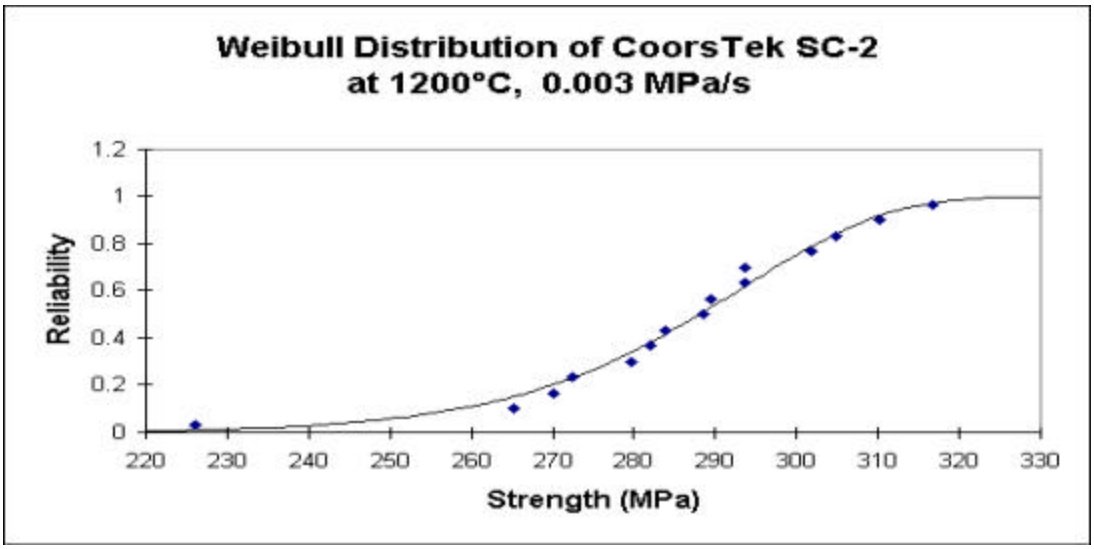

Weibull Modulus	16.3	RWMT	0.0615	WCS	416
Average Strength	402	Std. Dev.	31	BO	-98
Median Strength	406				

15 Specimens

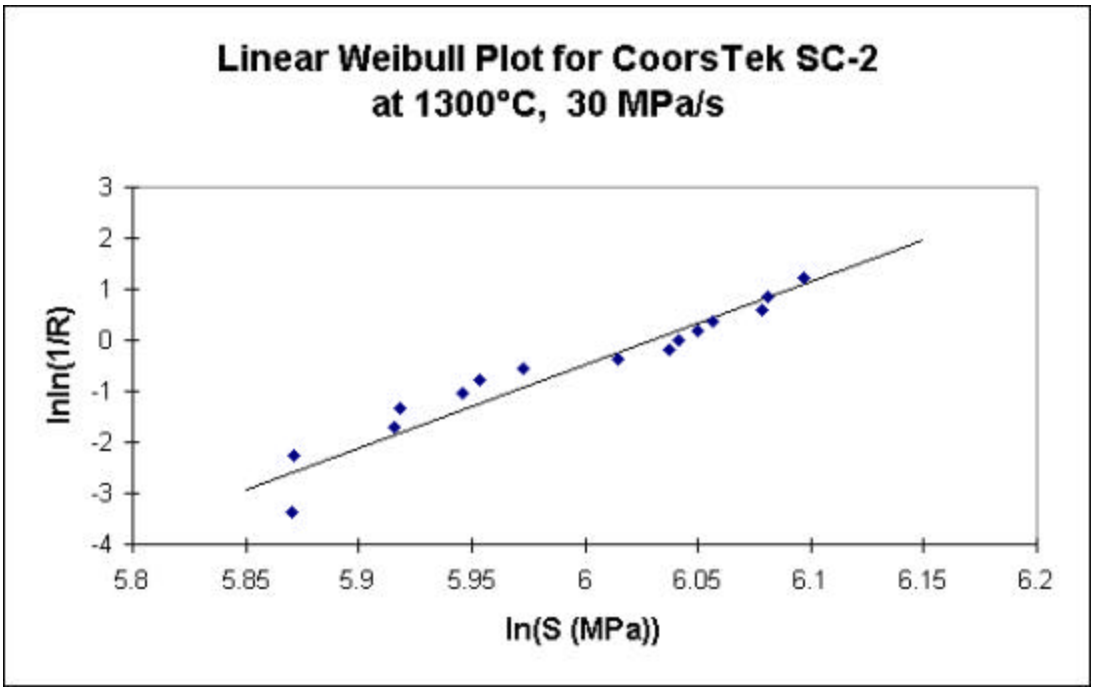

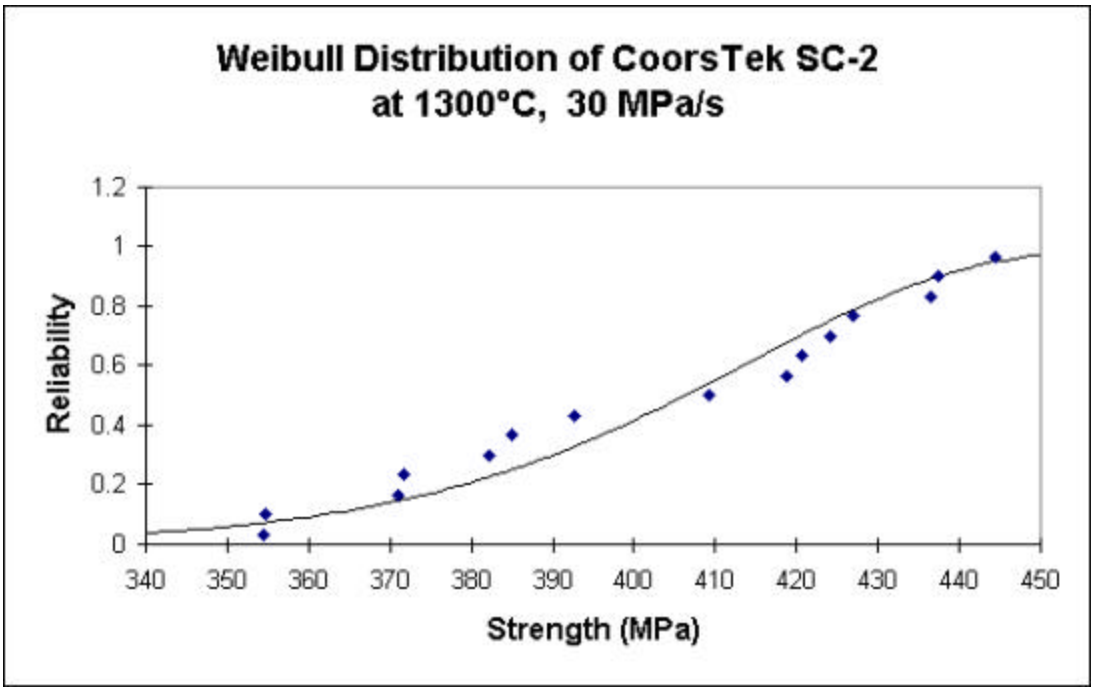

The tensile creep data collected so far are shown below:

Specimen Number	Applied Stress (Mpa)	Temp (°C)	Result
2	260	1100	Failed while loading
1	200	1100	Failed at 3mins
9	150	1100	Failed at 0.5hrs
8	100	1100	Failed at 22.5hrs
3	8	1100	Failed at 116.5 hrs
14	75	1100	Test stopped at 625.5hrs
12	75	1200	Still running 354 hrs

Status of Milestones

(a) Complete modification of six creep rupture frames to accommodate testing in water vapor and complete validation tests (Due August 1, 2001/Completed).

(b) Complete test matrix for Honeywell Ceramic Components and issue letter report (Due September 2002. No samples have been received yet. This milestone may have to be modified given the uncertainty concerning the availability of the Honeywell material.

Industry Interactions

Attended the Peer Review Meeting, March 12-14 in Fairfax, Virginia. Interacted with numerous researchers from GE, UTRC, St.Gobain, Kennametal, Precision Combustion, Ingersoll Rand, Caterpillar, Oak Ridge National Laboratory and the University of Connecticut.

The Ohio Department of Development is responsible for the Microturbine program in Ohio. Two Capstone Microturbines are being installed in the Canton school district. Microturbines are also operating at Wright Patterson Air Force Base and at Dayton Power and Light. There are probably others but no list exists for those operated by the Utility Companies.

Problems Encountered

None.

Publications/Presentations

None.

Microstructural Characterization of CFCCs and Protective Coatings

K. L. More
Metals and Ceramics Division
Oak Ridge National Laboratory
P.O. Box 2008, Oak Ridge, Tennessee 37831-6064
Phone: (865) 574-7788, E-mail: koz@ornl.gov

Objective

Characterization of CFCC materials and CFCC combustor liners after exposure to simulated (ORNL's Keiser Rig) and actual (engine tests) combustion environments

Exposures of candidate environmental barrier coatings (EBCs) to high water-vapor pressures (in Keiser Rig) to determine thermal stability and protective ability

Work with CFCC and coating suppliers/manufacturers to evaluate new/improved ceramic fibers, protective coatings, and composite materials

Highlights

Inner and outer CFCC/EBC combustor liners were removed from a Solar Turbines Centaur 50S SoLoNOx engine running at the Chevron test site in Bakersfield, CA after 13,937 h when a hole was observed in the inner liner during a routine borescope inspection. The liners were visually inspected by all the program collaborators after removal from the engine in order to decide how and where the liners would be sectioned following NDE evaluation at Argonne National Laboratory. ORNL received 8 large sections from each liner that were then cut into smaller sections and distributed to the other program participants for evaluation. ORNL's primary role was to lead the microstructural and mechanical characterization of the CFCCs and EBCs comprising each liner after engine testing for 13,937 h. The results from the characterization of the liners after engine testing were compared to results obtained from similarly-processed CFCC/EBCs exposed in the Keiser Rig. In previous quarterly reports, characterization results from Keiser Rig exposures of the EBC/CFCCs were summarized (January 1, 2001 – March 31, 2001) and results from the evaluation of the engine-exposed inner liner were presented (October 1, 2001 – December 31, 2001), In the current report, results from the evaluation of the engine-exposed outer liner will be presented.

Technical Progress

The outer CFCC combustor liner (30" diameter) used in the recent Chevron engine test (13,937 h engine test #5) was a liner produced by the chemical vapor infiltration (CVI) process and was manufactured by GE Power Systems Composites, Inc. The outer liner had an experimental EBC on the working surface, which will be referred to as the "mixed" layer EBC. This EBC was initially developed under the EPM Program and has been optimized by United Technologies Research Center (UTRC) for use on CFCC liners used in the Centaur 50S engine. An SEM image of the layered EBC structure used on the outer

liner in the engine test is shown in Fig. 1 and consists of a ~125 μm plasma sprayed Si layer (bond-coat), an ~125 μm plasma-sprayed mullite+BSAS mixed layer (intermediate layer), and a ~125 μm $Ba_{0.75}Sr_{0.25}Al_2Si_2O_8$ (BSAS) surface layer (top-coat). Mixed-layer EBCs, which were shown to be superior (protective) coatings compared to dual-layer EBCs after long-term Keiser Rig exposures, were used on both inner and outer liners for engine tests at the Malden Mills facility in Malden, MA.

In order to characterize the different types of damage present on the working surface of the outer liner after engine testing and to evaluate the effect of the damage on the mechanical properties, 1" wide strips (aft to fore length was 8") were cut from the liner within the different areas of observed surface degradation. Figure 2 is a photo series compiled to show the full working surface of the outer liner after 13,937 h engine exposure. Typical strips cut from the outer liner (strips are outlined in Figure 2) are shown in detail in Figure 3(a-c) and include (a) areas showing minimal EBC damage, (b) localized EBC loss associated with an injector impingement area, and (c) area showing patterned pinhole damage. There were areas where the EBC seemed completely intact on the surface of each of these strips.

Eight 1" sections were cut from each 8" long strip such that changes in the microstructure from the aft to fore end of each strip could be characterized in cross-section. Figures 4(a) and 4(b) show SEM cross-section images comparing the EBC on the outer liner from the aft end (cooler region) to an area from the center of the liner where the EBC appeared to be intact, respectively. A significant loss (~65%) of the BSAS top layer thickness was observed in this particular center section (from a strip similar to that shown in Figure 3(a) compared with the original thickness of the BSAS (Figure 4(a). In areas associated with fuel injector impingement in the center (aft to fore) of the liner (see Figure 3(b), full recession of the EBC layers was locally observed. The fuel injector impingement areas are usually associated with higher temperatures (>1200°C) and/or somewhat higher gas velocities. The dark area shown on the strip in Figure 3(b) is indicative of complete EBC loss such that the CVD SiC seal coat is exposed. However, this loss is due to BSAS recession, not EBC spallation. Volatilization of BSAS appears to be a dominant mechanism contributing to loss/recession of the top coat with time at temperatures ~1200°C. Similar observations were made on the BSAS top coat on the inner liner (see DER Materials quarterly report for October 1, 2001 – December 31, 2001), BSAS volatilization is relatively slow at these temperatures (at least compared with the volatilization of silica during the oxidation of Si-based materials such as CVD SiC and the underlying SiC/SiC CFCC in similar combustion environments) but is clearly a problem when considering pushing CFCC liner lifetimes to >25,000 h. Unfortunately, measuring the recession rates for BSAS after these engine tests is a difficult problem. Accurate temperature measurements on the liner surfaces during engine use are extremely difficult to measure, thus, associating a measured top coat "loss" with a temperature is not possible. Long-term exposures in a laboratory rig would be beneficial, however, actual burner-rig tests have traditionally been run for short times, usually 100-200 h, which is not long enough to start measurable recession of the BSAS top coat. Recession of BSAS has not been observed during long-term testing in the ORNL Keiser Rig because of the very low gas velocity in this rig (at least two orders of magnitude less than that in a combustion chamber). Thus, several questions still remain unanswered (more data from engine tests is required): (1) What are the volatilization mechanisms for BSAS? (2) What is the volatilization/recession rate for BSAS? (3) At what temperature does BSAS volatilization start? (4) Can the BSAS be stabilized (compositionally) for use in combustion environments?

As shown in Figure 3(c), a regular pattern of "pinhole" defects was observed on the working surfaces of both the inner and outer liners, but was especially prevalent across most of the surface of the outer liner. These defects were initially observed during borescope inspections in the early stages of the engine test and increased in number and severity as the engine test progressed. The spacing of the majority of the defects on the outer liner corresponded directly with the tooling used during the CVI processing of the outer liner. The pattern of "tool bumps" are always observed on the surface of as-processed CVI-produced CFCCs and are caused initially by the slight localized pulling or raising of the wound fibrous preform (usually a single fiber tow) during CVI. The tool bumps on the surface of the liner are still evident following the application of the CVD SiC seal coat, as shown in Figure 5. The surface asperities at this stage usually measure ~0.2-0.25mm in height. After application of the EBC, the surface asperities are still present on the surface of the as-processed EBC/CVI-CFCC. A cross-section directly through a typical tool bump shows that in the majority of cases, the asperity results in the formation of a through-thickness crack in the EBC, as shown in Figure 6. Clearly, a through-thickness crack in the EBC will lead to localized accelerated oxidation of the Si bond coat below the surface. In fact, rapid oxidation of the constituents below the surface caused these localized areas to oxidize at rates approaching those of the uncoated CFCCs and severely limited the lifetime of the liner. Figure 7 shows a tool bump area from a relatively cool section (fore end) of the outer liner. In this case, the formation of excessive SiO_2 just below the EBC nearly resulted in the spallation of the EBC. Oxidation did not progress through the CVD SiC seal coat and into the CFCC. However, in much hotter areas near the center of the outer liner, pinholes formed when the rapid oxidation progressed down through the Si bond coat, the CVD SiC, and well into the CFCC, as shown in Figure 8. In several cases, localized loss of the entire liner thickness resulted from the accelerated oxidation associated with the tool bumps.

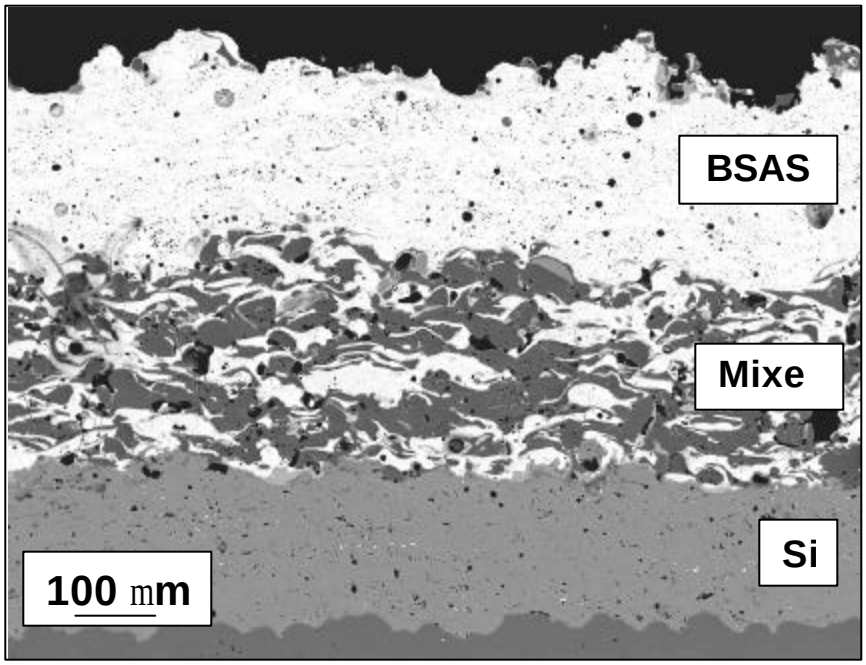

Figure 1. SEM image of the mixed-layer EBC used on the outer liner for the 13,937 h engine test.

Figure 2. A series of compiled images showing the entire working surface of the outer liner after 13,937 h engine test.

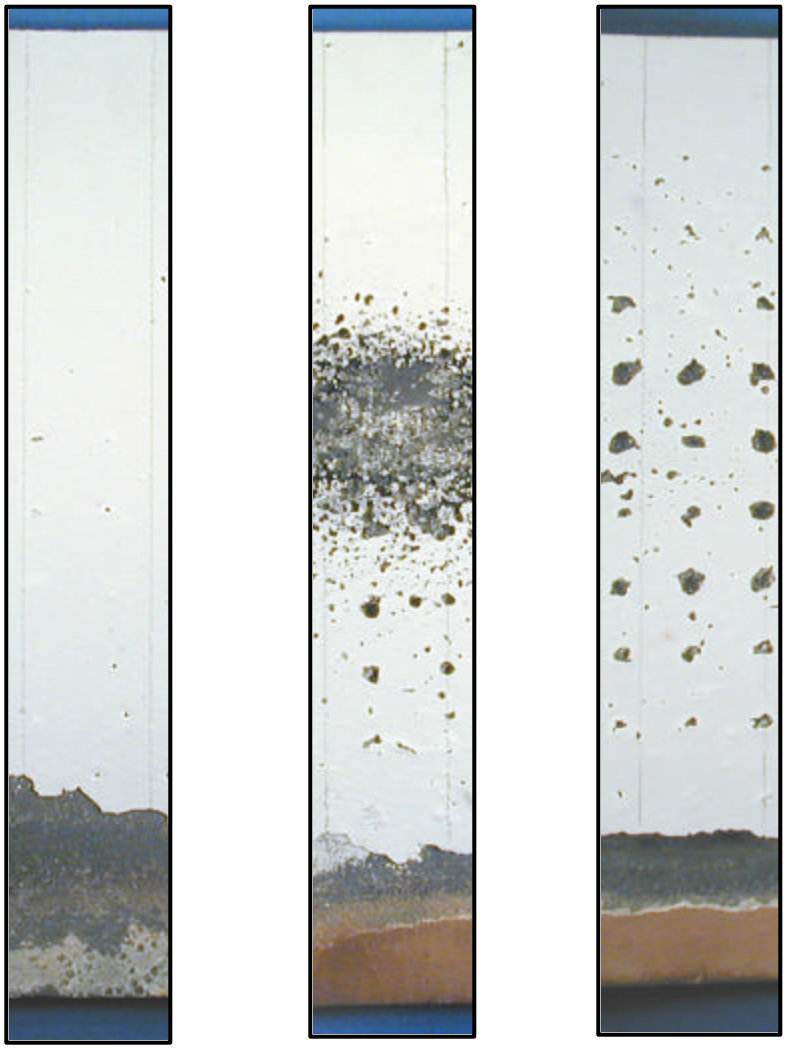

(a) (b) (c)

Figure 3. Typical strips (aft to fore) cut from different damaged areas of outer liner after 13,937 h engine test: (a) little observed EBC damage, (b) fuel injector impingement area, and (c) patterned pinhole damage.

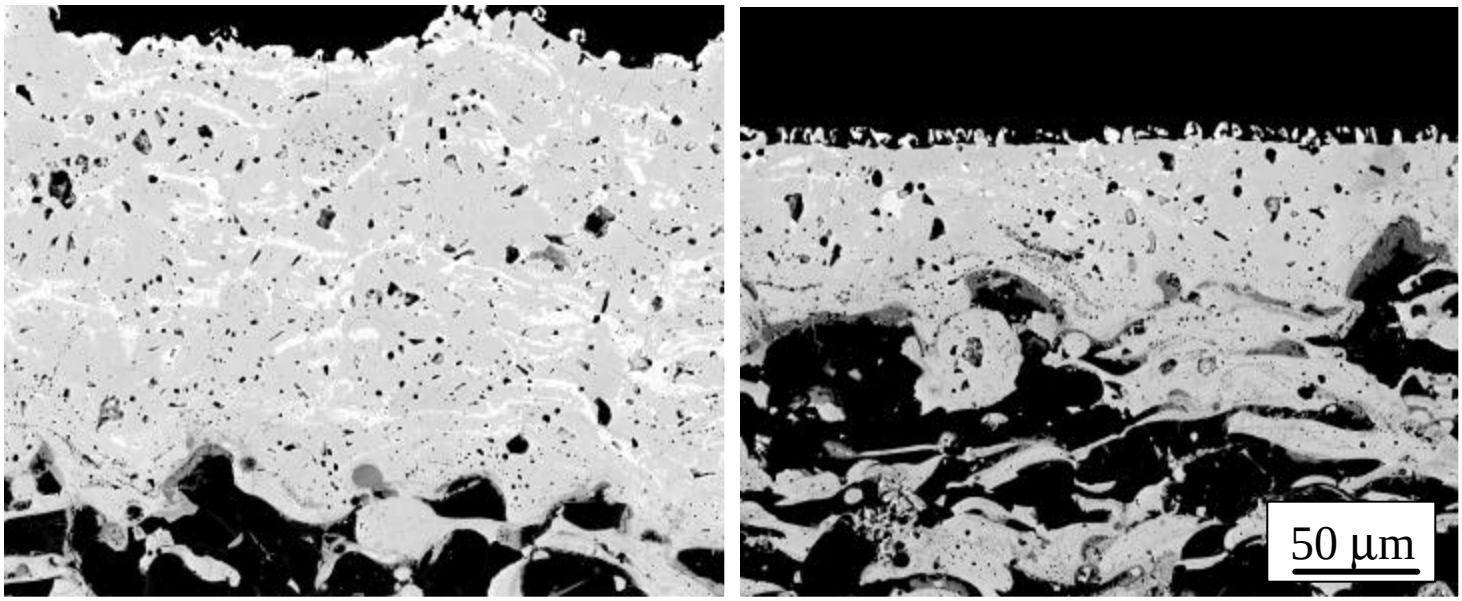

(a) (b)

Figure 4. SEM image of EBC from (a) aft end of outer liner and (b) center of outer liner showing BSAS recession.

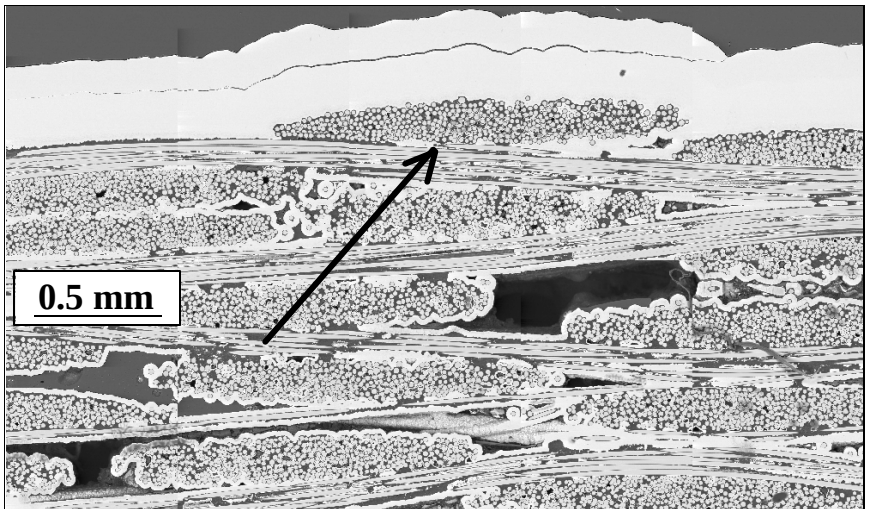

Figure 5. SEM cross-section image through a tool bump before EBC has been applied.

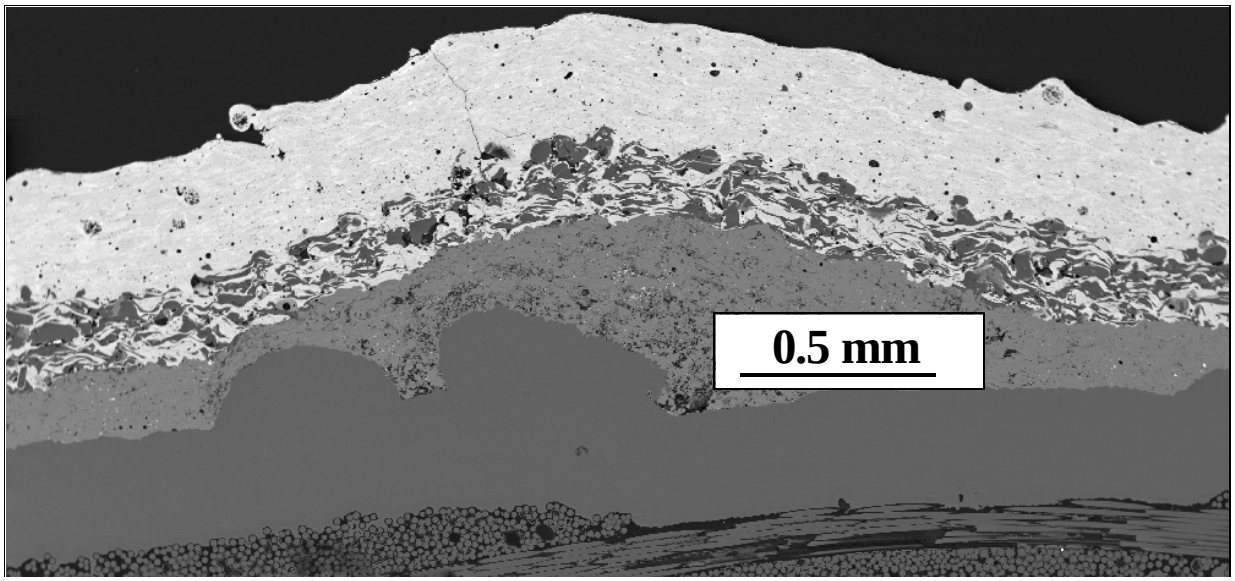

Figure 6. Through-thickness crack in the as-processed EBC associated with a tool bump.

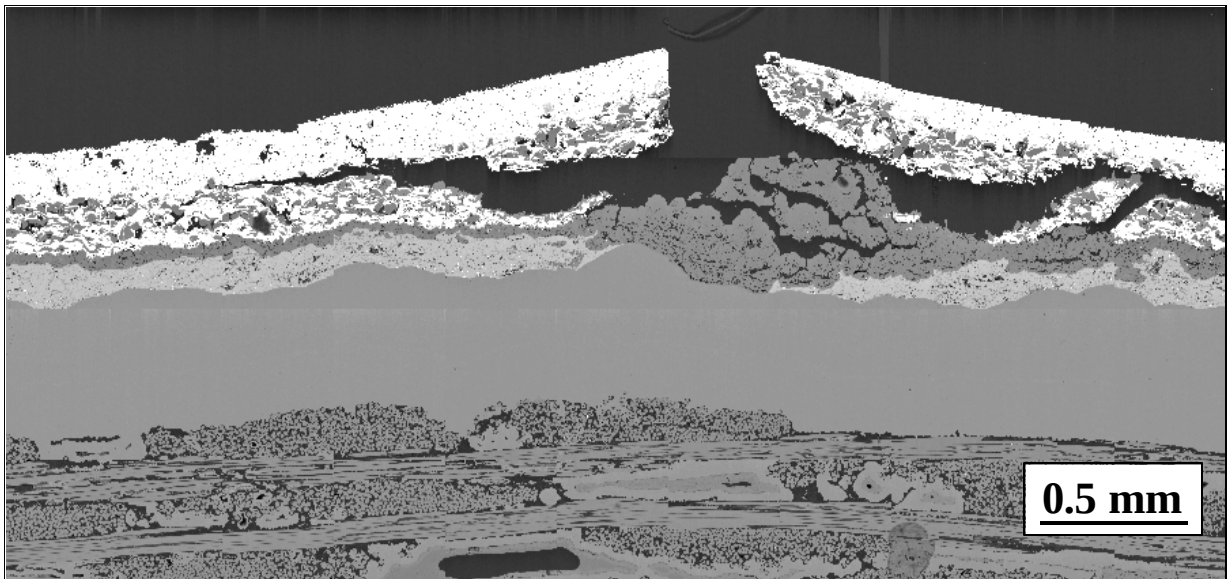

Figure 7. Accelerated oxidation below the EBC associated with a tool bump area.

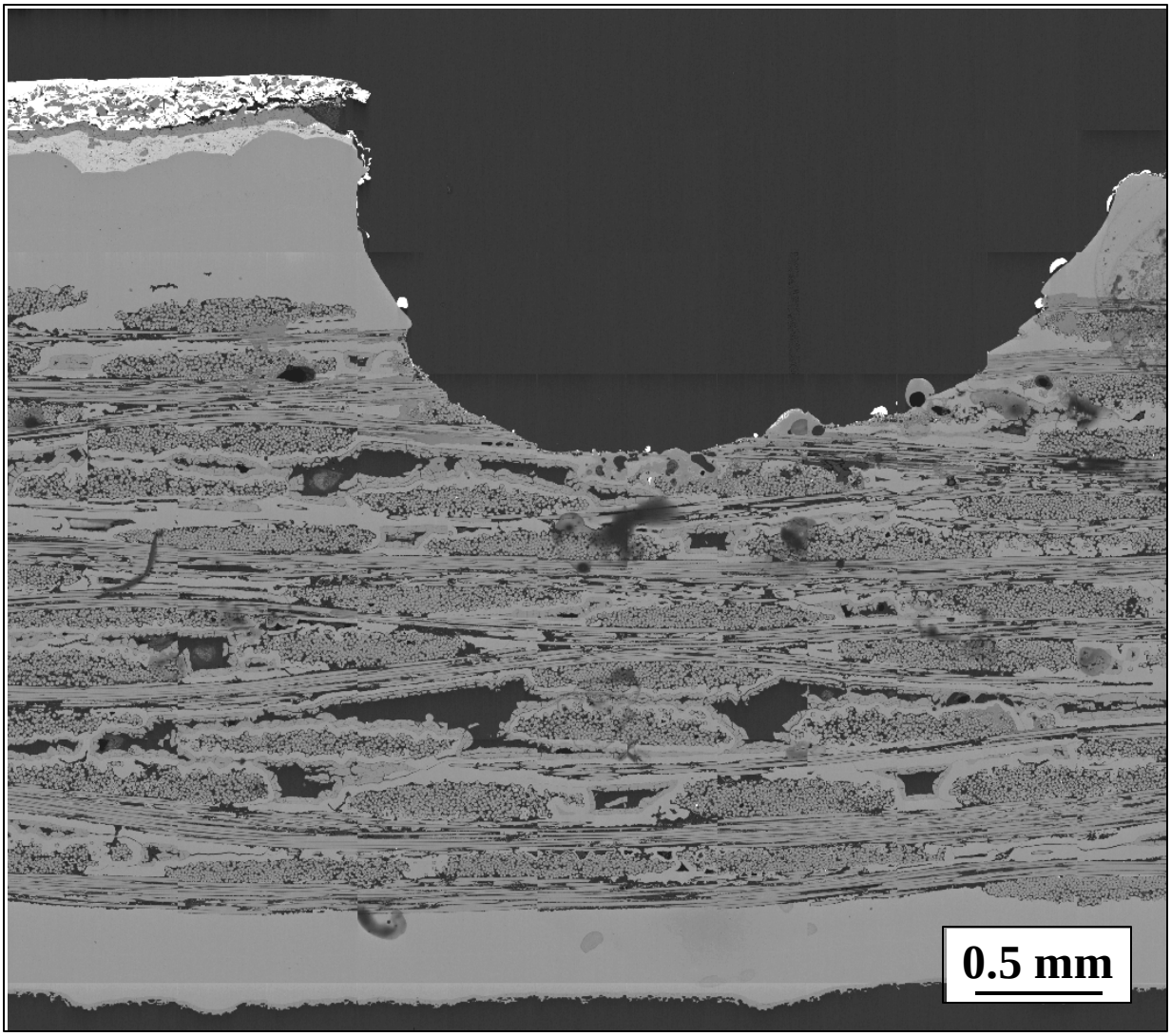

Figure 8. Cross-section SEM image through a "pinhole" defect caused by a tool bump.

Status of Milestones

04/02 Milestone

Prepare a report and present results on the evaluation of the set of 14,000h Texaco (Chevron) combustor liners. This milestone has been met. A manuscript has been accepted for publication by ASME and will be part of the proceedings of the IGTI meeting in Amsterdam, June 3-6, 2002. K.L. More, P.F. Tortorelli, L.R. Walker, J.B. Kimmel, N. Miriyala, J.R. Price, H.E. Eaton, E.Y. Sun, and G.D. Linsey, "Evaluating EBCs on Ceramic Matrix Composites After Engine and Laboratory Exposures."

Industry Interactions

Attended DER Materials Peer Review Meeting, March 12-14, 2002 in Fairfax, VA and met with several CFCC industrial collaborators to discuss program status.

Problems Encountered

None.

Publications/Presentations

K.L. More and P.F. Tortorelli, "Continuous-Fiber Ceramic Composites (CFCCs) For Industrial Gas Turbines," presentation at the DER Materials Peer Review Meeting, Fairfax, VA, March 14, 2002.

K.L. More, P.F. Tortorelli, L.R. Walker, N. Miriyala, J.R. Price, M. van Roode, H.E. Eaton, E.Y. Sun, and G.D. Linsey, "The High-Temperature Stability of SiC-Based Composites In High H2O Pressure Environments," presentation at the TMS Annual Meeting, Seattle, WA, February 19, 2002. To be published in *Journal of The American Ceramic Society*.

Symposium Co-Organizer at TMS Annual Meeting, February 18-20, 2002 in Seattle, WA. "Water Vapor Effects on Oxidation of High-Temperature Materials." Papers to be published in Special Edition of *The Journal of The American Ceramic Society*.

High-Temperature Environmental Effects on Ceramic Materials

P. F. Tortorelli, K. L. More, and L. R. Walker
Metals and Ceramics Division
Oak Ridge National Laboratory
P.O. Box 2008, Oak Ridge, TN 37831-6156
Phone: (865) 574-5119, E-mail: tortorellipf@ornl.gov

Objective

The overall objective of this task is to examine the trends and mechanisms of high-temperature degradation and their effects on the properties and life of ceramics and ceramic composites used in combustion environments in order to improve their environmental stability through changes in composition, structure, and design. This is accomplished by investigating the effects of combustion-relevant high-temperature environments on material stability and properties, evaluating the effectiveness of coatings in ameliorating such degradation, and examining the range of conditions and root causes of environmental susceptibility for a given ceramic or ceramic composite system.

Highlights

A study of the exposure of SiC at 1200°C and high water vapor pressures (1.5 atm) has shown SiC recession rates that significantly exceed what is predicted based on parabolic oxidation at elevated H_2O pressures. After exposure under these conditions, distinct silica scale structures were observed; thick, porous, non-protective cristobalite scales formed above a thin, dense SiO_2 layer. The porous cristobalite thickened with exposure time, while the thickness of the underlying dense layer remained constant. Recession measurements quantitatively agreed with what was predicted from a paralinear oxidation model.

Technical Progress

Significant advances in SiC-based continuous fiber-reinforced ceramic matrix composite (CFCC) development and design have been made over the past decade and have led to the evaluation of these materials in several high-temperature applications, including combustor liners in land-based gas turbines.[1,2] As part of this effort, the influence of high water-vapor pressures (>1 atm) found in higher-pressure-ratio gas turbines on the oxidation of SiC has been one of the areas of study. Specimens of sintered α (SA) and chemical-vapor-deposited (CVD) SiC were exposed at 1200°C to slowly flowing (~ 0.5 mm/s) air or air+ 15 vol% H_2O at a total pressure of 10 atm in an experimental facility described elsewhere.[3] After each exposure interval of 500 h, the specimens were carefully removed and examined. After sectioning to obtain a small

representative piece for microstructural analysis, selected specimens were then placed back in the furnace for additional exposure cycles. Microstructural examinations by scanning and transmission electron microscopy and electron microprobe analysis were used to measure the thickness of the oxidation product and of the unaffected material remaining (surface recession) and to assess the nature of the oxides that formed.

The presence of water vapor at an elevated partial pressure had a dramatic effect on the oxidation of SiC. The silica that formed on SiC exposed to 8.5-atm air + 1.5-atm H_2O at 1200°C (see, for example, Fig. 1) was much thicker than that exposed to 10-atm air (~25 versus ~3 µm, respectively, after 100 h). The silica structures formed on the SA and CVD SiC exposed to the air-1.5 atm H_2O environment, described in more detail elsewhere,[4,5] were characterized by a thin, dense vitreous SiO_2 layer under a much thicker, porous silica scale (Fig. 1). X-ray diffraction identified the thick, porous surface SiO_2 layer as cristobalite. (Such oxide morphologies have been observed under similar exposure conditions for CVD SiC seal

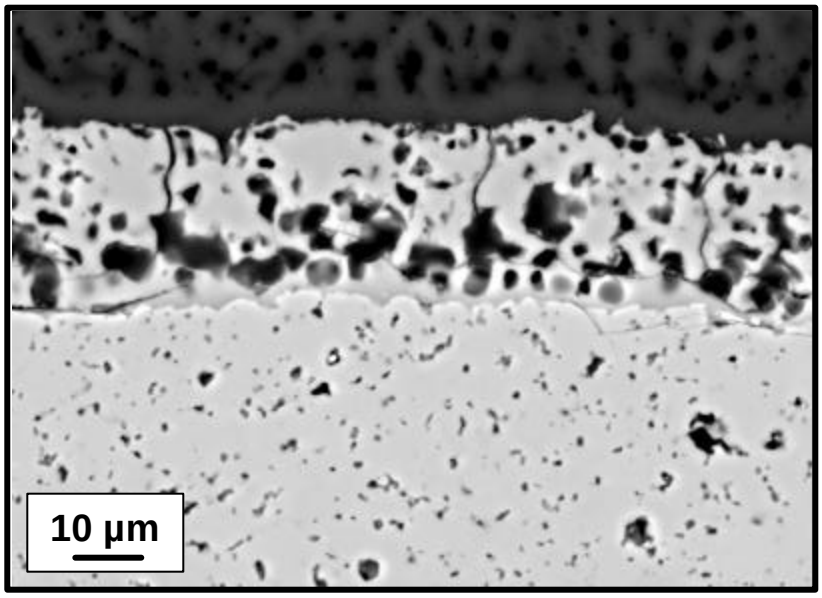

Figure 1. SA SiC exposed in 8,5 atm air-1.5 atm H_2O for 100 h at 1200°C.

coats used to protect SiC-based, fiber-reinforced composites.[1]). The thickness of the porous cristobalite product continually increased with exposure time while that of the dense vitreous SiO_2 underlying it remained constant.

As mentioned above, microstructural analysis of polished cross sections was used to directly determine the amount of SiC converted to SiO_2 as a function of time by measuring the thickness of unaffected material remaining after each exposure cycle. (Such recession measurements proved to be more reliable than mass changes or oxide product thickness data because of silica spallation during cooling or handling.) The SiC recession data are plotted in Fig. 2. The measured values are fairly well described by a linear fit over exposure time, which yields

recession rates of ~0.06 μm/h for CVD SiC and ~0.04-0.08 μm/h for SA. These rates are higher than that predicted by the well-established models for SiC oxidation as a function of the water vapor pressure and gas velocities.[6,7]

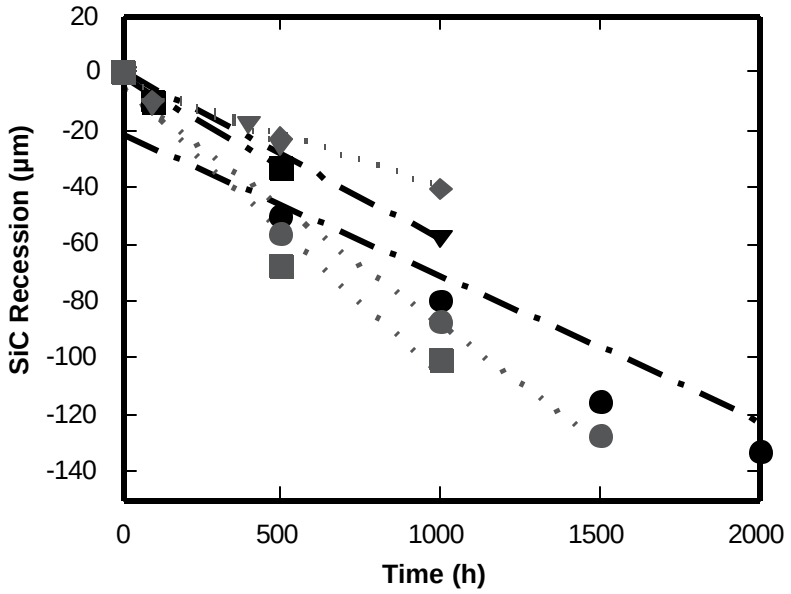

The observation that the thin, dense SiO_2 layer did not thicken with time suggests a paralinear kinetic process.[6] Applied in the present case, a layer of fixed thickness is maintained when the oxidation front proceeds into the SiC at the same rate at which the dense silica is converted to a porous, crystalline oxide and recession is thus linear with time. In such a paralinear kinetic

Figure 2. Recession as a function of time for SA (gray) and CVD (black) SiC, 1200°C, 8.5-atm air + 1.5-atm H_2O.

model, the invariant thickness of the dense silica, d, is proportional to the ratio of the paralinear rate constant for the solid-state oxidation of SiC to SiO_2, k_p, to the linear recession rate, k_l:

$$d = k_p/2k_l.$$

As the current microstructural measurements give experimental values of d (~4 μm) as well as k_l (0.06 μm/h for CVD SiC and 0.04-0.08 μm/h for SA), k_p can be calculated from the above equation. Doing so yields

$$k_p = 0.5\ \mu m^2/h \text{ for CVD SiC}$$

and

$$k_p = 0.3\text{-}0.7\ \mu m^2/h \text{ for CVD SiC.}$$

These k_p values can be directly compared to the expected value of the parabolic rate constant based on its functional dependence on temperature and water vapor partial pressure as determined by Opila for CVD SiC.[8] Using the present experimental conditions of 1200°C and 1.5 atm of H_2O, a k_p of 0.5 $\mu m^2/h$ is calculated for SiC. The excellent agreement between the predicted parabolic rate constant and the experimentally determined values of k_p (through its dependence on k_l and d) is strong evidence for the applicability of the paralinear kinetic model to the present case of high-temperature oxidation of SiC at high water vapor pressures and low gas flow velocities. This model has relevance for combustion conditions with respect to oxidation of SiC within a composite[9] or underneath a defective protective coating,[10] where conditions of high water vapor pressure and low gas velocity exist.

The type of paralinear kinetic process described above is quite distinct from a model of similar form that describes the oxidation of SiC at elevated H_2O pressures and high gas velocities, where the rate-controlling step is the volatilization of the constant-thickness SiO_2.[7,11,12] As such, this latter type of model, based on the low gas-flow rate employed in this study, would predict much less SiC recession than what is reported here.

Status of Milestones

To address concerns with long-term environmental stability of Si-based ceramics, complete a comprehensive paper or report on oxidative degradation mechanisms and rates of such materials at high temperatures and high water-vapor pressures typical of gas turbines. (March 2002) – paper to be submitted to journal by June 30, 2002

Industry Interactions

P.F. Tortorelli attended a combustor liner project update meeting with personnel from Solar Turbines, UTRC, Argonne National Laboratory, and DOE on January 30, 2002 during the Annual Conference on Composites, Materials and Structures in Cape Canaveral..

P.F. Tortorelli and K.L. More organized (with E.J. Opila of NASA-Glenn), and participated in, the Symposium on Water Vapor Effects on Oxidation of High Temperature Materials at the TMS Annual Meeting in February 2002.

P.F. Tortorelli and K.L. More attended a status review for the Honeywell high-velocity burner rig held at Honeywell Engines Systems in Phoenix on March 20, 2002.

Problems Encountered

None.

Publications/Presentations

P.F. Tortorelli, "Effects of High Water-Vapor Pressures on the Oxidation of Si-Based Materials at High Temperatures," presentation at Symposium on Water Vapor Effects on Oxidation of High Temperature Materials, TMS Annual Meeting, February 19, 2002.

Reference

1. K. L. More *et al*., *J. Eng. Gas Turbines and Power* 122 (2000) 212-18.

2. N. Miriyala and J. R. Price, *Proc. of ASME TURBOEXPO 2000*, Paper 2000-GT-648, ASME International, New York (2000).

3. J. R. Keiser, M. Howell, J. J. Williams, and R. A. Rosenberg, *Proc. Corrosion/96*, Paper. 140, NACE International, Houston, TX (1996).

4. K. L. More, P. F. Tortorelli, M. K. Ferber, and J. R. Keiser, *J. Am. Ceram. Soc.* 83 (2000) 211-13.

5. P. F. Tortorelli and K. L. More, to be submitted to *J. Am. Ceram Soc.*, 2002.

6. E. J. Opila and R. E. Hann *J. Am. Ceram. Soc*., 80 (1997) 197-205.

7. J. L. Smialek, R. C. Robinson, E. J. Opila,, D. S. Fox, and N. S. Jacobson, *Adv. Composite Materials*, 8 (1999) 33-45.

8. E. J. Opila, *J. Am Ceram. Soc.* 82 (1999) 625-36.

9. P. F. Tortorelli, K. L. More, and L. R. Walker, *DER Materials Quarterly Progress Report for Period Ending December 2001*.

10. K. L. More *et al.*, accepted for publication in *Proc. of ASME TURBO/EXPO 2002*, ASME International, New York (2002).

11. R. C. Robinson and J. L. Smialek, *J. Am. Ceram. Soc.* 82 (1999) 1817-25.

12. E. J. Opila, J. L. Smialek, R .C. Robinson, D. S. Fox, and N. S. Jacobson, J. Am. Ceram. Soc. 82 (1999) 1826-34.

High Speed Burner Rig Development

B. Schenk and G. Schroering
Honeywell Engines, Systems & Services
2739 E. Washington Street
P.O. Box 5227, Phoenix, AZ 85010
Phone: (602) 231-4130, E-mail: bjoern.schenk@honeywell.com

Objective

Design, build, and operate a burner rig facility which

- will provide ability to expose most promising ceramics and coatings at environmental conditions typical of turbine nozzles and blades
- will provide oxidation information at conditions well beyond current experimental database

Test section maximum operating conditions

- Gas Temperature - 3000°F
- Average Gas Velocity - 2700 ft/s
- Partial Pressure of Water Vapor - 70 psia (in combustor)
- Stress Rupture Test Capability
- Durability for extended unmanned operation (100's of hours)
- Operating costs to be minimized

Highlights

- Conceptual and preliminary design completed
- Facility resource equipment specified, ordered, and received 3rd Qtr 2001
- Building modifications underway
- Tensile Stress rupture frame, Instron 1362, arrived
- Failure Mode and Effects Analysis (FMEA) of rig layout completed
- Conducted Program Status Review with customer 3/20/02
- No cost extension to March 31, 2003 has been approved by ORNL

Technical Progress

Facility resources (dedicated air compressor, steam boiler, super heater, gas compressor, etc.) were sized to match the operating envelope of the burner rig. The specified equipment has been ordered and completely received to date. All construction drawings for the facility have been completed. Building permits were submitted for approval to and in the meantime granted by the City of Phoenix.

Canned control system software has been purchased. Software development to link all instrumentation and valves required for monitoring rig safety and flow control using the canned software has been initiated. The design objective of the control system is to automatically handle any alarm and take corrective action.

The burner rig is being designed to mimic the flow field experienced by ceramic airfoils. It will incorporate a modular design to simplify repairs and specimen replacement. The test section will house multiple ceramic test samples and is designed to minimize the temperature gradients along the length of the specimen as well as from the first specimen to the last specimen downstream.

Long lead time parts to manufacture have been identified and preliminary drawings were sent to potential vendors for a rough order of magnitude (ROM) quote (including lead time estimates).

The flow field of the combustor has been analyzed by Computational Fluid Dynamics (CFD) at the extreme test section condition of 2700 ft/s @ 3000°F. This will aid in combustor optimization and provide temperature profiles for a detailed stress analysis of structural test section and rig components. At least one other flow condition at the opposite end of the operating envelope will be analyzed for this combustor design.

A Failure Mode and Effects Analysis (FMEA) of the rig conceptual design has been conducted and identified two major potential failure modes, i.e. thermal barrier coating (TBC) reliability and the specimen retention scheme. Potential TBC failure was reduced by improving the cooling system design which resulted in lower (≈1500°F) bond coat temperatures. Various specimen retention schemes (zirconia blocks, ceramic rope seals, cooled metal retainer seals) are currently under analytical evaluation.

Status of Milestones

Combined conceptual & preliminary design review with the customer was held on 3/20/02.

Survey of similar test facilities to capture best practices to incorporate into design concept was completed in the conceptual design phase of this program.

SOW for facility control system has been completed.

Preliminary site plan (power & utility for facility) has been completed and approved.

Industry Interactions

Dr. Schenk is actively participating in a working group to establish Oxidation Test Standards for Ceramic Materials.

Problems Encountered

Test specimen retention and test section assembly is still an issue with the current design. Design iterations and refinements are still being conducted to achieve a design robust enough to withstand many assembly/disassembly cycles, as well as the hostile operating environment, while allowing easy assembly and installation.

Thermal Barrier Coating (TBC) thickness and bond coat temperature were the critical issues of the design concept. Honeywell's experience is to keep the bond coat temperature at or below 1600°F. The design was optimized through thermal analyses in order to achieve this limit. A TBC-system capable of surviving the flow conditions has been identified. The rig layout has been sent to various vendors for ROM quotes.

Publications/Presentations

Program overview and progress presentations were given by Dr. Schenk at the International Conference on Advanced Ceramics & Composites, Cocoa Beach, FL, January 13-18, 2002.

DOE Microturbines Peer Review, Fairfax, VA, March 12-14, 2002.

A customer review was held at ES&S on March 20, 2002.

DEVELOPMENT OF HIGH-TEMPERATURE COATINGS

Environmental Protection Systems for Ceramics in Microturbines and Industrial Gas Turbine Applications, Part A: Conversion Coatings

S. D. Nunn and R. A. Lowden
Metals and Ceramics Division
Oak Ridge National Laboratory
P.O. Box 2008, Oak Ridge, TN 37831
Phone: (865) 576-1668, E-mail: nunnsd@ornl.gov

Objective

Silicon-based monolithic ceramics are candidate hot-section structural materials for microturbines and other combustion systems. The performance of silica-forming ceramic materials in combustion environments is, however, severely limited by rapid environmental attack caused by the combination of high temperature, high pressure, and the presence of water vapor. Thus, the development of environmental protection systems has become essential for enabling the long-term utilization of these materials in advanced combustion applications.

Similar to thermal barrier coatings for nickel-based super alloys, successful environmental protection systems for ceramics and ceramic composites will likely utilize multiple layers, i.e. surface layers and bond coats, and complex combinations of materials. A challenge in the development of current protection systems, most of which employ oxide surface layers, is the formation of silica at the oxide-bond coat or the oxide-substrate interface. The oxide ceramic layers cannot prevent oxygen diffusion to the underlying materials; therefore the formation of silica at this boundary is inevitable.

A solution to the formation of this weak link is the development of substrate compositions or bond coatings that form more thermochemically and thermomechanically stable compounds. A common practice used to improve the performance and extend the life of TBCs for Ni-based super alloys is to enrich the alloy surface with aluminum. The Al surface enrichment using pack cementation or chemical vapor deposition produces a surface layer that forms a stable alumina layer upon oxidation. Similar approaches can be applied to silicon-containing ceramics to produce a bond layer that does not form silica but a more stable oxide. Diffusion processes for surface treatment of silicon-based ceramics will be explored to produce "bond coatings" that will enhance the performance and life of environmental protections systems.

Highlights

The surface of silicon nitride is being enriched with aluminum and other metals using pack cementation to produce a coating or bond layer that does not form silica but a more stable oxide. Silicon nitride specimens have been heat treated in packed beds with chemistries similar to those used in the treatment of super alloys prior to the deposition of a thermal barrier coating. Initial experiments with aluminum-containing beds have produced surface layers containing silicon nitride and aluminum nitride. It appears that during the treatment, the glassy grain boundary

phase near the outer edges of the silicon nitride is replaced with nano-crystalline aluminum nitride. These layers should oxidize to form aluminosilicate (preferably mullite), which should exhibit improved stability as compared to silica.

Technical Progress

The pack cementation process looks very promising as a method for developing a thin conversion-coating layer on silicon nitride (Si_3N_4) components. Experiments have shown that a wide variety of reactive materials can be used to form a conversion layer on dense Si_3N_4 samples. Tests are now being conducted using a number of different Si_3N_4 compositions to help understand the effect of the different additives on the resulting coating composition. These additives form crystalline or amorphous grain boundary phases in the Si_3N_4 material. Some of the variations in the pack cementation process that are being investigated are summarized in Table 1.

Table 1. Process and material variations

Si_3N_4 Compositions	Reactive Powders	Temperatures	Times	Atmosphere	Filler
Honeywell AS800	Al, NH_4Cl	1000°C	2 hr.	Ar	Al_2O_3
Honeywell GS-44	Al, $ZrCl_4$	1175°C	5 hr.		
Norton NT154	$AlCl_3$	1410°C			
Kyocera SN281	$ZrCl_4$				
	$AlCl_3$, $ZrCl_4$				

In each pack cementation experiment, the reactive powder is blended with alumina (Al_2O_3) filler powder and loaded into a graphite crucible. Small bars of the Si_3N_4 materials are placed in the blended powder and the crucible is closed with a screw cap. The crucible is then placed in a furnace containing an argon atmosphere and heated to the desired temperature for a selected time. After the thermal treatment, the samples are examined to characterize the coating.

As noted in an earlier report, all of the samples treated in the beds exhibit a distinct color change after processing. A cross-section of one of the aluminized samples is shown in Figure 1. This image clearly shows the uniform surface layer that was formed on the sample. The interior of the sample was unchanged from the starting material. The modified samples were initially analyzed using x-ray diffraction, and then in more detail employing scanning and transmission electron microscopy, to identify the compounds that were formed during the treatments, and to examine microstructural changes.

The best-characterized samples are those exposed in packing beds containing Al metal and various activators. The SEM analysis revealed a change in the distribution of the rare earth containing grain boundary phases used in the processing of the silicon nitride substrates. The oxide grain boundary phases were not present in the reaction zone near the outer surfaces of the samples. This is highlighted in the SEM images in Figure 2.

Further analysis using TEM found nano-crystalline aluminum nitride (< 25 nm) along the grain boundaries in the conversion zone (Figures 3 and 4). The elemental dot maps displayed in

Figure 5, supported the observation that the grain boundary phase(s) are replaced with AlN during the conversion process. The dot maps indicate the presence of Al, N, O, and some Cl at the grain boundaries near the outer surfaces of the as-treated samples. As shown in Table 1, additional treatments are being conducted to explore improved penetration and other effects. Heat treatments will also be conducted to examine removal of residual chlorine and investigate other potential benefits.

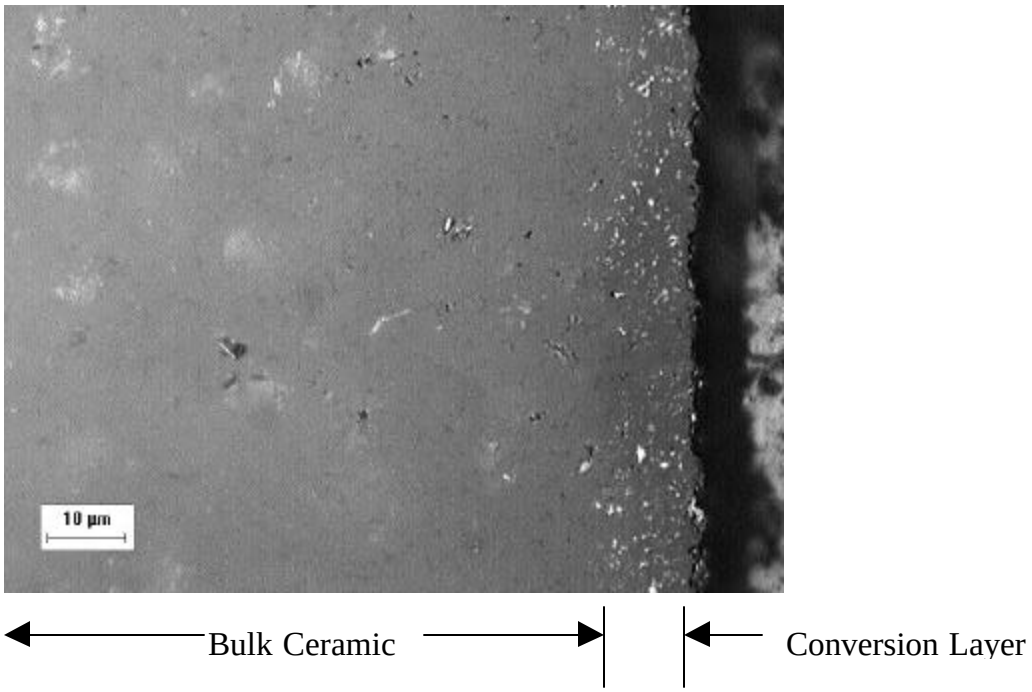

Figure 1. High magnification image of AS800 Si_3N_4 after pack cementation processing showing the thin conversion layer that was formed on the surface of the sample.

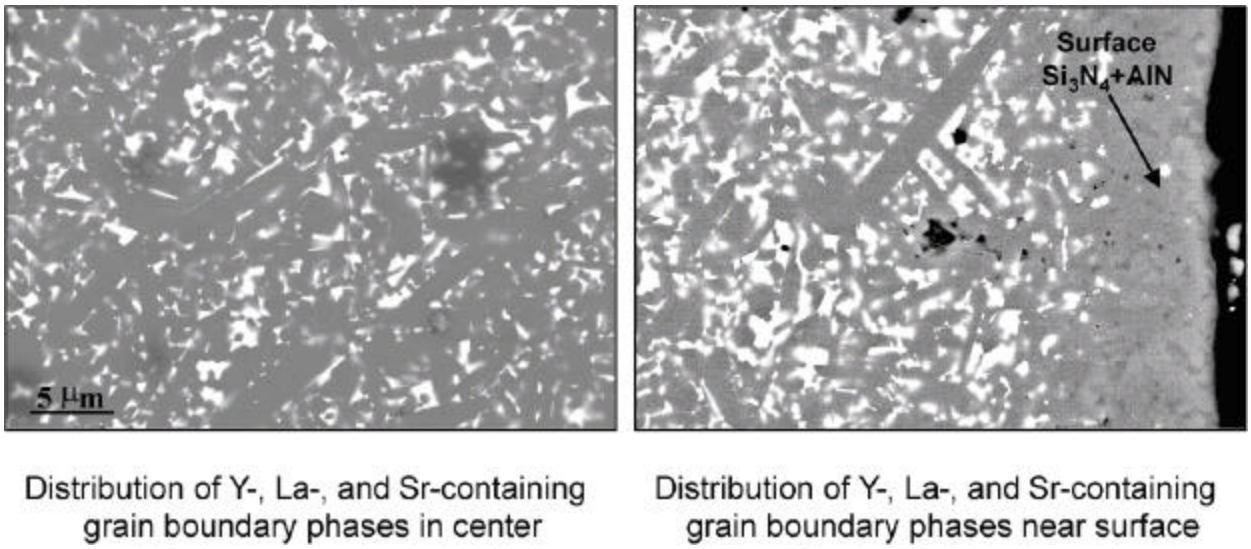

Figure 2. SEM image of AS800 Si_3N_4 after pack cementation processing showing the removal of the grain boundary phases in the conversion zone.

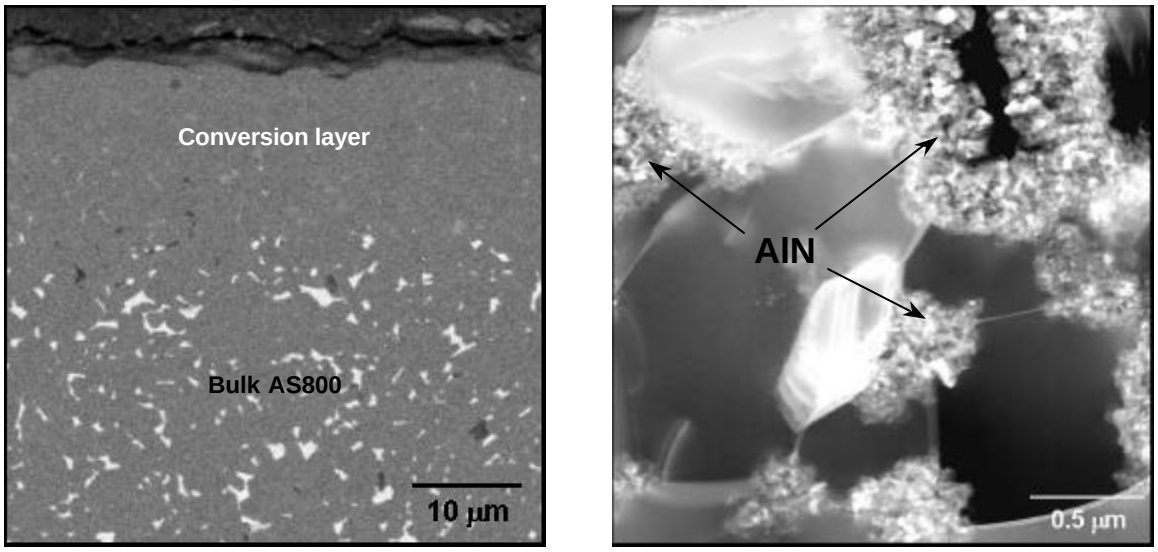

Figure 3. The ~ 10 µm conversion layer on AS800 is clearly shown in the backscatter scanning electron microscope image (left). More detailed analysis using transmission electron microscopy revealed the presence of the nano-crystalline AlN at the grain boundaries (right).

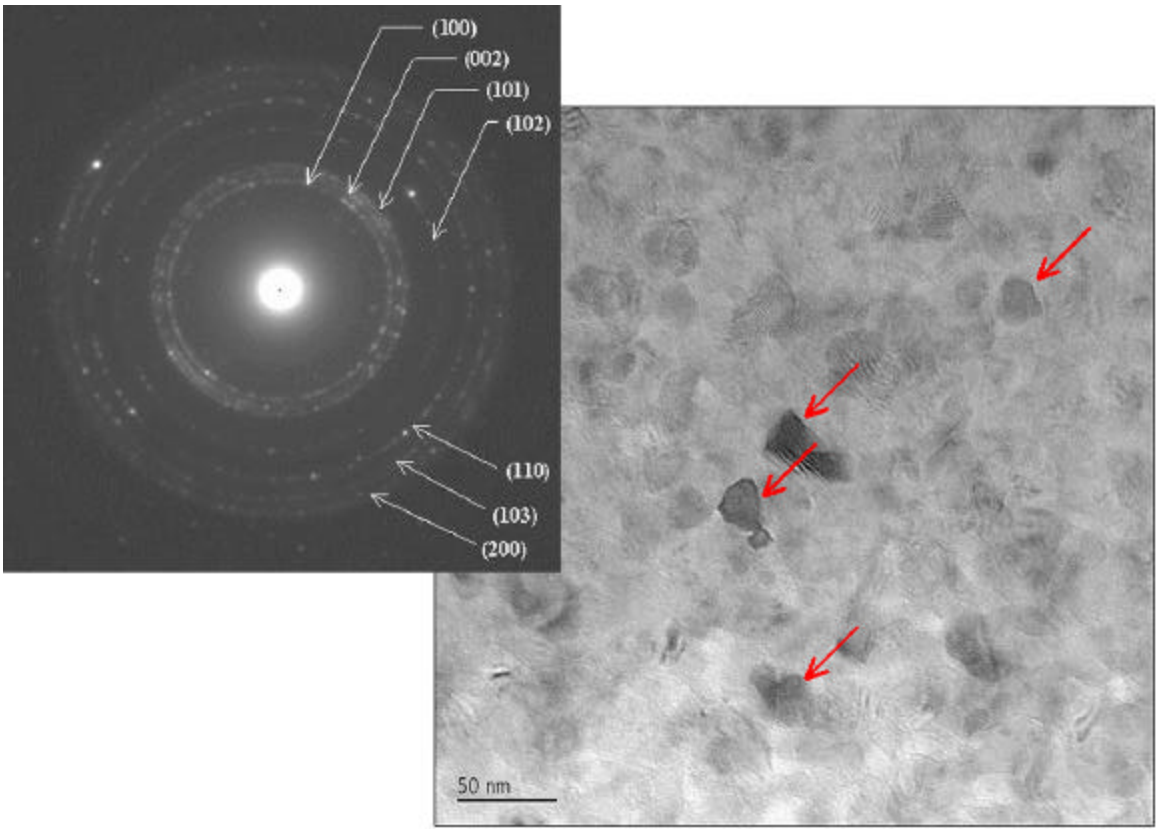

Figure 4. Fine-grained hexagonal AlN (<25 nm) was identified between Si_3N_4 grains using electron diffraction.

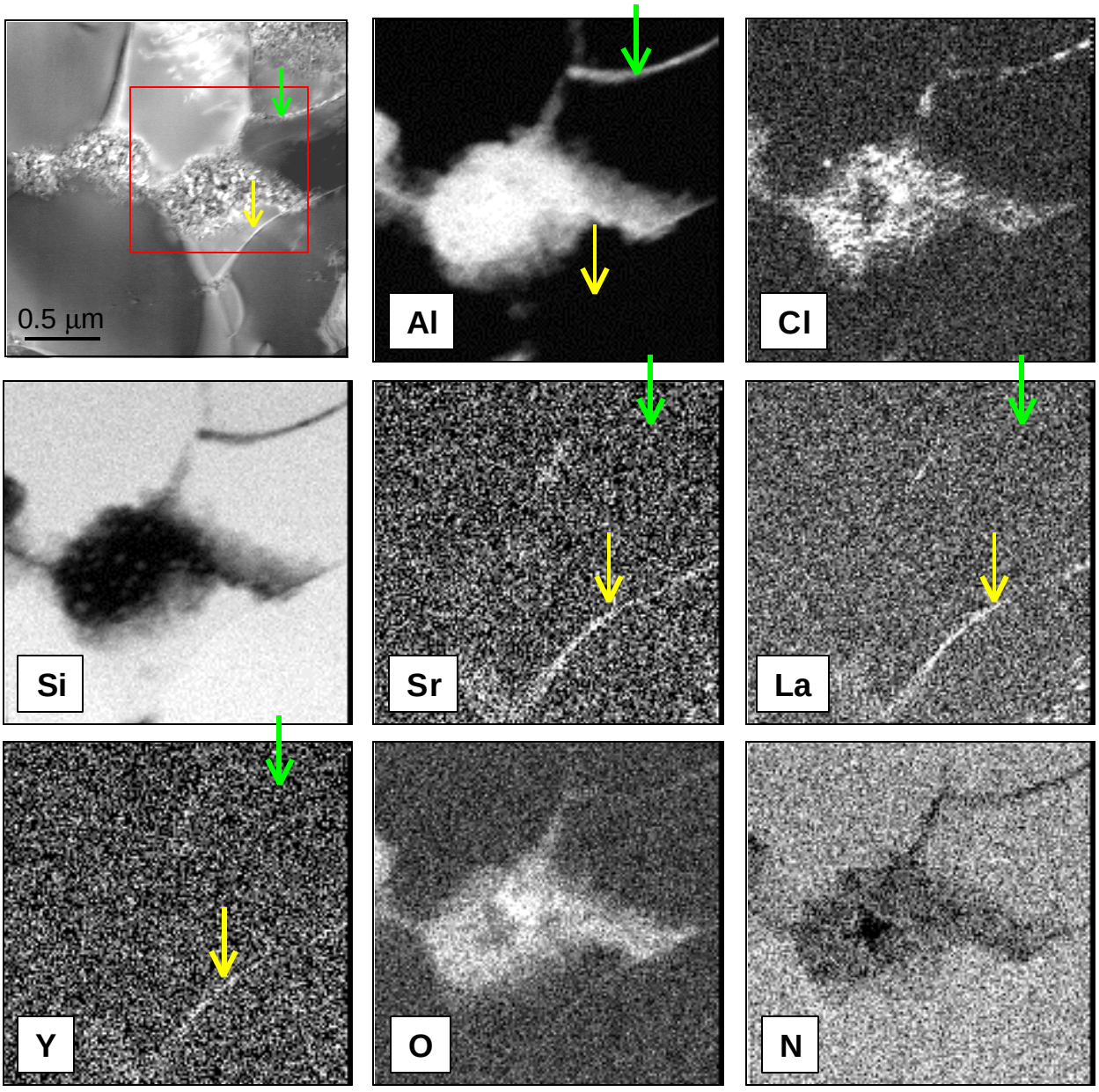

Figure 5. When AlN was found at Si_3N_4 grain boundaries, standard sintering aids (Sr, La, Y) were not present (green arrows) but when the AlN has not penetrated along certain Si_3N_4 grain boundaries, the sintering aids were found (yellow arrows).

Status of Milestones

Examine diffusion bond coatings containing aluminum for silicon-based ceramics (09/02).

Industry Interactions

A presentation on environmental protection systems produced by pack cementation was given at Honeywell Engines and Systems in Phoenix on March 20, 2002.

Problems Encountered

None.

Publications/Presentations

None.

Environmental Protection Systems for Ceramics in Microturbines and Industrial Gas Turbine Applications, Part B: Slurry Coatings and Surface Alloying

B. L. Armstrong, K. M. Cooley, M. P. Brady, H-T Lin, and J. A. Haynes
Oak Ridge National Laboratory
P.O. Box 2008, Oak Ridge, Tennessee 37831-6063
Phone: (865) 241-5862, E-mail: armstrongbl@ornl.gov

Objective

Silicon-based monolithic ceramics are candidate hot-section structural materials for microturbines and other combustion systems. The performance of silica-forming ceramic materials in combustion environments is, however, severely limited by rapid environmental attack caused by the combination of high temperature, high pressure, and the presence of water vapor. Thus, the development of environmental protection systems has become essential for enabling the long-term utilization of these materials in advanced combustion applications.

Similar to thermal barrier coatings for nickel-based super alloys that utilize a specialized oxide surface layer and a metallic bond coat, successful environmental protection systems for ceramics and ceramic composites will likely utilize multiple layers and complex combinations of materials. Most recent efforts have focused on the selection and deposition of the oxide surface layer, and due to numerous factors, the majority of the candidates have been from the aluminosilicate family of oxide ceramics. Stable rare-earth silicate deposits have been found on component surfaces after recent engine and rig tests, indicating there may be other stable oxide compositions that have not been fully investigated. Thin coatings of selected silicate compositions will be deposited on test coupons using a variety of techniques. The specimens will then be exposed to simulated high-pressure combustion environments and materials that demonstrate good potential will be investigated further.

Highlights

Initial results showed interaction between BSAS and some of the silicon nitride substrates. Feasibility of the concept of utilizing a sacrificial coating that forms a protective scale was demonstrated.

Technical Progress

Work continued on the characterization of the BSAS screen-printed coatings and the development of a sacrificial coating that oxidizes and/or diffuses via a heat treatment or in-situ to form a stable oxide, such as alumina.

Characterization of the BSAS Screen-Printed Coatings

A 35.0 volume percent BSAS ink was fabricated and deposited on Honeywell AS800 and Norton NT154 silicon nitride coupons at a gap height of 0.035". The resulting coatings were densified in argon at 1400°C for 2 hours then subsequently heat treated at 1000°C in air. The BSAS coating reacted with the AS800 substrate. Image analysis shown in Figure 1 shows that the

"reaction" areas were enriched with lanthanum. A control sample, an AS800 substrate without any coating, was also densified under the same processing conditions. As shown in Figure 2, the substrate surface shows less severe reaction areas, and the reaction areas are composed needle-like grains composed of lanthanum, yttrium, silicon and oxygen. The cause of the reaction of the coating with the AS800 substrate is still under investigation. The NT154 silicon nitride substrate coated with BSAS did not show the same reaction areas when densified under the same processing conditions as shown in Figure 3. Although slightly microcracked, the coating survived and was dense.

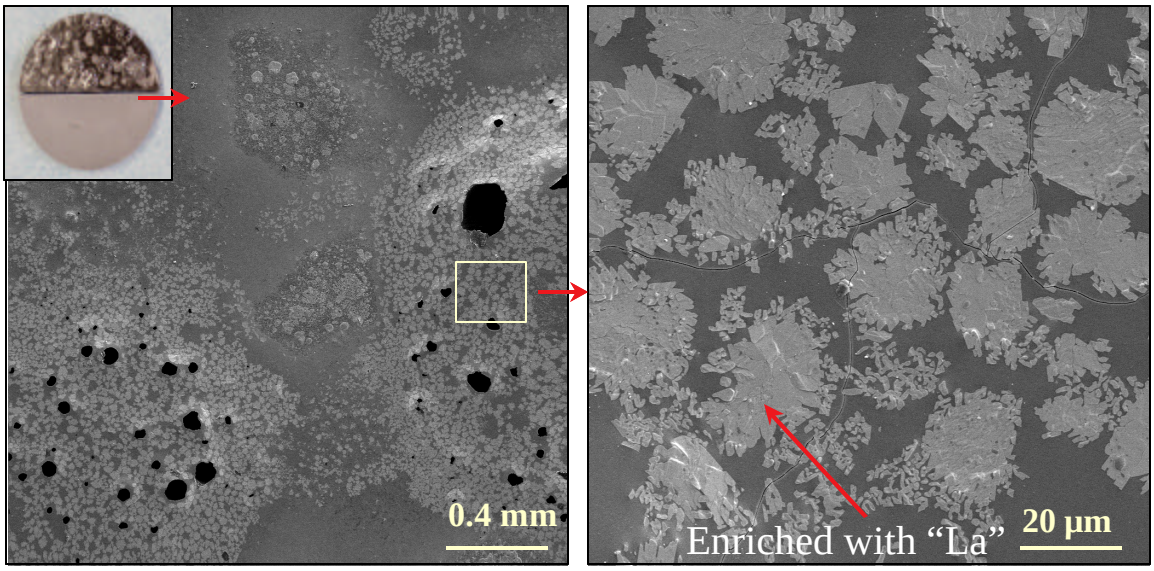

Figure 1. Top surface of the BSAS coated AS800 silicon nitride substrate after densification at 1400°C in argon for 2 hours and subsequent heat treatment in air at 1000°C for 2 hours.

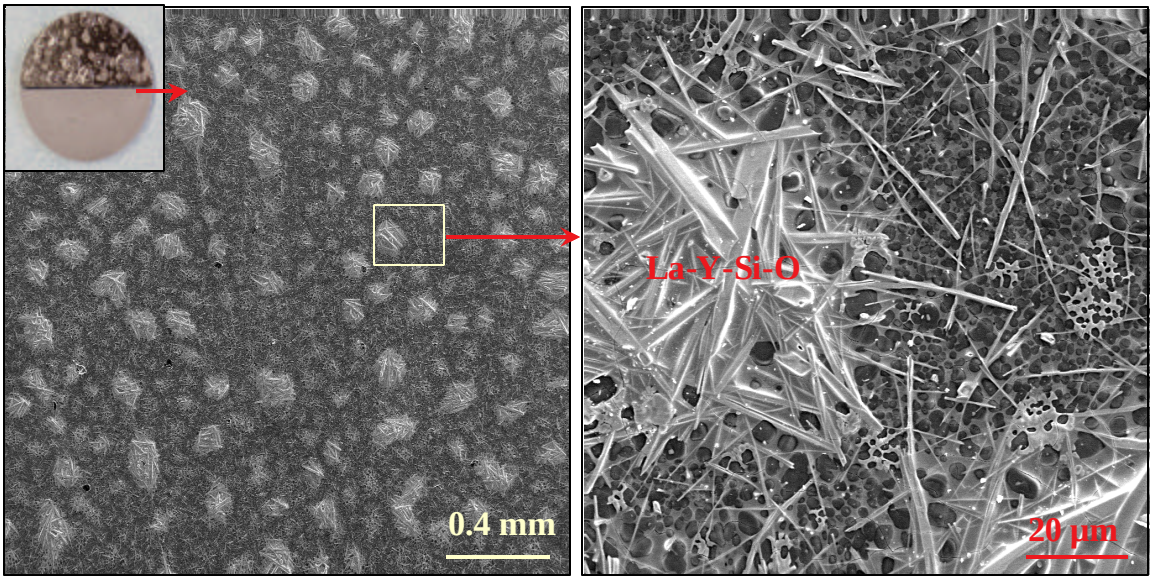

Figure 2. Top surface of the uncoated AS800 silicon nitride substrate after densification at 1400°C in argon for 2 hours and subsequent heat treatment in air at 1000°C for 2 hours

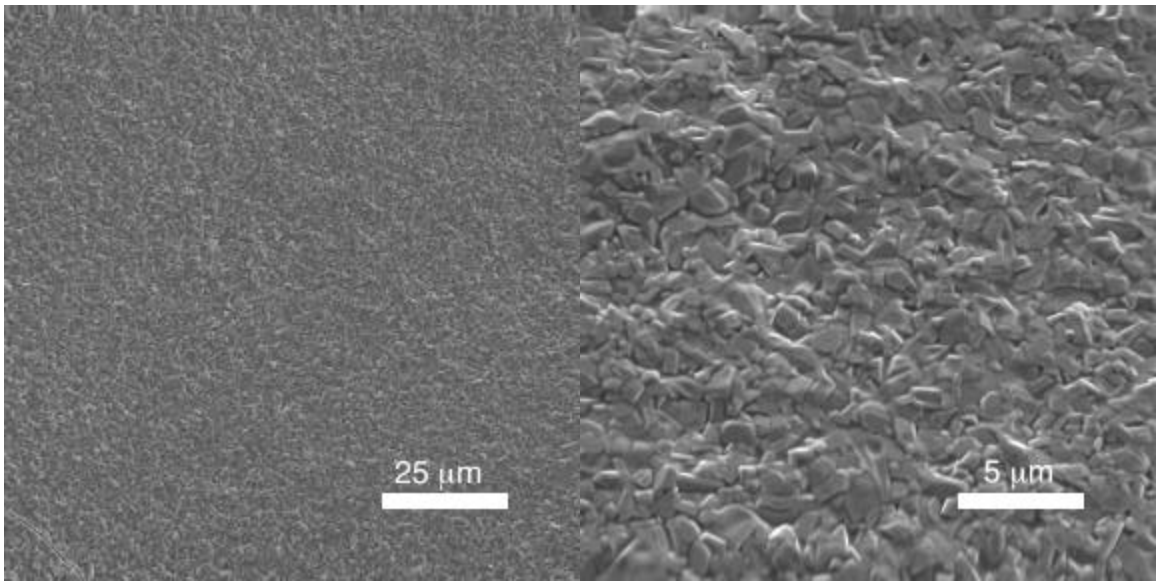

Figure 3. Top surface of the BSAS coated NT154 silicon nitride substrate after densification at 1400°C in argon for 2 hours and subsequent heat treatment in air at 1000°C for 2 hours

Development of a Sacrificial Coating

One challenge in the densification of a slurry coating is the prevention of silica formation at the coating – substrate interface. Oxygen will diffuse to the substrate during the sintering process until densification is complete. Even if steps are taken to limit the oxygen diffusion during this densification process, the formation of a silica layer at the coating – substrate interface can still occur if the coating does not completely prevent oxygen transport. Thus, the development of a sacrificial coating that oxidizes and/or diffuses via a heat treatment or in-situ to form a volatility barrier has been proposed to address these concerns. Thus, the concept of looking at the use of thin metallic precursor layers as a route to forming self-graded oxide surface layers that can act as volatility barriers or protect against aggressive species that would degrade a silica layer was proposed. In this case, the metal layer would completely convert to ceramic by an oxidation pretreatment.

For a feasibility evaluation, the authors proposed using four of the well characterized alumina-forming intermetallic systems, yttrium doped chrome aluminide (Cr_2AlY), hafnium doped nickel aluminide (NiAlHf), and chromium/yttrium doped nickel aluminide (NiCrAlY. These compositions were selected with a range of CTE, high temperature strength properties in the metal layer, and base metal component chemistries in order to explore what the key issues are regarding the conversion of the metal layer to ceramic and the formation of a dense, adherent oxide after oxidation pretreatment. It is anticipated that the oxide layer formed will be a duplex with an outer layer of alumina and an inner layer of graded oxide layer of the base metal of the aluminide, Si and Al.

Feng Huang and Mark L. Weaver of the University of Alabama, Tuscaloosa sputtered 2-3 μm coatings of Cr_2AlY, NiAlHf and NiCrAlY on to NT154 and SN282 substrates. The resulting substrates were exposed to 1150°C in flowing oxygen for 0.5 hour to convert the coating to alpha alumina prior to stability testing. The resulting microstructures of the SN282 substrates exposed at 1150°C are shown in Figures 4 through 6. In each of the three coating conditions, Cr_2AlY,

NiAlHf and NiCrAlY, a 0.5 µm layer of alumina formed at the surface. Chrome, nickel and both nickel and chrome, respectively, were also found in the alumina layer. A 2.5 µm alumino-silicate layer formed underneath the doped alumina layer. As before, chrome, nickel and both nickel and chrome, respectively, were also found in the alumina-silicate layer. All of the coatings were adherent in spite of the thermal expansion coefficient mismatch from the starting materials. The substrates were subsequently exposed to 72 hours at 1000°C in 100% humidity, and analysis is currently being completed.

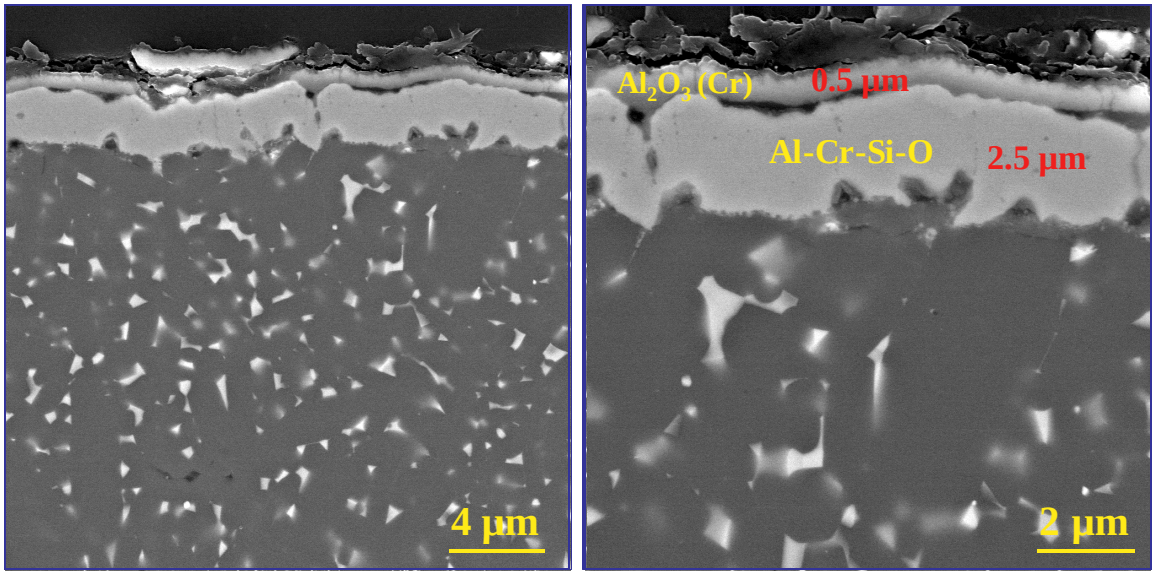

Figure 4. Polished cross section of Cr_2AlY coating on SN282 silicon nitride substrate exposed to oxygen at 1150°C for 30 minutes

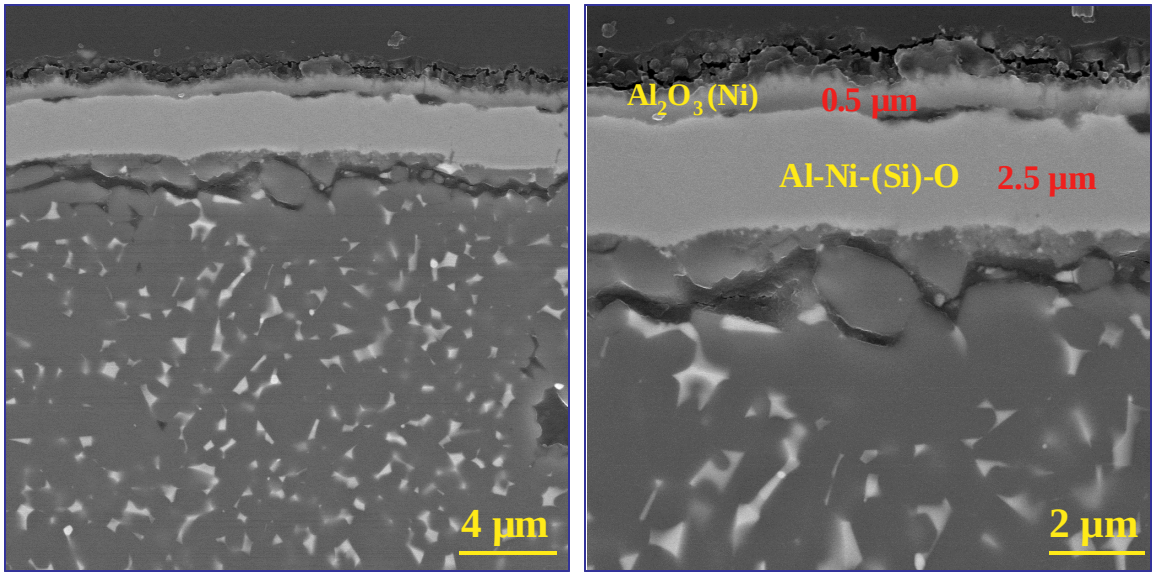

Figure 5. Polished cross section of NiAlHf coating on SN282 silicon nitride substrate exposed to oxygen at 1150°C for 30 minutes

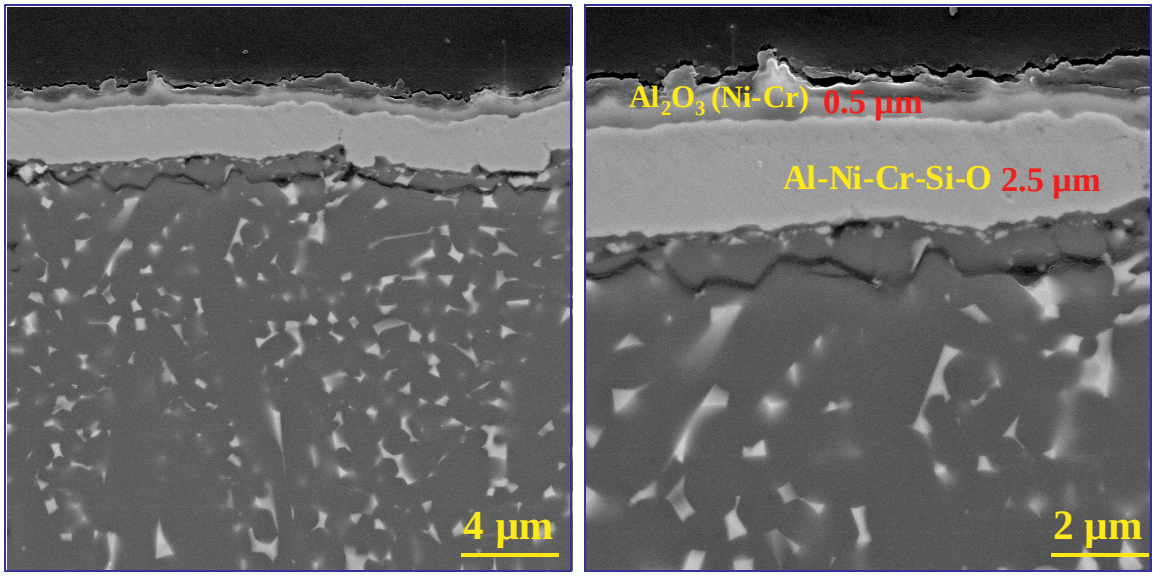

Figure 5. Polished cross section of NiCrAlY coating on SN282 silicon nitride substrate exposed to oxygen at 1150°C for 30 minutes

Status of Milestones

Evaluate the protective capacity of new silicate coatings on Si3N4 in simulated combustion environment. (June 2002)

Industry Interactions

Discussions with UTRC and GE Corporate R&D have continued. This project has collaborated with an ARTD Fossil Energy project on Corrosion Resistant Coatings.

A presentation on environmental protection systems produced by surface alloying was given at Honeywell Engines and Systems in Phoenix on March 20, 2002.

Problems Encountered

None.

Publications/Presentations

None.

High-Temperature Diffusion Barriers for Ni-Base Superalloys

B. A. Pint, J. A. Haynes, K. L. More and I. G. Wright
Metals and Ceramics Division
Oak Ridge National Laboratory
Oak Ridge, TN 37831-6156
Phone: (865) 576-2897, E-mail: pintba@ornl.gov

Objective

Aluminide coatings for high-temperature corrosion resistance are degraded by the loss of Al due to oxidation but much more Al is lost due to interdiffusion with the underlying Ni-base superalloy substrate. The goal of this program is to fabricate and assess potential compounds for use as high-temperature diffusion barriers between coating and substrate. Ideally, the barrier would act to reduce the inward diffusion of Al as well as the outward diffusion of substrate elements (such as Cr, Re, Ta, W) which generally degrade the oxidation resistance of the coating. The work is motivated by previous experimental results which suggested some compositions that exhibited diffusion-barrier capabilities. A secondary objective will be to demonstrate routes to fabricating diffusion aluminide coatings incorporating a diffusion barrier.

Highlights

Nickel-base superalloy substrates were coated by an outside vendor and initial aluminizing has been conducted. The rate of coating growth during aluminizing was significantly reduced by the presence of the metallic sputter coating. This result agreed with previous observations and supports the premise of a diffusion barrier compound being formed via the proposed process.

Technical Progress

Superalloy substrates were machined from single-crystal René N5 ingots obtained from Howmet Corporation (Whitehall, MI). These superalloy castings were electro-discharge machined into substrate discs (1.65 cm diameter x 0.16 cm thick). Hafnium was chosen to form a potential diffusion barrier during aluminizing by chemical vapor deposition (CVD). It was deposited onto one surface of a large batch of René N5 disc substrates via magnetron sputtering by a commercial source (Surmet Corporation, Boston, MA). Three different thicknesses were deposited.

The sputter-coated superalloys were aluminized in a laboratory-scale CVD reactor in order to determine the feasibility of the proposed process. Some initial problems were encountered with bubbling of the coatings (which is common for sputter coated specimens), after which a pre-aluminizing heat treatment was added to the process. Coating mass gains were used to measure the amount of Al deposited. After deposition, coating surfaces were characterized by scanning electron microscopy (SEM) and metallographic cross-sections were made.

Table I compares fabrication conditions and mass gains of the first three batches of CVD aluminide coatings with diffusion barriers (2 specimens per batch). The last four coatings on the list are CVD NiAl coatings that were previously fabricated on the same superalloy substrates under identical aluminizing conditions (6h, 1150°C), but with no sputter coating. The table also indicates which of the sputtered specimens were heat-treated prior to aluminizing to reduce the bubbling.

Table I. Fabrication of CVD aluminide coatings with and without sputtered diffusion barriers

CVD Batch	Hf Thickness* (μm)	Heat Treat	Mass Gain (mg)
1	7	No	7.6
1	4	No	13.6
2	4	Yes	6.8
2	1	Yes	10.7
3	1	Yes	20.4
3	7	Yes	4.9
(Previous work)	0	No	21.0
(Previous work)	0	No	20.6
(Previous work)	0	No	21.2
(Previous work)	0	No	21.0

* Specimens were sputter coated on one side prior to aluminizing.

Comparison of mass gains for the diffusion barrier specimens and CVD NiAl specimens showed that the presence of the sputtered material reduced the specimen mass gain (implying a reduced thickness of the aluminide layer), especially for the thicker sputter coatings. The average mass gain for the CVD NiAl coatings with no sputter layer was approximately 21 mg. In contrast, diffusion barrier specimens with 7μm sputter layers on one surface showed total mass gains of just 4.9 and 7.6 mg. Clearly, aluminizing mass gain decreased as coating thickness increased. However, decreases in mass gain with a 7μm thick coating were substantial and higher than expected, considering that one side of the specimen was not sputter coated. It is possible that the mass gains were affected by the loss of sputtered material during the early stages of aluminizing due to reactions with the chloride atmosphere.

The surfaces of an aluminide coating with a 7μm sputtered diffusion barrier were examined by SEM. The coatings consisted of large polygonal grains (20 – 100 μm diameter) with ridges over the grain boundaries, similar to the structure formed without a sputtered coating. Thus, it appears that the presence of the diffusion barrier slows coating growth, but does not prevent normal formation of the aluminide grains, as expected.

Figure 1 shows polished cross-sections of the first specimen aluminized with a 7μm thick sputter coating. Microchemical analysis has not been completed but certain microstructural differences between the sputtered and non-sputtered sides are clear. First, Figure 1a shows a typical CVD NiAl coating formed on the side without a sputtered coating. There is a single-phase aluminide surface layer with an underlying multi-phase interdiffusion zone.. The original superalloy surface is the interface between the aluminide layer and the interdiffusion zone.

Figure 1b shows the cross-section of the Hf-coated surface of the same specimen. In this case, extra layers are present and the outer single-phase layer of aluminide is of reduced thickness as suggested by the mass change difference (Table I). The bright-contrast region beneath the single-phase

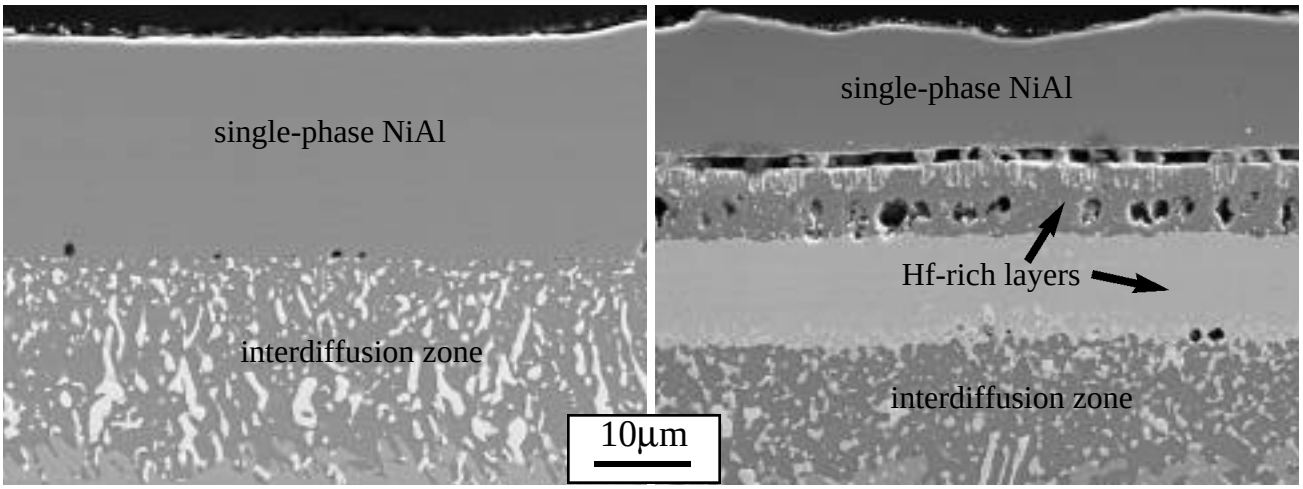

Figure 1. SEM secondary electron images of polished cross-sections of the first coating formed on a René N5 substrate with a sputter coating on one side. (a) uncoated side with a single-phase NiAl outer layer and interdiffusion zone and (b) the sputter-coated diffusion barrier side of the same specimen.

(β-NiAl) layer and another as-yet-unidentified layer is rich in Hf. The thickness of the single-phase region was about 60% that of the β-NiAl layer on the uncoated side. However, the differences in mass gain suggest an even greater difference in thickness, part of which may be explained by a reduced interdiffusion region beneath the sputtered layer (due to reduced inward diffusion of Al). Further characterization is necessary to better understand the coating formed on the sputter-coated side. After characterization, specimens will be tested under cyclic oxidation conditions in order to determine the high-temperature performance of the Hf-modified coatings.

Status of Milestones

FY2002
Develop methods for fabricating nickel-based aluminide bond coatings requiring no Ni diffusion from the superalloy substrate.
(September 2002)

Industry Interactions

The project team had interactions with Surmet Corporation regarding diffusion barrier compound fabrication. Bond coating performance and diffusion barrier concept were discussed with representatives of General Electric Power Generation and Siemens-Westinghouse.

Problems Encountered

None

Publications

None

POWER ELECTRONICS

Development of High-Efficiency Carbon Foam Heat Sinks for Microturbine Power Electronics

J. W. Klett, A. D. McMillan, N. C. Gallego
Metals and Ceramics Division
Oak Ridge National Laboratory
P.O. Box 2008, Oak Ridge, TN 37831-6087
Phone: 865-574-5220, E-mail: klettjw@ornl.gov

Objective

Conventional heat sinks are used to cool the power electronics of today's microturbines. Unfortunately, there are situations in hot climates or enclosed spaces where it is very difficult to sufficiently cool the electronics. Furthermore, these heat sinks become very large and heavy when scaled up to be suitable for larger (several hundred kilowatts) advanced high-efficiency microturbines. Therefore, ultra-efficient heat sinks that utilize high conductivity, high surface area graphite foam are being developed.

Highlights

Two new heat sinks based upon evaporative cooling have been designed and fabrication is almost complete.

Technical Progress

Two designs were developed to take advantage of the unique characteristic of the graphite foam: specifically the combination of high ligament thermal conductivity and high specific surface area. The basic premise of the evaporative cooling is illustrated in Figure 1. The Passive Evaporative Cooling Sink (PECS) is designed to be a retrofit or replacement for current machined finned aluminum or copper heat sinks and the principle is quite simple. The PECS system is hollow and contains an evaporator (graphite foam) and a working fluid at a reduced pressure equal to the fluids vapor pressure at room temperature. Heat is added to the bottom of the PECS and passes through the metal base plate (Figure 1). This heat is then transferred to the graphite foam through a soldered or brazed joint. The extremely high ligament thermal conductivity (equivalent to diamond) rapidly transmits the heat to all the internal surfaces of the foam. Concurrently, capillary action wicks the working fluid (perflurocarbon or water) into the foam and coats the internal surfaces. After all the permanent gases (gases which do not condense such as oxygen or nitrogen) are removed, any heat that is added to the system disturbs the equilibrium and the working fluid evaporates (or boils) since the system's pressure maintained the boiling point of the fluid at room temperature. The vapor then traverses the foam and the evaporative chamber to condense on a wall of the chamber that is cooled externally (typically with air). In this manner, the fluid condenses at the same temperature that it was evaporated, and thus the system is isothermal. The advantage of the graphite foam is that its extremely high surface area results in dramatically higher heat fluxes that can be transmitted to the working fluid. This has been demonstrated in collaboration with the National Security Agency and the University of Maryland. In recent tests, heat fluxes as high as 115 W/cm^2 have been reported at chamber temperatures of 85°C.

The biggest issue in the current designs is that when more fluid is vaporized at higher heat fluxes, there is a limiting amount of surface area for condensation (Figure 1). A limit in the area to transfer the heat from the chamber to the air results in a rise in the internal pressure of the system which, in turn, changes the thermodynamic equilibrium (vapor pressure) of the system and increases the chamber temperature. This rise in chamber temperature results in a decrease in effective heat flux. So the key has been to optimize the internal surface area for condensation of the working fluid.

Many designs of these types of systems simply add a finned heat sink to the outer chamber, but the heat is limited by thermal conduction of the metal, and the advantages of the evaporation is negated. The key is to have the heat pass through a thin layer of metal directly to the cooling fluid and minimize any thermal conduction in the system. As more of the system relies on thermal conduction, the effectiveness of the devices will be limited. Therefore, it is critical that the heat is removed from the system at the point where it is condensed and no thermal conduction to an external surface area is required (like the finned heat sink we are replacing)

The first design (illustrated in Figures 3-5) is a simulation of a standard finned heat sink as the method for improving the internal surface area. The concept is to use a hollow finned heat sink to be the location of the surface for condensing the working fluid. This will increase the surface area for heat transfer by more than 20x and, therefore, should improve the heat fluxes by a similar amount. However, to construct this design, a series of corrugated aluminum fins was made as the hollow fin structure. A support structure was designed for the corrugated fins to slide onto, thus sealing the ends and producing a hollow finned structure that is hermetic. Then, this hollow finned chamber is bolted the bottom plate which has the graphite foam bonded to its cavity (see Figure 3-5).

Knowing that this first concept is difficult to construct and will be very difficult to manufacture, a second design was developed in which the hollow finned cavity was replaced with a simple box with many tubes passing through it (Figure 6). This will allow air or water to be passed through the cooling tubes to facilitate the rapid transfer of the latent heat of condensation to the cooling fluid while still maintaining a significant increase in condensation area.

After receiving the two new designs, they will be assembled at ORNL and tested on a model system that is capable of delivering 3600 watts for simulating a microturbine power electronic system. After testing the sub-scale designs, a full-scaled design will be fabricated and tested on a complete microturbine.

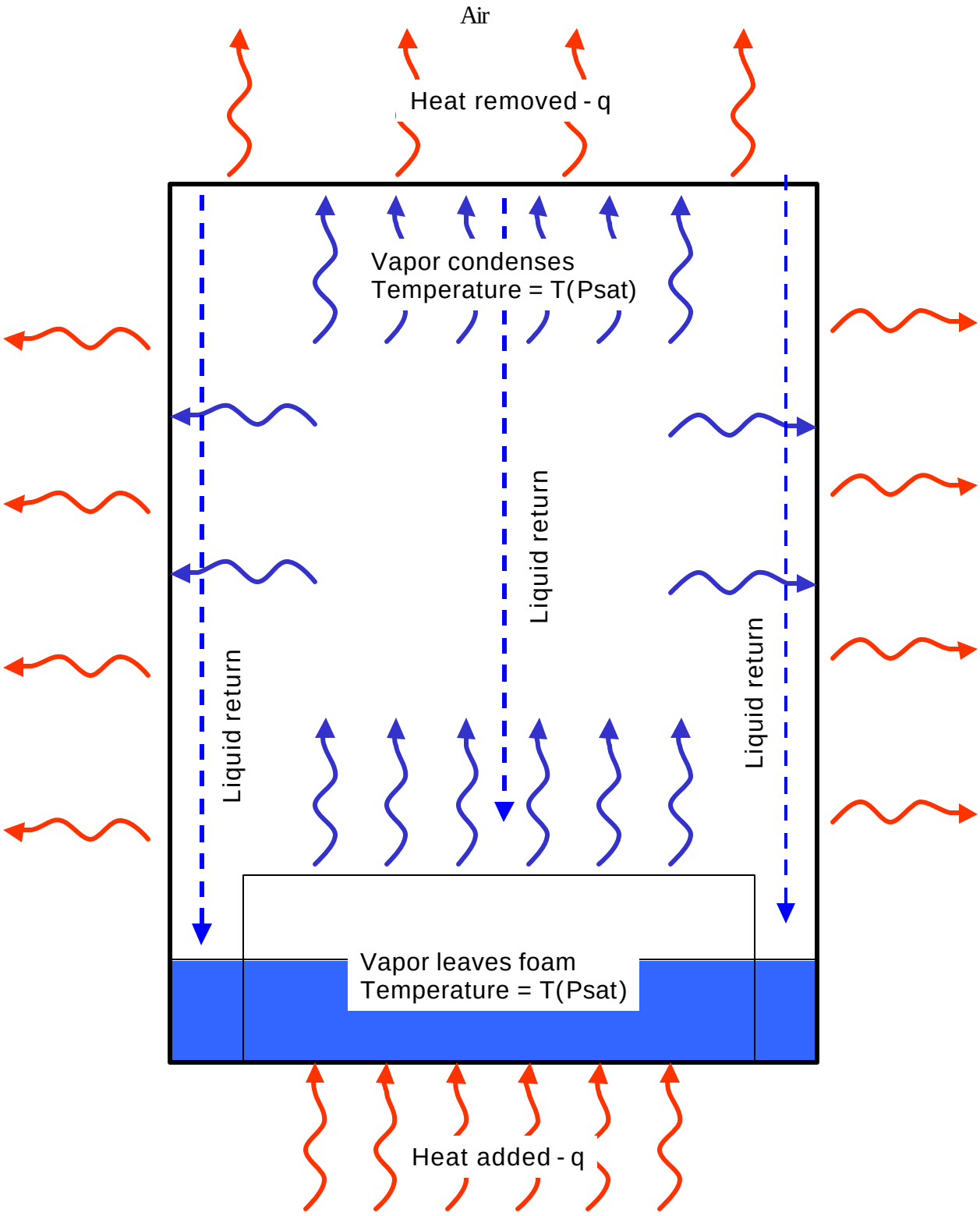

Figure 1. Illustration of concept of evaporative cooling with graphite foam.

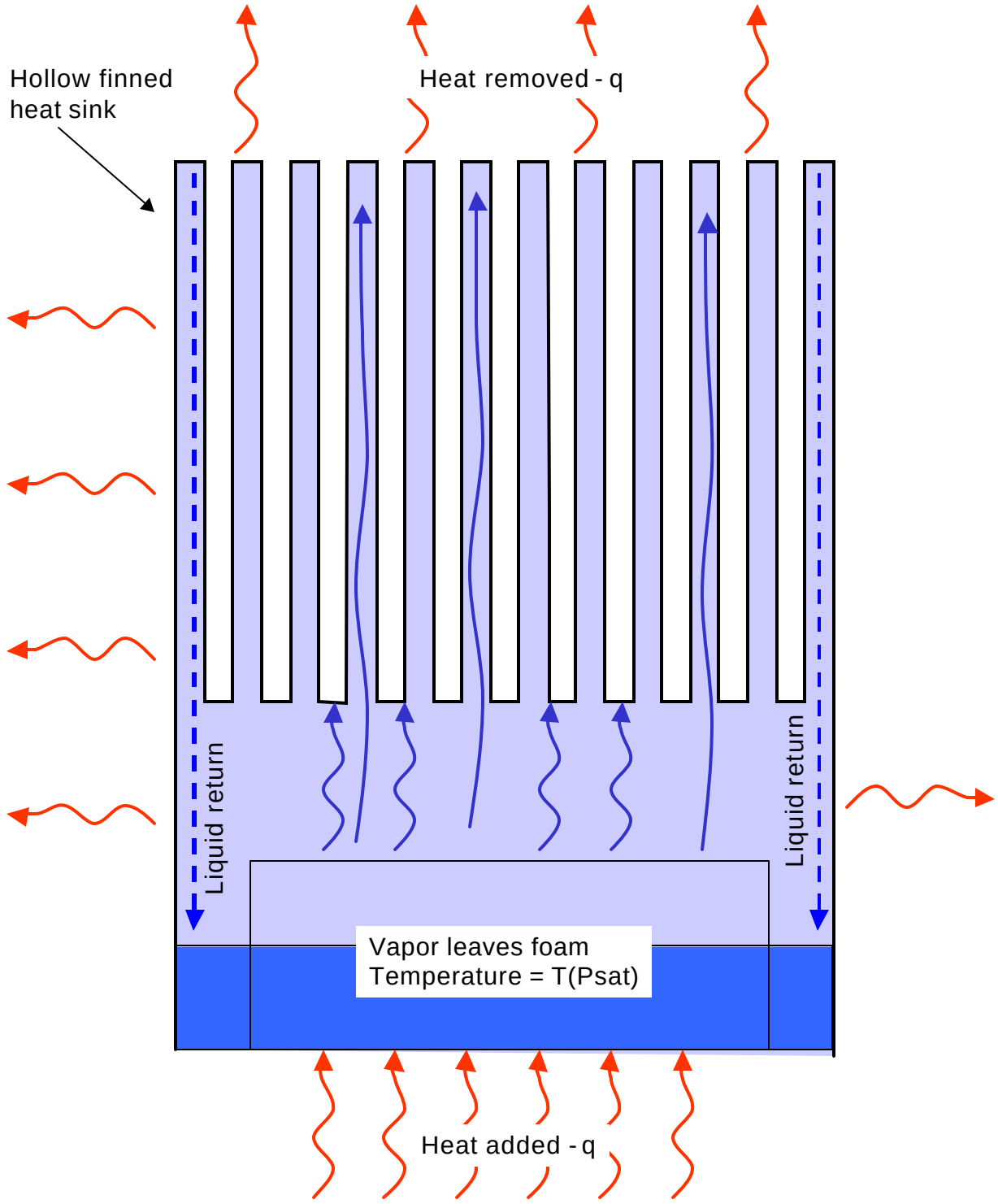

Figure 2. Schematic of improved design to enhance internal surface area for condensation.

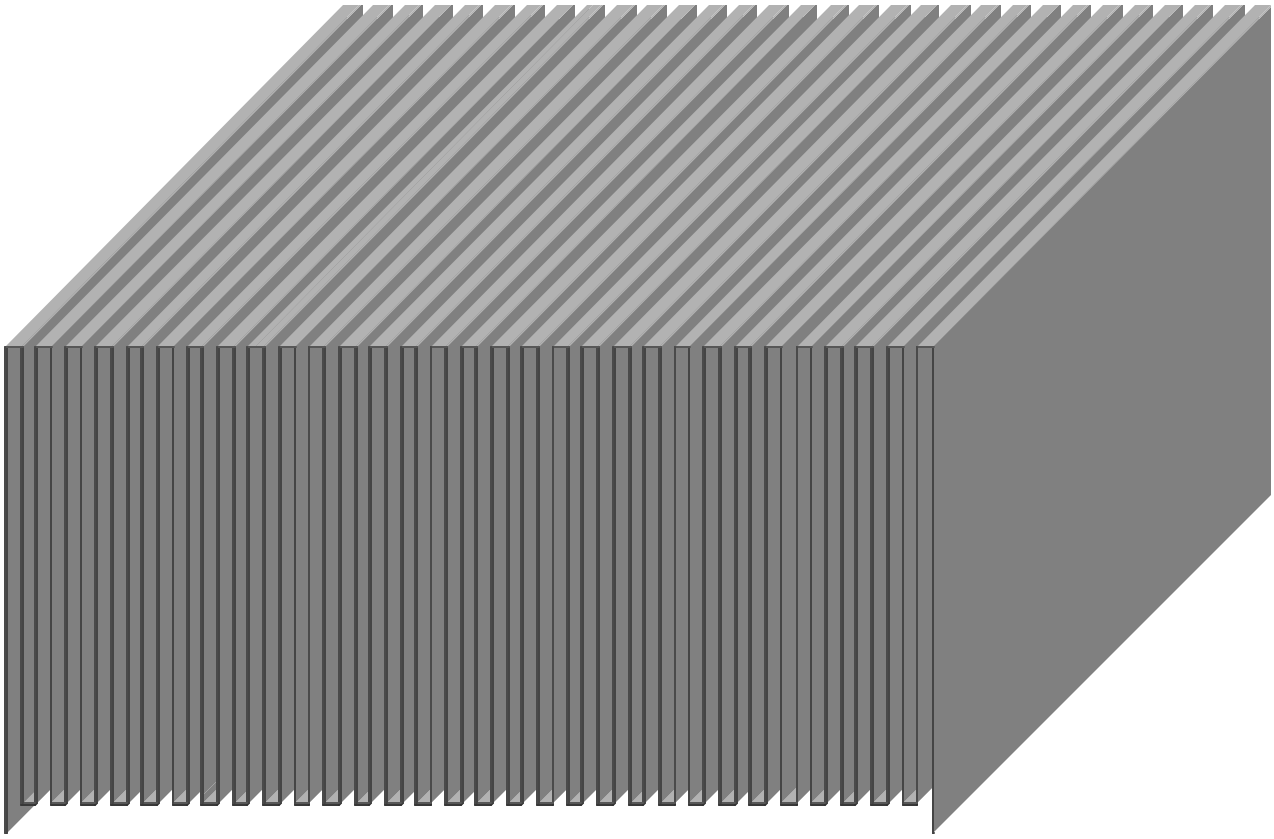

Figure 3. Corrugated aluminum fins to mount over support structure shown in figure 4. Ends will be soldered, brazed, or epoxied, depending on best method of providing hermetic seal.

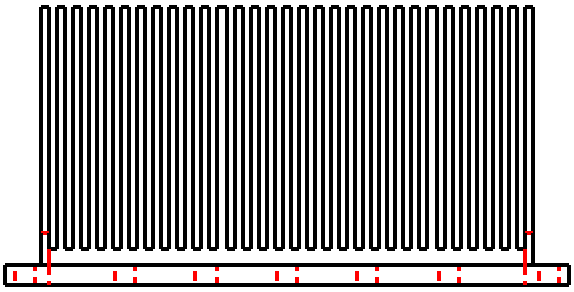

Side view

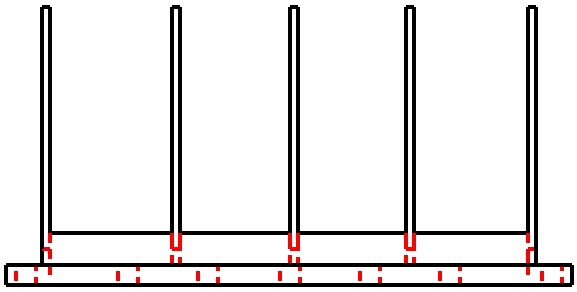

Front view

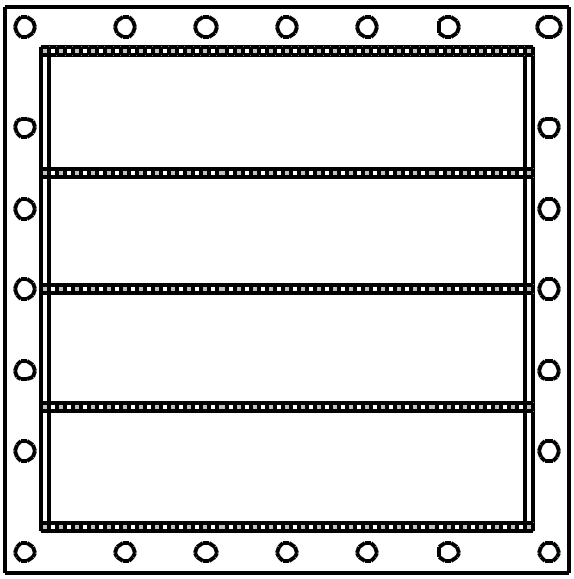

Top view

Figure 4. Support structure for corrugated fins shown in Figure 3. The result will provide a hollow finned heat sink to be placed over a graphite foam evaporator (illustrated in Figure 5). The evaporation of the working fluid will remove significantly more heat than standard heat sinks and the hollow heat sink will provide the proper surface area for condensation of the working fluid in a small package.

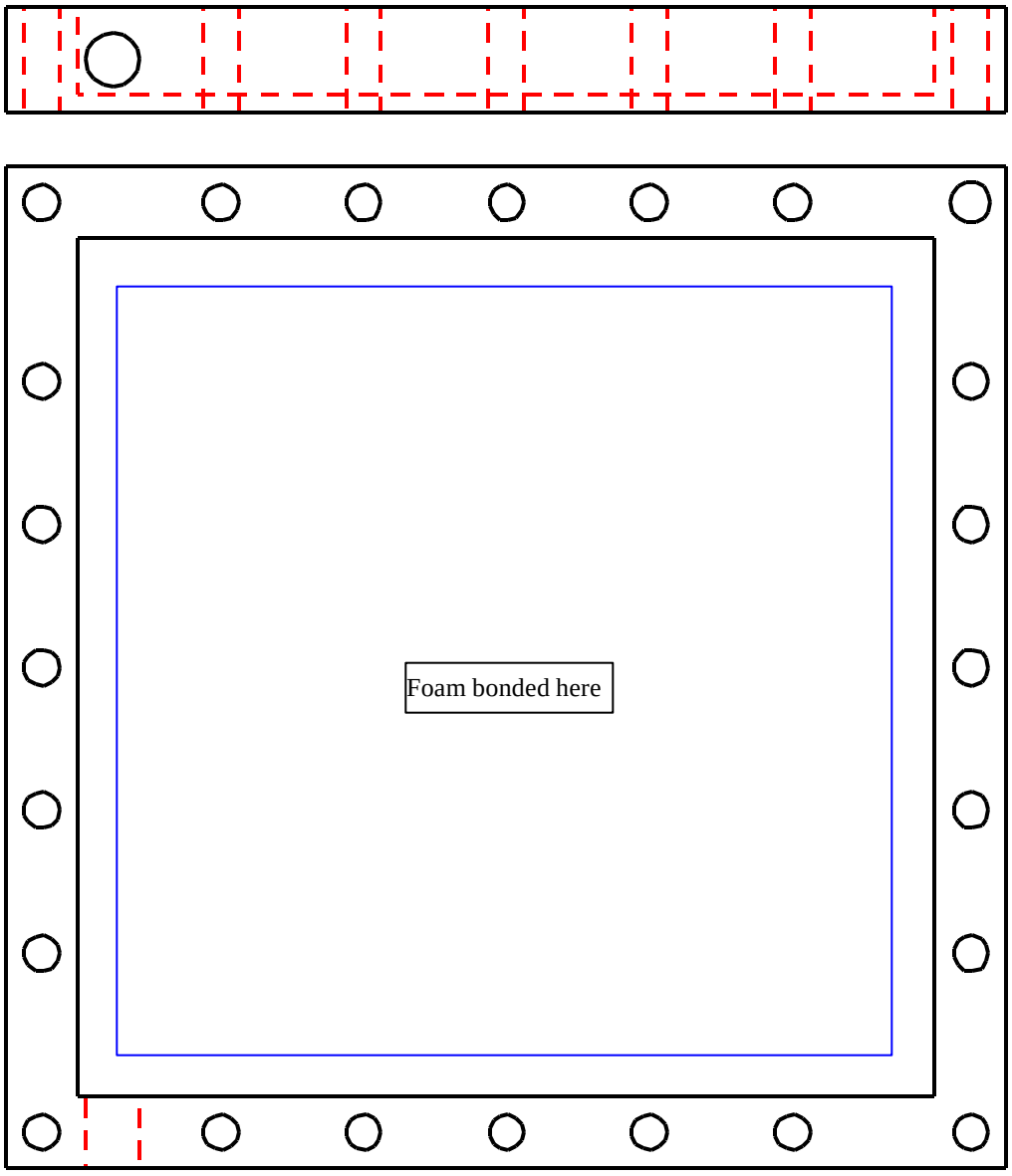

Figure 5. Base plate of evaporative chamber. Foam will be bonded to the inside of the base plate to facilitate evaporation.

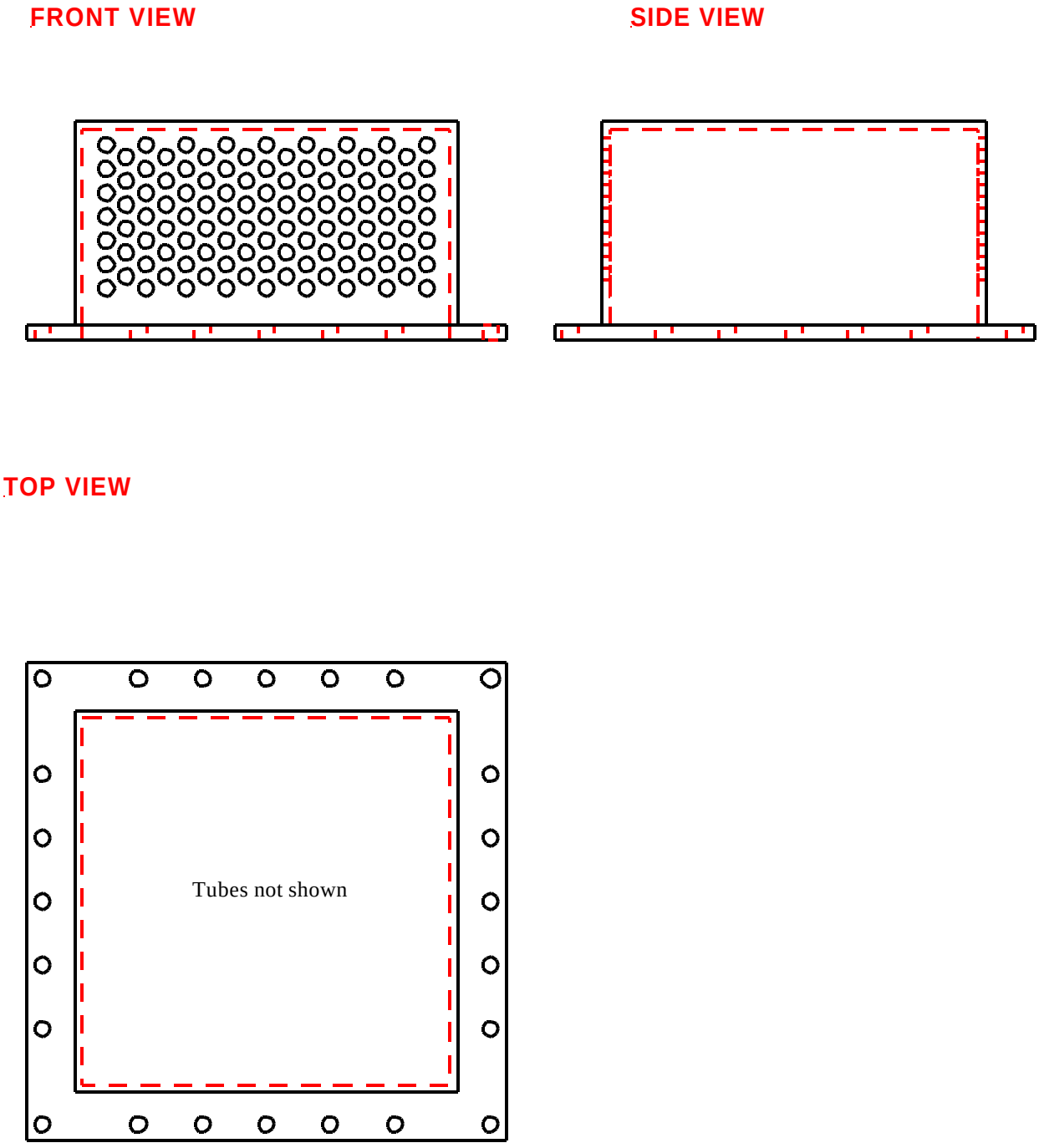

Figure 6. Design 2 incorporates tubes to increase surface area of condensation and improve performance.

Status of Milestones

Milestone 1: Design, fabricate, and evaluate an improved heat sink based on evaporative cooling for power electronics on microturbines (September 2, 2002).

- This milestone in nearly complete in that the heat sinks have been designed and are being fabricated. The devices will then be installed in the test device and evaluation should be completed in the next several months.

Problems Encountered

None.

Publications/Presentations

None.

MATERIALS FOR ADVANCED RECIPROCATING ENGINES

Development of an Ultra Lean Burn Natural Gas Engine

R. M. Wagner, T. J. Theiss, J. H. Whealton, J. M. Storey, and J. B. Andriulli,
Oak Ridge National Laboratory
2360 Cherahala Blvd.
Knoxville, TN 37932
Phone: 865/946-1348; E-mail: Theisstj@ornl.gov

Objective

Distributed generation (DG) is becoming an increasingly important factor in our nation's energy infrastructure. The restructuring of the electrical grid coupled with increased electrical demand could have a negative environmental impact if older, less efficient power plants are forced back into service. Natural gas (NG), however, is a relatively "clean" fuel source especially while alternative technologies are being investigated to take advantage of renewable energy sources. The use of NG reciprocating engines for DG is an important step toward meeting the energy demand while minimizing the environmental impact. The objectives of this NG reciprocating engine program are to improve electrical efficiency, reduce NO_x emissions, and reduce operating and maintenance costs. The results of this endeavor will be available to industry for use in their own evaluations and testing to aid in commercialization of the technology.

Highlights

The rotating arc spark plug (RASP) has been used in the Kohler engine for a short period of time. Design modifications have been incorporated to correct difficulties experienced with the plug during this run.

Technical Progress

Ignition System Development Task

The ignition system for the rotating arc spark plug was integrated into the engine timing circuits. An inductance ignition is being used to fire the rotating arc spark plug (RASP). During this reporting period, the RASP successfully fired the Kohler engine. During testing, it was discovered that the initial RASP design was prone to overheating of the magnet since the magnet experiences the combustion temperature. Overheating of the magnet can and did reduce the magnet strength to a point where it is no longer effective.

A second iteration of the RASP designed to reduce the magnet temperature was fabricated during the reporting period. The original and modified RASP plugs are shown in Fig. 1. The modified RASP is currently undergoing bench testing at elevated pressure in a spark plug test chamber.

Engine Integration and Demonstration Task

A 9.5 kW Kohler NG generator is being used to evaluate the new technologies proposed for achieving ultra lean burn combustion. The generator set is a stationary system sized for a small home and provides an excellent platform for demonstrating the new technologies outlined in the

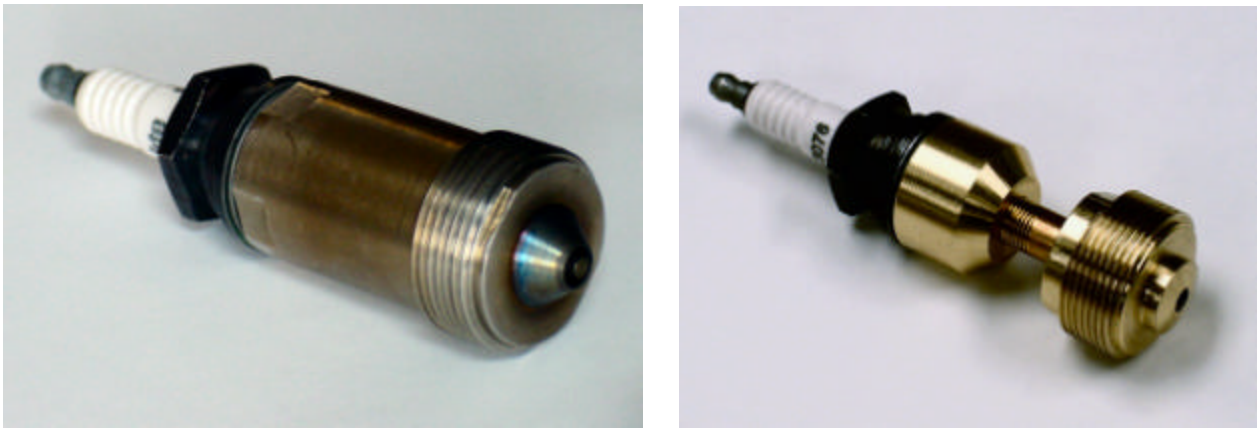

Fig. 1 Original (left) and modified (right) rotating arc spark plugs.

original proposal. The generator set is based on an 18 kW natural gas Kohler Command two-cylinder engine. The key feature of this engine is aluminum heads, which is currently a requirement for use with the new ignition system. In addition, the intake manifold is well suited for converting the engine to port fuel injection if necessary.

An after-market engine control system has been installed on the dynamometer engine and is now fully operational. The system controls ignition timing and fuel injection parameters based on lookup tables. The lookup tables currently use engine speed, air-fuel ratio, and manifold absolute pressure (MAP) to determine the proper ignition and fuel injection parameters. Due to issues with the MAP reading, instrumentation is being added to replace MAP with throttle position in the lookup tables. Referencing of the ignition and fuel injection events was an issue since the Kohler engine does not have a synchronizing cam sensor. This issue was resolved by interfacing the control system with an in-cylinder pressure transducer and the shaft encoder via electronics to properly synchronize the events to the engine.

Preliminary lean burn characterization experiments were performed during this reporting period to shake out any remaining problems with the setup. Several minor issues with the low-speed data acquisition system were encountered. These issues are currently being resolved. The lean burn characterization is on schedule to be completed in June 2002.

Status of Milestones

The milestones for the duration of this project are listed below.

Ignition system development (Due December 2001)- This milestone has been met. The RASP system has been demonstrated on the bench and reported. The RASP will be integrated into the engine ignition system and demonstrated in a later milestone. We are continuing work on the follow up milestone and expect to meet it on schedule.

Characterize engine under lean burn conditions (Due June 2002) – The lean burn characterization of the Kohler engine has been started. We are on schedule to meet this milestone.

Characterize engine with hydrogen addition under lean conditions (Due September 2002) - Hydrogen will be added to the engine to quantify lean burn improvement due to the hydrogen addition. Bottled gases will be used for the hydrogen in a mixture simulating reformer composition.

Characterize engine with RASP under lean conditions (Due December 2002) - The rotating arc spark plug will be re-introduced to the engine and the system will be characterized under lean conditions. This will determine the extent of improvement associated with the new spark plug and provide a basis for combining the above two tasks.

Demonstrate lean burn with hydrogen addition and RASP (Due June 2003) - The previous three tasks will be combined and the engine will be operated under lean burn conditions using the new spark plug with the addition of hydrogen from bottled gas.

Industry Interactions

Ron Fiskum, DOE/OPT, visited the NTRC during this reporting period and was shown this and other related activities.

Tim Theiss has been asked to manage for ORNL one of the Integrated Energy Systems projects (formally Building, Cooling, Heating, and Power Program) - "Wakeusha Engine Modular BCHP System". He visited with Gas Technology Inc., and participated in a kick-off meeting with GTI, Ballard Engineering, and Trane Inc. on this project. This is the only IES project that uses a reciprocating engine as its prime mover.

Tim Theiss, John Whealton, and Jim Conklin, visited with Cummins Inc. during the reporting period to discuss ignition system issues. The project discussed is not funded by ARES but definitely underscored the importance of ignition development.

Problems Encountered

None.

Publications/Presentations

None.

Advanced Materials for Exhaust Components of Reciprocating Engines

P. J. Maziasz
Metals and Ceramics Division
Oak Ridge National Laboratory
P.O. Box 2008, Oak Ridge, TN 37831-6115
Phone: (865) 574-5082, E-mail: maziaszpj@ornl.gov

Objective

The goal of this program is to address the specific high-temperature and performance limitations of austenitic stainless steels and alloys either being used (i.e. wrought stainless steel exhaust valves) or being considered (i.e. cast stainless steels) for various critical exhaust components (exhaust valve, exhaust manifold, turbocharger housing) for advanced natural gas reciprocating engine systems (ARES). At 650-800^{o}C, stainless steels can replace low-cost materials that have exceeded their temperature capabilities in some cases (i.e., SiMo ductile cast iron), while in other cases stainless steels must give way to much stronger and more expensive materials like Ni-based superalloys. The approach will be to define the problem through careful comparison of fresh and engine-exposed austenitic stainless steel and alloy components (if available), and then improving performance, aging resistance and reliability through judicious modifications of alloy composition and/or processing.

Highlights

This is a new project that began during FY2002. Prior interactions with Waukesha Engine Dresser, Inc. and their component supplier, TRW, Inc., reached agreement for them to provide several exhaust valve components to ORNL for characterization and analysis. This quarter (2nd, FY2002), stainless steel and nickel-based superalloy valves that fresh (as-made) and tested for significant times in natural gas reciprocating engines without failure were received at ORNL from Waukesha Engine Dresser, Inc. These valves are currently being sectioned for microstructural characterization and analysis, particularly define and understand the effects of high-temperature aging. These observations will provide the basis for defining either alloy composition or processing modifications to improve the high temperature performance and durability of both kinds of valves.

Discussion also continued this quarter with Cummins Power Generation to better define their interest in similar analysis of several different kinds of exhaust components.

The goal of this project is to define the metallurgical effects of engine service and aging on various exhaust components, particularly those made of austenitic stainless steel. Such information will then be used to improve the high-temperature performance and durability of

wrought and cast austenitic stainless steels, with input from the commercial parts supplier, to enable their use in advanced reciprocating engines.

Technical Progress

New program in 1st quarter FY2002.

Status of Milestones

New Program

FY 2003 – Obtain and characterize fresh and engine-exposed exhaust components (i.e. valves, manifolds) from current engines and define metallurgical effects related to performance limitations (Nov. 2002).

Industry Interactions

Discussions continued with Waukesha Engine Dresser, Inc. (R.J. Kakoczki, Director of Technology) about examining exhaust valves. A non-disclosure agreement was signed this quarter. Discussions also continued with Cummins Engine Company, Inc.(D.A. Bolis, Technical Advisor – Natural Gas Engines) to define their specific exhaust component interests and priorities with ORNL.

Problems Encountered

None.

Publications/Presentations

None.

Internal Distribution

B. L. Armstrong, 4515, MS-6063, armstrongbl@ornl.gov
P. F. Becher, 4515, MS-6068, becherpf@ornl.gov
T. M. Besmann, 4515, MS-6063, besmanntm@ornl.gov
C. A. Blue, 4508, MS-6083, blueca@ornl.gov
M. A. Brown, 4500N, MS-6186, brownma@ornl.gov
M. K. Ferber, 4515, MS-6069, ferbermk@ornl.gov
J. A. Haynes, 4515, MS-6063, haynesa@ornl.gov
D. R. Johnson, 4515, MS-6066, johnsondr@ornl.gov
M. A. Karnitz, 4500N, MS-6186, karnitzma@ornl.gov
J. O. Kiggans, 4508, MS-6087, kiggansjojr@ornl.gov
J. W. Klett, 4508, MS-6087, klettjw@ornl.gov
E. Lara-Curzio, 4515, MS-6069, laracurzioe@ornl.gov
H. T. Lin, 4515, MS-6068, linh@ornl.gov
R. A. Lowden, 4515, MS-6063, lowdenra@ornl.gov
P. J. Maziasz, 4500S, MS-6115, maziaszpj@ornl.gov
K. L. More, 4515, MS-6064, morekl1@ornl.gov
B. A. Pint, 4500S, MS-6156, pintba@ornl.gov
D. T. Rizy, 3147, MS-6070, rizydt@ornl.gov
D. P. Stinton, 4515, MS-6063, stintondp@ornl.gov
R. W. Swindeman, 4500S, MS-6155, swindemanrw@ornl.gov
P. F. Tortorelli, 4500S, MS-6156, tortorellipf@ornl.gov
I. G. Wright, 4500S, MS-6157, wrightig@ornl.gov
A. Zaltash, 3147, MS-6070, zaltasha@ornl.gov

External Distribution

ALLISON ADVANCED DEVELOPMENT CO., 1100 Wilson Blvd., Suite 1450, Arlington, VA 22209
J. Miles, r.jeffrey.miles@allison.com

ALM SYSTEMS, INC, 1920 N Street, NW, Suite 750, Washington, DC 20036
M. Kalin, mkalin@ibek.com

ARGONNE NATIONAL LABORATORY, 9700 S. Cass Ave., Argonne, IL 60439-4838
W. Ellingson, ellingson@anl.gov

BATTELLE MEMORIAL INSTITUTE, 505 King Avenue, Columbus, OH 43201
D. Anson, ansond@battelle.org

BAYSIDE MATERIALS TECHNOLOGY, 21150 New Hampshire Ave., Brookville, MD 20833
D. Freitag, dfreitag@ix.netcom.com

BCS, INC., 5550 Sterrett Place, Suite 216, Columbia, MD 21044
D. Bartley, dbartley@bcs-hq.com

BOWMAN POWER, 20501 Ventura Boulevard #285, Woodland Hills, CA 91364
T. Davies, tdavies@bowmanpower.demon.co.uk
T. Hynes, adh.bowmanpower@att.net
K. Mehrayin, kmehrayin@bowmanpower@com

CALIFORNIA ENERGY COMMISSION
A. Soinski, asoinski@energy.state.ca.us

CANNON-MUSKEGON CORP., Box 506, Muskegon, MI 49443-0506
J. Wahl, jwahl@canmkg.com

CAPSTONE TURBINE CORP., 6430 Independence Ave., Woodland Hills, CA 91367
P. Chancellor, pchancellor@capstoneturbine.com
K. Duggan, kduggan@capstoneturbine.com
M. Stewart, mstewart@capstoneturbine.com
J. Willis, jwillis@capstoneturbine.com
M. Rodrigues, mrodrigues@capstoneturbine.com
B. Treece, btreece@capstoneturbine.com

CLEMSON UNIVERSITY, South Carolina Institute for Energy Studies, 386-2, Clemson, SC 29634-5180
L. Golan, glawren@clemson.edu
R. Wenglarz, rwnglrz@clemson.edu
J. Hinson, jhinson@clemson.edu

CONNECTICUT RESERVE TECHNOLOGIES, 2997 Sussex Ct., Stow, OH 44224
E. Baker, baker@crtechnologies.com
S. Duffy, sduffy@crtechnologies.com
J. Palko, jpalko@crtechnologies.com

DTE ENERGY, 37849 Interchange Dr., Suite 100, Farmington Hills, MI 48335
M. Davis, davism@dteenergy.com

ELECTRIC POWER RESEARCH INSTITUTE, 3412 Hillview Ave., Palo Alto, CA 94303
J. Stringer, jstringe@epri.com

ELGILOY SPECIALTY METALS, 1565 Fleetwood Drive, Elgin, IL 60123
T. Bartel, terryb@elgiloy.com

ELLIOTT ENERGY SYSTEMS, 2901 S.E. Monroe Street, Stuart, FL 34997
D. Burnham, dburnham@elliott-turbo.com

ENERGETICS, INC., 501 School St., SW, Suite 500, Washington, DC 20024
R. Scheer, rscheer@energeticsinc.com

ENERGY TECHNOLOGIES APPLICATIONS, 5064 Camino Vista Lujo, San Diego, CA 92130-2849

T. Bornemisza, borneger@ix.netcom.com

GAS TURBINE ASSOCIATION, 1050 Thomas Jefferson St., NW, 5th Fl, Washington, DC 20007

J. Abboud, abboud@advocatesinc.com

GENERAL ELECTRIC (GE) CR&D, 1 Research Circle, Building K1-RM 3B4, Niskayuna, NY 12309

S. Correa, correa@crd.ge.com
K. Luthra, luthra@crd.ge.com
J. VanDerwerken, vanderwerken@crd.ge.com
C. Johnson, johnsonca@crd.ge.com

GENERAL ELECTRIC AIRCRAFT ENGINES, One Neumann Way, Mail Drop M89, Cincinnati, OH 45215-1988

R. Darolia, ram.darolia@ae.ge.com

GENERAL ELECTRIC POWER SYSTEMS, One River Rd., 55-127, Schenectady, NY 12345

R. Orenstein, robert.orenstein@ps.ge.com

GENERAL ELECTRIC POWER SYSTEMS, Gas Technology Center, 300 Garlington Road, Greenville, SC 29615

P. Monaghan, philip.monagham@ps.ge.com

HAYNES INTERNATIONAL, INC., 1020 W. Park Avenue, P.O. Box 9013, Kokomo, IN 46904-9013

V. Ishwar, vishwar@haynesintl.com
D. Klarstrom, dklarstrom@haynesintl.com

HONEYWELL CERAMIC COMPONENTS, 2525 W. 190th St., Torrance, CA 90504

D. Foley, dan.foley@honeywell.com
C. Li, chien-wei.li@honeywell.com
D. Newson, danielle.newson@honeywell.com
M. Savitz, maxine.savitz@honeywell.com
J. Wimmer, jim.wimmer@honeywell.com
M. Mitchell, michele.mitchell@honeywell.com

HONEYWELL COMPOSITES, 1300 Marrows Rd., PO Box 9559, Newark, DE 19714-9559

R. Matsumoto, roger.matsumoto@honeywell.com

HONEYWELL ENGINES, SYSTEMS, & SERVICES 2739 E. Washington St., PO Box 5227, Phoenix, AZ 85010

B. Schenk, bjoern.schenk@honeywell.com
M. Masoudipour, mike.masoudipour@honeywell.com

HONEYWELL POWER SYSTEMS, 8725 Pan American Freeway NE, Albuquerque, NM 87113

S. Wright, e.scott.wright@honeywell.com

HOWMET RESEARCH CORP., 1500 South Warner St., Operhall Research Center, Whitehall, MI 49461-1895

B. Mueller, bmueller@howmet.com
R. Thompson, rthompson@howmet.com

INGERSOLL-RAND ENERGY SYSTEMS, 32 Exeter St., Portsmouth, NH 03801

A. Kaplau-Colan, alex_haplau-colan@ingersoll-rand.com
M. Krieger, michael_krieger@irco.com
J. Johnson, jay_johnson@ingersoll-rand.com
J. Kesseli, jim_kesseli@ingersoll-rand.com
J. Nash, jim_nash@ingersoll-rand.com

KINECTRICS NORTH AMERICA, 124 Balch Springs Circle, SW, Leesburg, VA 20175

B. Morrison, blake.Morrison@kinectrics.com

KRUPP VDM TECHNOLOGIES CORP., 11210 Steeplecrest, Suite #120, Houston, TX 77065-4939

D. Agarwal, dcagarwal@pdq.net

NASA GLENN RESEARCH CENTER, 21000 Brookpark Rd., MS 49-7, Cleveland, OH 44135

D. Brewer, david.n.brewer@grc.nasa.gov
J. Gykenyesi, john.p.gyekenyesi@lerc.nasa.gov
S. Levine, stanley.r.levine@lerc.nasa.gov
N. Nemeth, noel.n.nemeth@grc.nasa.gov
B. Opila, opila@grc.nasa.gov

NATIONAL RURAL ELECTRIC COOPERATIVE ASSOC., 4301 Wilson Blvd., SS9-204, Arlington, VA 22203-1860

E. Torrero, ed.torrero@nreca.org

NATURAL RESOURCES CANADA, 1 Haanel Drive, Nepean, Ontario, Canada K1A 1M1

R. Brandon, rbrandon@nrcan.gc.ca

PCC AIRFOILS, INC., 25201 Chagrin Blvd., Suite 290, Beachwood, OH 44122

C. Kortovich, ckortovich@pccairfoils.com

PENN STATE UNIVERSITY, Applied Research Laboratory, PO Box 30, State College, PA 16823

J. Singh, jxs46@psu.edu

PRAXAIR SURFACE TECHNOLOGIES, 1500 Polco St., Indianapolis, IN 46224

R. Novak, richard_c_novak@praxair.com

RICHERSON AND ASSOC., 2093 E. Delmont Dr., Salt Lake City, UT 84117
D. Richerson, richersond@aol.com

ROLLS-ROYCE ALLISON, 2925 W. Minnesota St., PO Box 420, Indianapolis, IN 46241
S. Berenyi, steve.g.berenyi@allison.com
P. Heitman, peter.w.heitman@allison.com
F. Macri, francis.g.macri@allison.com

SAINT-GOBAIN CERAMICS & PLASTICS, INC., Goddard Road, Northboro, MA 01532
R. Licht, robert.h.licht@saint-gobain.com
M. Abouaf

SEBESTYEN, T., Consultant, 6550 Mission Ridge, Traverse City, MI 49686-6123
T. Sebestyen, sebestyen@chartermi.net

SIEMENS WESTINGHOUSE POWER CORP., 1310 Beulah Rd., Pittsburgh, PA 15235-5098
M. Burke, michael.burke@swpc.siemens.com
C. Forbes, christian.forbes@swpc.siemens.com

SOLAR TURBINES, INC., TurboFab Facility, 16504 DeZavala Rd., Channelview, TX 77530
B. Harkins, harkins_bruce_d@solarturbines.com

SOLAR TURBINES INC., 818 Connecticut Ave., NW, Suite 600, Washington, DC 20006-2702
R. Brent, solardc@bellatlantic.net

SOLAR TURBINES, INC., 2200 Pacific Highway, PO Box 85376, MZ R, San Diego, CA 92186-5376
P. Browning, browning_paul_f@solarturbines.com
M. Fitzpatrick, fitzpatrick_mike_d@solarturbines.com
P. Montague, montague_preston_j@solarturbines.com
M Van Roode, van_roode_mark_x@solarturbines.com
M. Ward, ward_mike_e@solarturbines.com

SOUTHERN CALIFORNIA EDISON COMPANY, 2244 Walnut Grove Avenue, Rosemead, CA 91770
S. Hamilton, hamiltsl@sce.com

SOUTHERN COMPANY, 600 N. 18th Street, 14N-8195, P.O. Box 2641, Birmingham, AL 35291
S. Wilson

STEVEN I. FREEDMAN, Engineering Consultant, 410 Carlisle Ave., Deerfield, IL 60015
S. Freedman, sifreedman@aol.com

STAMBLER ASSOCIATES, 205 South Beverly Drive, Suite 208, Beverly Hills, California 90212
I. Stambler

THE BOEING COMPANY, Rocketdyne Propulsion & Power, 6633 Canoga Avenue
MC: GB-19, P.O. Box 7922, Canoga Park, CA 91309-7922
G. Pelletier, gerard.pelletier@west.boeing.com

TELEDYNE CONTINENTAL MOTORS, 1330 W. Laskey Rd., PO Box 6971, Toledo, OH 43612-0971
J. T. Exley, texley@teledyne.com

TURBEC
L. Malmrup, lars.malmrup@turbec.com

UCI COMBUSTION LABORATORY, U. of CA, Irvine, Irvine, CA 92697-3550
V. McDonell, mcdonell@ucic1.uci.edu

UDRI, Ceramic & Glass Laboratories, 300 College Park Ave., Dayton, OH 45469-0172
A. Crasto, allan.crasto@udri.udayton.edu
G. Graves, gravesga@udri.udayton.edu
N. Osborne, osborne@udri.udayton.edu
R. Wills, roger.wills@udri.udayton.edu

UNITED TECHNOLOGIES RESEARCH CENTER, 411 Silver Lane MS 129-24, East Hartford, CT 06108
H. Eaton, eatonhe@utrc.utc.com
J. Holowczak, holowcje@utrc.utc.com
T. Rosfjord, rosfjotj@utrc.utc.com
J. Smeggil, smeggijg@utrc.utc.com
G. Linsey, linseygd@utrc.utc.com
J. Shi, shij@utrc.utc.com
E. Sun, suney@utrc.utc.com
D. Mosher, mosherda@utrc.utc.com

UNIVERSITY OF CALIFORNIA, Department of Mechanical Engineering, Berkeley, CA 94720
R. Dibble, rdibble@newton.berkeley.edu

UNIVERSITY OF MARYLAND, Department of Mechanical Engineering, College Park, MD 20742-3035
R. Radermacher, rader@eng.umd.edu

US DOE-NETL, P. O. Box 880, MSO-D01, 3610 Collins Ferry Rd., Morgantown, WV 26507-0880
C. Alsup, Jr., charles.alsup@netl.doe.gov
A. Layne, abbie.layne@netl.doe.gov
L. Wilson, lane.wilson@netl.doe.gov

US DOE-NETL, PO Box 10940, Pittsburgh, PA 15236
N. Holcombe, norman.holcombe@netl.doe.gov
U. Rao, rao@netl.doe.gov

US DOE CHICAGO OPERATIONS OFFICE, 9800 S. Cass Ave., Argonne, IL 60439
J. Jonkouski, jill.jonkouski@ch.doe.gov
J. Mavec, joseph.mavec@ch.doe.gov
J. Livengood, joanna.livengood@ch.doe.gov
S. Waslo, stephen.waslo@ch.doe.gov

US DOE-HQ, 1000 Independence Ave., S.W., Washington DC 20585
R. Fiskum, ronald.fiskum@ee.doe.gov
D. Haught, debbie.haught@ee.doe.gov
P. Hoffman, patricia.hoffman@ee.doe.gov
W. Parks, william.parks@ee.doe.gov
M. Smith, merrill.smith@ee.doe.gov
C. Sorrell, charles.sorrell@ee.doe.gov

WILLIAMS INTERNATIONAL, 2280 West Maple Rd., PO Box 200, Walled Lake, MI 48390-0200
G. Cruzen, g.cruzen@williams-int.com
W. Fohey, w.fohey@williams-int.com
C. Schiller, cschiller@williams-int.com

WRIGHT PATTERSON AIRFORCE BASE,
R. Sikorski, ruth.sikorski@wpafb.af.mil